UNIVERSITEIT VAN PRETORIA
UNIVERSITY OF PRETORIA
YUNIBESITHI YA PRETORIA

Influential cooling of the free surface by jet impingement of aqueous nanodispersion dominant with hybridized nanoparticles

Research Thesis: MEng Master's Degree

Rajesh Singh Padiyaar

1/14/2022

Department of Mechanical and Aeronautical Engineering

Supervisor - Prof. M.Sharifpur

Abstract

The sustenance of industries depends on implementing energy conservation and sustainability concepts. They partially or wholly rely on thermal energy to fabricate products that are necessary for the paced livelihood. Amidst them, jet impingement cooling is one of the fast-emerging techniques due to its capability of producing very efficient localised heat transfer. The impinging jet cooling technology has been extensively employed in various industrial systems, such as cooling of gas turbine system and components, cooling of the rocket launcher, and cooling of high power density electrical density machines, to remove a considerable quantity of heat. However, it is vital to remember that increasing the impingement cooling magnitude isn't always the best design decision when trying to control the engine's thermal conditions and reactions. The bulk metal temperature and local thermal stresses have the most significant impact on the life expectancy of the hot gas path component. The component will break sooner if the bulk temperature is too high, but cracks will form, spread, and eventually collapse (cycles) if the thermal stress is too high. A high bulk temperature may be reduced by increasing the cooling flow; however, this might increase the problem of thermal stress. In order to eliminate local gradients, surface roughness or orientation of the impingement jets may be used to increase the heat transfer coefficient around a lower starting magnitude. Hence, the current study investigates the influence of free surface cooling by jet impingement of hybrid nanofluids prepared by dispersing MWCNT (5 nm) and Al_2O_3 (<7 nm) in DI water in the ratio of 90:10. The fluid was characterised by TEM and DLS to understand the dispersion and hydrodynamic size. The fluid stability was evaluated and quantified by visual inspection, zeta potential and transient viscosity approach. The nanofluid properties such as viscosity, thermal conductivity and surface tension were measured at different volume concentrations (0.025, 0.05, 0.1, 0.15%) and temperatures (10 to 60°C). The heat transfer experiments were focused on cooling the targeted copper round surface (D=42 mm) using a jet nozzle (D_j=1.65mm inner diameter) to impinge the HNFs at a constant jet-surface distance at H/D_j=4 susceptible to a turbulent flow regime. Numerical studies by the Eulerian-Eulerian approach were also carried out by assuming that both gas and solid phases are at interpenetrating continua with the k-w SST model evaluating the changing velocity and turbulent viscosity. Furthermore, we investigated a transient cooling rate for varying particle vol% concentrations. The effect of flow rate, advection, and surface tension on the thermal performance of the nanofluid in cooling the surface is measured by relating the Nusselt number with Reynolds number ($6000 \leq Re$

≤ 16500), Peclet number (80000 ≤ Pe ≤ 205000) and Weber number (1000 ≤ We ≤ 7000) respectively. The maximum augmentation in Nu number is at 0.05% HNF with a 17% increase compared to DI water. From the CFD study, a maximum improvement of 19.7% in Nu number is seen by the 0.15% HNF, and the improvement in the 0.05% particle concentration fluid is 13.7%. The impinging Nu number for HNF with 0.05% stands at 180, 18.7% augmentation compared to DI-water and has the maximum improvement than any other particle vol% concentration fluids. It was concluded that the 0.15% HNF is the worst performing fluid at the jet-surface domain and hurts the Nu number. However, this trend was not shown in the CFD analysis and could be caused by other factors of the experiment such as size and shape of nanoparticles, mixing methods, surfactant amount and heat loss. In terms of the transient cooling rate investigated, the best-performing fluid is 0.15% particle concentration fluid with relaxations time 1 second and 1.75 seconds in CFD and experiment, respectively. The steady-time (the time the cooling curve is approaching the infinity line) is 23 seconds and 33 seconds in CFD and experiment, respectively. Correlation for Nusselt number as a function of Re and volume concentration was also proposed.

Acknowledgements

The author of this report would like to thank Prof Mohsen Sharifpur, Doc. Suseel Jai Krishna and Doc. Mostafa Mahdavi for their continuous support and guidance throughout the project.

Table of Contents

Abbreviations

- NFs = Nanofluids
- HNFs = Hybrid nanofluids
- HTF = Heat transfer fluid.
- LPM = Litres per minute
- CFD = Computational fluid Dynamics
- MWCNT =Multi-wall carbon nanotubes
- vol% = Volume percentage (%)

Symbols

- k =Thermal conductivity (W/mK).
- μ = Dynamic Viscosity (kg/m.s)
- v = Kinematic viscosity (m^2/s)
- ρ= Density (kg/m^3)
- C_p= Specific heat (J/kg.K)
- β= Volume expansion coefficient (1/K)
- α= Thermal diffusivity(m^2/s)
- σ= Stefan-Boltzmann constant
- g = Gravitational force (9.815 m/s^2)
- $\dot{m}$= Mass flow rate(kg/s)
- V= Volume(m^3)
- A= Area(m^2)
- D= Diameter(m)
- H = Height (m)
- T= Temperature (°C or K)
- φ= Particle concentration percentage (%)
- ϕ= Volume fraction of particle
- ψ = Weight concentration fraction
- V = Voltage(V)

- I = Current (amps)
- θ = Cooling rate
- R = Correlation coefficient
- EB = Energy balance
- X = Percent weight of nanoparticles
- M = Mass of nanoparticle

Subscripts

- eff = effective
- p = particle
- bf = base fluid
- nf = nanofluid
- hnf = hybrid nanofluid
- bf = base fluid
- j = jet
- e = exit
- s = surface
- bf = base fluid
- *0* = at stagnation
- *ip* = at impinge surface
- *Cu* = copper
- MWCNT = Multi-wall carbon nanotubes
- Al_2O_3 = Aluminium oxide
- elec = electrical

List of Figures and Tables

1. Introduction:

Industrial applications, including transport, energy, HVAC, and electronic cooling, have used heat transfer fluids (HTF) for centuries. Some of the traditional methods of increasing cooling rate are usually increasing flow rate or increasing surfaces of fins or fan. With the increase in flow rate, more pump power is needed to transport the fluid, and increasing the system's surface gets compromised for its space and design. Therefore, a new type of HTF called Nanofluid is studied for its remarkable thermal properties. Nanofluid is now in the centre of being one of the best fluids to use in any fluid dynamics application. Fluids with nano-sized solid particles suspended in them have been called nanofluids (NFs), which have shown to be suitable heat transfer fluids in recent studies. Conventionally, nanofluids were used as mono-particle fluids. In recent years, new NFs have been developed where Bi- and Tri-nanoparticle ratios are prepared to achieve even higher thermos-physical property enhancements. Some of these fluids have exceptional heat transfer properties due to the interactions between the particle interfacial boundaries. In fact, Nanofluids are non-homogenous suspensions in which the nanoparticles are added to the base fluid to increase the effective surface of heat transfer. In other words, nanoparticles could be considered as the nanofins in the suspensions that improve the conduction heat transfer. In addition, by adding nanoparticles to the base fluid, the Brownian motions could be improved due to the increment in the values of Reynolds (Re) number. This simple definition could bring a valuable understanding of the application and importance of nanofluid. Furthermore, nowadays, nanofluids have become one of the tools in biomedical engineering. Drug delivery and cancer treatment are the ones well-known applications in medicine (Constanza Toledo, 2021).

Jet cooling is effectively used in industries for various applications such as microelectronic components cooling, heat transfer in electronic parts, cooling of combustion engines, thermal photography, cooling of turbines, and used in the food and textile industry. Jet cooling is known for its enhancement of heat and mass transfer coefficients. It is achieved by high-speed jet impingement on the surface of the fluid, which creates a local thin boundary layer around the surface, which behaves like a cooling blanket around the target surface.

We did experimental tests to analyse the MWCNT/Al2O3(90:10) -DI water hybrid nanofluid (HNFs) for their thermal-physical properties and the experimenting of jet impingement using the HNFs. We investigated steady- and transient states for both experiment and numerical study. In

the steady-state analysis of the MWCNT/Al_2O_3(90:10)-DI water HNFs, we investigated heat transfer coefficient (HTC), Nusselt (Nu) number enhancement at the jet nozzle and the impinged surface region with varying Volume Fraction, Reynolds, Webers and Péclet number; furthermore, the pumping power for varying volume fractions only was investigated.

Many studies are performed using mono nanofluids in literature, but HNFs are not researched much for their thermal properties, nor in an application of jet cooling; hence, this project will provide critical findings on the thermo-physical property enhancement and application in jet impingement. The jet impingement problem is analysed with two models, the analytical-experimental and numerical simulations; not many researches are done with both types of analysis, it is critical to gather information from both experimental and numerical to validate the work due to the rarity and limited amount of literature for both the HNFs and jet impingement studies.

2. Literature Review:

2.1 Jet cooling configuration and flow characteristics

Before carrying out the research study, we studied the flow regime for its thermal and dynamic behaviour. The experiment deals with high flow speed and Re number. It, therefore, falls under the turbulence flow regime due to the internal flow Re number of the jet being more significant than 2300. The term turbulence for the problem in jet impingement is defined as the unsteady, irregular (aperiodic) motion of fluid transportation. These characteristics are even more prevalent in the NF flow because of the particle effect on the transport qualities, such as mass momentum fluctuations in time and space. Large Turbulent eddies are present in turbulence flow, and the size and velocity of these large eddies are in order of mean flow. Energy is derived from the mean flow by these large eddies and then transferred to smaller eddies. Turbulent energy is converted to internal energy by viscous dissipation in the smallest eddies. The small and large eddies can be seen in the microscopic view of a typical turbulence flow structure provided by (Richardson Energy cascade, 1922) and are shown in Figure 1 below.

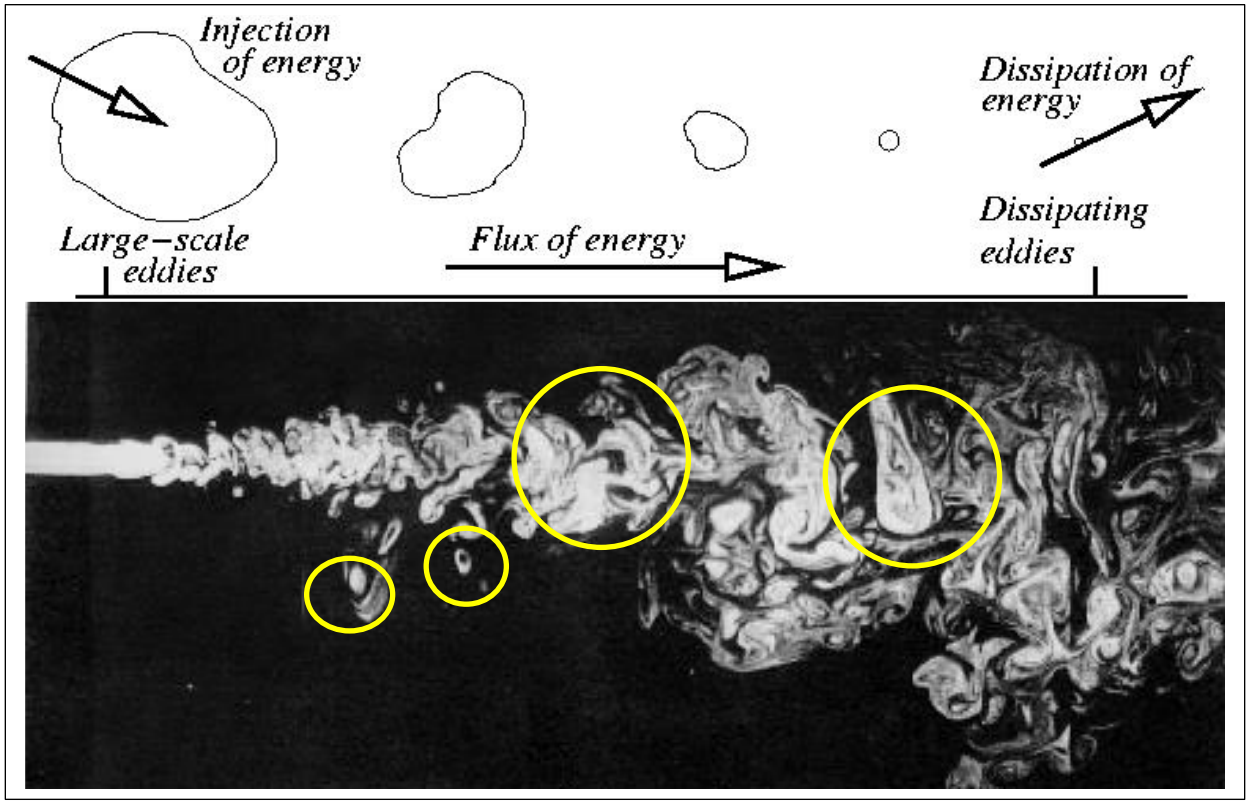

Figure 1 Microscopic view of energy transportation in fluid flow by Eddies (Energy Cascade Richardson (1922)

Impinging jet can be classified into two main categories, a free surface or submerged and further separated into confined and unconfined setup (M. Molana, 2013), as shown in Figure 2. In submerged jets, the jet exudes the same liquid as the liquid between the target space and jet, which can be configured as confined or unconfined, depending on the target distance. The jet stream forms a potential core centreline during a submerged jet unaffected by other disturbances such as entertainment (Webb, 1995). In the confined configuration, such as the jet coming in from a long tube, the jet interaction with ambient and other surroundings has a higher HTC because the heated fluid is not causing disturbance to the incoming jet (Lupton T. L, 2008). The fluid is discharged into a gas space such as air before impingement with the target surface in free surface jets configuration. The disturbances from the jet fluid are negligible, and the potential core is not relevant in this case. The space between jet and target surface is usually limited in a free surface configuration. The different configuration is shown below in Figure 2 and explained in Table 1. A flow field is characterized by a jet zone, a stagnation zone, and a wall jet zone(K Marzec, 2014).

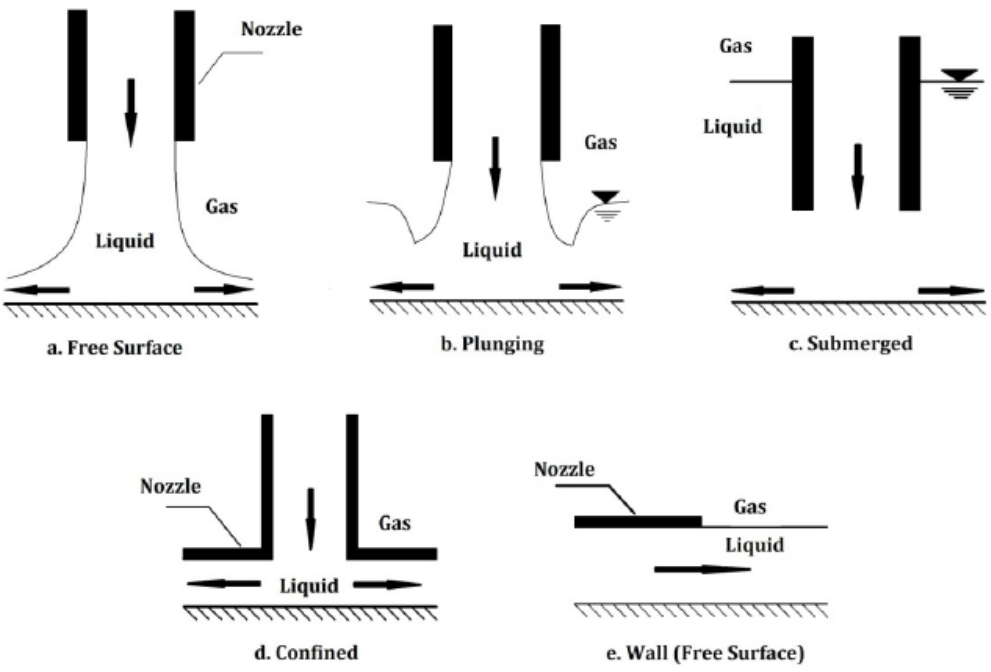

Figure 2 Various Jet -Surface Configurations types in jet cooling applications (M. Molana, 2013)

Table 1 Various types of Jet-Surface Configuration descriptions

A. Unconfined Free surface	The jet inlet is in the gas space, and the nozzle exudes liquid through the gas onto a target surface,
B. Plunging	The nozzle is submerged in liquid space; the liquid is exuded through the fluid area onto the target surface.
C. Submerged	The jet liquid is bounded with walls which creates several exits.
D. Confined	The jet liquid is bounded with walls which creates several exits.
E. Wall confined free surface.	The jet is targeted along a wall surface in a parallel direction.

2.2 Jet cooling Experimental and Numerical review

Many researchers have come up with different experiments to find the various impact of jet parameters on the flow's heat transfer and dynamic properties. Many of these studies provide critical conclusions compared to the investigation carried out. Few published pieces of research are discussed below, and these researches include jet impingement cooling by NFs and HNFs for both steady and transient states.

Al_2O_3 Aluminium oxide nanoparticle-based fluid was used to perform a jet cooling experiment by (O. Zeitoun, 2013). A round water jet with the horizontal circular surface as the target was used. The study was performed to find different effects on heat transfer from different flow rates, jet diameter, and nanoparticle concentration. For a constant Re number, the Nu number was increased, indicating an increase in HTC. Furthermore, changing nanoparticle concentrations (0,6.6 and 10%) of NFs were considered in the study. For equal Re numbers, the experimental data showed an increase in Nu numbers that can reach up to 75%.

(Mingzheng Zhou, 2015), used water and silver-based NF of different concentrations to perform a jet cooling experimental study. They investigated the heat sink's thermal performance and flowed characteristics with confined and submerged liquid jet array impingement. The HTC of pin fin heat sink and plate heat sink increases with particle mass fraction at constant jet speed. For the three NFs, 0.02, 0.08, and 0.12 wt%, the HTCs are enhanced by 6.23, 9.24, and 17.53%, respectively, compared with base fluid at the same jet-velocity. For a constant Re number, the Nu number was increased as the concentration of particles increased, indicated by the increase in HTC. AISI 304 steel plate was used with alumina NF jet impingement at different particle concentrations by (A. M. Tiara, 2016) to study the heat transfer characteristics of the fluid. At a low concentration of below 10ppm, the thermal conductivity increased slightly. They showed the nucleate sites on the roughness test increase significantly, indicating that NF enhances the heat transfer rate. At low concentrations, they improved the cooling rate considerably, but at high concentrations, it was shown to decrease slightly—the HTC increases with reduced surface temperature.

(Kulkarni G.A, 2018), experimentally studied the jet impingement quenching on a moving metal sheet with several jets. They analysed the boiling curve and the width of the wetting region for different metals and different mould moving speeds and the initial temperature. The results are compared and analysed to identify influencing parameters during the continuous quenching process. Metals with high thermal conductivity have more prominent cooling regions than other materials, and the areas increase in size with the decrease in speed of the metal sheet. The maximum heat flux is seen to be decreasing with decreasing metal sheet velocity. Generally, metals with high conductivity are suitable for industrial applications, but one should consider the stress that the maximum temperature during quenching causes on the metal.

(Bin Sun, 2019), studied the heat transfer characteristic of HNFs when used on an impinging jet setup. The HNF is prepared at the same ratios of Ag and MWCNT nanoparticles. They selected at various mass fraction deionized water and the optimal balance of the mixed solution. The study encompasses conventional impinging and swirling impinging jets for the conditions of varying heat flux surface, length to diameter (L/D) ratios, and various swirling ratios. The conventional and swirling jet HNF showed a better HTC when compared to mono NFs and deionized water only. The results showed that the HTC increased with an increase in the mass fraction of particles due to an increased concentration, which caused the thermal conductivity of the fluid to rise. The HNFs Nu number increased as the L/D value rose between 2 and 6 then reduced at the given Re

number. Nu number is maximum, when L/D=4 for the swirling impinging jet, the conventional jet did not perform well in terms of heat transfer effect. For a ratio higher than L/D=4, the HTC effect is high. The heat transfer effect of the conventional impinging jet was not excellent in terms of revolving. At the constant L/D values, the Nu number increased as the Re number was increased. They examined how various target surface structures affect heat transfer. They found that the effectiveness of heat transfer in the concentric circular groove target surface was better rather than that of the concave and the mirror surface because of the small kinetic energy of the jet working fluid when Re is less than 10,000. The concave target surface's heat transfer was best when Re was more than 15000. This is because the kinetic energy of the working fluid was substantial. The concave surface also acts as a pool for diverging jet fluids, which in turn increases the efficiency of the heat transfer.

(Mohsen Amjadiana, 2020), experimentally studied the heat transfer characteristics of Cu_2O water-based nanofluid used in Jet Impingement. They explored different factors such as Re number and particle concentration on the nanofluid flow and heat transfer characteristics. The target surface of the circular aluminium plate was kept at constant heat flux. The nanofluid concentration of 0.03 to 0.07 wt% was examined, and at 0.07 wt% concentration, the convective heat transfer increased by 45%. The stagnation zone is at the centre of the plate because of the highest intensity. The maximum local HTC appears in the stagnation point and reduces in the radial direction. Increasing the Re number increased the turbulence intensity, enhancing the HTC.

(Ishita Sarkar, 2019) , used TiO_2 nanofluid as a base coolant in a jet impingement quenching of a hot steel plate experiment. There experiment aimed to improve the cooling performance in the jet impingement process. Different nanofluid concentrations were used for a hot steel plate at 900°C. They found that the higher concentration, the better the thermal conductivity increased. An 8.3 % improvement in the thermal conductivity and 19 % improvement in cooling was observed when using a 40 ppm TiO_2 nanofluid compared to water. They also found that the nanoparticles form nuclei on the surface, increasing the wettability and improving the cooling performance. Optimal heat flux was also found at 40ppm and decreased due to the coating of nanoparticles on the plate. The surface temperature at different times was recorded for different nanofluid concentrations; again, the 40ppm nanofluid coolant is the most effective. It has the steepest slope indicating that the cooling rate is maximum at 40 ppm.

Jet impingement cooling of an isothermal surface with Al_2O_3 water nanofluids were investigated with the presence of a magnetic field by (Fatih Selimefendigila, 2020). Galerkin weighted residual finite element approach was used for governing Equations. The simulation was performed at various Re numbers (100-400), solid particle concentration (0-4%), and Hartmann number (0-2.5). The distance was varied for slot distance (jet to surface distance). The magnetic field affected the fluid flow and reduced the local Nu number to the best that of Hartmann. They found that because of Lorentz's force, fluid is unable to gain stagnation. When nanofluids are utilized, the average Nu number is greater in the magnetic area because of increasing the electrical conductivity, resulting in more convection suppression. There was a tiny change in the average Nu number as they raised distance spacing in the slots. But, increasing the jets to the bottom plate has deterioration effects on the average Nu number and stagnation. They achieved a moderate heat transfer increase, and the average Nu number can change linearly with a solid particle volume fraction.

Much numerical research has been carried out on Jet Impingement; some of the relevant literature to work is discussed below. This section of this research aims to help develop a numerical model to cater to all boundary conditions and parameters of the experimental work. A CFD approach (Muhammad Ali Rob Sharif, 2009) was used to investigate several turbulence models in a jet-wall problem to predict the convective heat transfer. The turbulence models considered for investigation were the Standard, realizable and RNG k – ϵ model, the SST k – ω model, and the LRR Reynolds stress transport model. The turbulence models were also implemented near-wall treatments such as wall-function and multi-layer enhanced wall. Using various validation research was used to compare the results of the five turbulence models. The results showed that most turbulence models predicted accuracy for core region local Nu number and wall jet region; however, the model did not predict well for impinging region Nu number. In both surfaces investigated, the concave and flat surface, the SST k – ω model and k – ϵ model with the enhanced wall functions predicted the Nu number well. The Dynamic profile of flow was not predicted well using the SST k – ω model for the concave surface profile. The RNG k – ϵ model predicted dynamic profile correlates with the experiment. The LRR Reynolds stress model is not superior to other eddy viscosity models for Dynamic studies.

(Oronzio Manca, 2011), they investigated the effect of confined impinging jet slots working with Al_2O_3 -water NF. The study involved the turbulent flow regime of the impingement process at a constant temperature, with a simple Single-phase model for the numerical simulation. Behavioural

changes examined geometric ratio, particle concentration, and Re number in Nu number, convective HTC, and pumping power. Using the stream function, they concluded that the geometric ratio of H/W, Re, and Particle concentration is responsible for the intensity and vortex structure. The highest local Nu number profile is evident at the stagnation point, and at the end-plate region, it is seen to be the lowest. The average Nu number increases with increased particle concentration and Re number. Furthermore, as particle concentration and Re number were raised, the power required for fluid flow increased.

A review study by (Wang Peng, 2014) was done on different turbulence models and wall function. The temperature and velocity behaviours were studied in single and various multi-phase models. The investigation was carried out to find how particle concentration, Re number, physical properties, and geometric configuration affect the impingement cooling process with nanofluid. From all the literature reviews, they concluded that the standard k-ω turbulence model, k-ε turbulence model, low-Re turbulence model, k-k_t-ω turbulence model, transition SST turbulence model, RSM and, a VoF turbulence model are not appropriate choices in numerical simulation of impingement jet. However, the k-ε turbulence model gives a better prediction for wall function; but, the standard, no equilibrium, and scalable wall function cannot be reasonably predicted. The single-phase models expected the HTC better; however, this was due to the physical properties derived from the experiment. The single-phase cannot capture critical information as its error increases significantly with volume fraction. They found that adding nano-particles improves the momentum exchange in phases and increases the temperature field uniformity. It strengthens the capacity in overall heat, which is not predictable in the single phase. The Eulerian-Eulerian multi-phase and the SST κ-ω turbulence model are more suitable for the impinging jet cooling of nanofluids. The proper turbulence model should be on the basis of the computational cost and accuracy.

(Miroslave kmecova, 2019), investigated the dynamic behaviour of Circular free jets with various turbulence models. The theoretical models were compared to the CFD models to provide a dynamic model that can be used to improve air quality in breathing zones. They investigated. The five turbulence models considered for investigation were namely the Standard, RNG and realizable $k - \epsilon$ model, the standard and SST $k - \omega$ model and Reynold's stress model (RSM). The turbulence models were verified for accuracy using the centreline velocity profile captured from the different models and the theoretically calculated velocity profile. The results show that the k-omega SST

turbulence model prediction is best compared to theoretical data. The model with the worst prediction was the k-epsilon standard turbulence model, followed closely by the standard k-omega turbulence model. All other turbulence models predicted well when compared to theoretical data.

(Fei Xue, 2019), investigated cooling of a Rib-Roughened trailing edge with high-speed impingements in a crossover formation. Two adjacent channels performed the numerical study where eleven racetrack-shaped holes were created as jets. The target surface consists of four ribs arrangements. Four different turbulence models were investigated: standard k-ε, realizable k-ε, and k-ω with shear stress transport (SST). They compared experimental data results. All four turbulence models predicted were compared to experimental data; the best performing model for predicting HTC was the k-ω-SST turbulence model.

(Mostafa Mahdavia, 2020), investigated the surface roughness effect on the jet cooling process by using nanofluid. VoF model in a multi-phase approach was used to simulate the interactions between the air and fluid. The nano-particles were tracked in the flow using a discrete phase model to understand the surface roughness effect on the cooling of the surface. Their result showed optimum surface roughness's where the heat transfer increases until and eventually decreases. The reduction in mean velocity of flow caused after a particular surface roughness reduces the cooling rate. The study showed that thermal conductivity significantly improved the heat transfer on rough surface profiles. As with the other studies, the most significant heat transfer occurred at the stagnation point.

(B. Boudraa, 2021), conducted a numerical study of jet impingement cooling using Al_2O_3-MgO HNFs to cool isothermal surfaces with extended jet holes. The Al_2O_3 and MgO nanoparticles were spherical, while the MgO particle was changed to see the particle shape effect of the cooling process. The analysis was carried out at Re number 5000 to 15000, with a 0-5% volume concentration. The ratio of Jet diameter to height of jet from the target surface is varied from 0 to 4. The numerical analysis revealed that the highest value of Re and the highest concentration of HNFs lead to the most remarkable enhancement in heat transfer rate, leading to more significant pressure loss in the system. The most considerable enhancement was seen by Al_2O_3- sphere and MgO- platelet shows that using different shape particles to formulate HNFs can significantly enhance its heat transfer capacity. The Nu number is at maximum at the stagnation point of the flow.

(Enrique-Manuel Garcia-Merida, 2021), carried out a numerical analysis on jet impingement of Al_2O_3 using ANSYS as the CFD software. The jet distance, surface distance, the volume fraction of nano-particle, and Re number effect on heat transfer performance were studied using the average Nu number on the plate. The heat transfer was minimal at the surface edge and 25% higher at the stagnation point for laminar flow. The maximum absolute uniformity (minimum σ) occurs at a maximum jet-to-plate distance, minimum nano-particle concentration, and minimum Re number. Specific improvements of the heat transfer can be achieved as ϕ and H/D increase, resulting in higher Nu numbers. Indeed, the average Nu number increased, at least up to 21.1%, when a 10% volume fraction of nano-particles is used compared to plain water. On the other hand, the Nu number can increase at least up to 19.7%. Regarding the uniformity of the heat transfer, the highest uniformity occurs when using plain water: the addition of nano-particles gives rise to certain regions efficiently cooled. In contrast, others are less cooled, which finally means a low uniformity heat transfer.

In the Jet cooling literature study, it was found that metals with high thermal conductivity have more prominent cooling regions than other materials, and the regions increase in size with the decrease in speed (Kulkarni G.A, 2018). Generally, metals with high conductivity are suitable for industrial applications, but one should consider the stress that the maximum temperature during quenching causes on the metal. For a non-uniform temperature, there is a decrease in convective heat transfer, which becomes higher with an increase in jet distance (Bin Sun, 2019). In jet cooling by nanofluid specifically; Increasing the Re number leads to more turbulence intensity which enhances the HTC—also, increasing the concentration leads to a significant increase in the heat transfer by convective and conductive. An increase in distance from the stagnation point decreases the local convective HTC, which is verified by increasing temperature. For a constant Re number, the Nu number was raised as the concentration of particles increased, indicated by the increase in HTC. Low particle concentration between 0- 4 % is an excellent range to investigate the enhancement of heat transfer using jet cooling and nanofluid. At high concentrations, the particles form large aggregation and malfunction of heat transfer between surfaces.

In jet cooling by nanofluid transient case, the nanoparticles form nuclei on the surface, increasing the wettability and improving the cooling performance. Optimal heat flux was also found at specific low concentrations and decreased due to the coating of nanoparticles on the plate. The

cooling rate was enhanced significantly (O. Zeitoun, 2013), but it was shown to decrease slightly at high concentrations—the HTC increases with reduced surface temperature. The Prandtl and Nu number values decrease with the rise in nanofluid concentration, and the HTC increases with an increase in the concentration of nanofluid (Kashinath Barik, 2020).

Regarding the numerical study of Jet cooling, most of the studies done in high Re number all show a positive outcome in heat transfer improvement in the jet cooling process. All past studies concluded that the average and local Nu number increases as particle concentration increases, indicating convective heat transfer improvement. (Oronzio Manca, 2011), concluded that the power required to carry the nanofluid to reach the same Re number is more significant than its base fluid, which increased as the particle concentration increased. It is due to the overall density increase in the fluid and flows property change of fluid. All studies reveal that the highest heat transfer occurs at the centre of the stagnation point and is the lowest at its surface edges.

(Wang Peng, 2014) express an SST κ-ω turbulence model, and the Eulerian-Eulerian multiphase model is more suitable to impinge nanofluids' jet cooling. Not much research was done on the shape or state of the surface. However, (Mostafa Mahdavia, 2020) investigated the effect of roughness on the heat transfer capabilities and concluded that the heat transfer is enhanced till an optimum surface roughness and after that decreases due to the damping of velocity.

HNFs are relatively new in jet cooling and have not been tested numerically; however, (B. Boudraa, 2021) conducted a numerical analysis using HNFs $Al_2O_3 - MgO$ to cool isothermal surfaces with extended jet holes. The results were the same as other research. It revealed that as Re number and particle concentration increased, the heat transfer performance was improved. They also tested with other shapes of nanoparticles, and the most prominent enhancement was seen by Al_2O_3- sphere and MgO- platelet revealed that using different shape particles to formulate the HNFs can significantly enhance its heat transfer capacity.

The SST k–ω turbulence model form part of the Reynolds-Averaged Navier Stokes (RANS) models; this approach solves ensemble-averaged (or time average) Navier stoke equations. The RANS models are the most widely used approach in the industry, and all turbulent lengths scales are modelled in RANS. The other two, namely Large Eddy Simulation (LES) and Direct Numerical Simulations (DNS), are not appropriate for turbulence flow modelling (Wang Peng,

2014). The SST k–ω turbulence model is one of the better approaches than the other RANS model, although the cost is significantly higher per iteration than different standard and realizable RANS models. The k–ω family of turbulence models is most widely used because all terms are defined in an equation at the wall, and they can be integrated into the wall without using wall functions.

2.3 Rayleigh-Taylor instability (RTI)

The Rayleigh-Taylor instability (RTI) is the evaluation of the interpenetration of materials. The RTI happens when a less density fluid pushes on a high-density fluid. Dynamic processes reduce the combined potential energy of the two fluids; this, in turn, ensures mixing and turbulence (Andrew W. Cook, 2009). To explain the formation of cirrus clouds, Lord Rayleigh first derived an interface movement as a heavy fluid is supported by a lighter one (Rayleigh, 1883). The study of (Rayleigh, 1883) only considered constant acceleration; however, in 1950, Sir. G.I. Taylor realized that Rayleigh's interfacial instability also accelerates other than gravity (Taylor, 1950).

Many researchers have conducted RTI scaling properties and mixing rates for variable and constant accelerations since 1950. The RTI's evolution has four main steps (Andrew W. Cook, 2009). In the initial stage, the perturbation amplitudes are small compared to their wavelengths. The motion's equations can be linearized, causing exponential instability is growing. An initial sinusoidal perturbation protects the sinusoidal shape at the first of this stage. However, nonlinear effects emerge at the end. In the beginning stages, the formation of mushroom-shaped spikes (heavy fluid changing into light ones) and bubbles (light fluid changing into rich ones) are observed. The mushroom structures still grow in the next stage. It can be used in buoyancy drag models, causing a constant growth rate in time. So, they can no longer ignore nonlinear terms in the movement's equations. In the third step, the bubbles and spikes start interacting. The nonlinear interaction of mode coupling merges smaller bubbles and spikes to create bigger ones. Now, bubble competition happens, where spikes and bubbles of smaller wavelengths that are saturated covered by larger ones are still not saturated. In the final step, It is evolved into a turbulent mixing region. The mixing area eventually extends for high Re numbers.

2.4 Preparation and stability methods

The preparation of nanofluids is the key step in the use of nanoparticles to improve the thermal conductivity of fluids. Due to the nature of the nanoparticles causing aggregations and settling due to the downward gravitational pull, it is critical to synthesize the particle in the base fluid to correct for the nanofluid to be effective in application and testing. Preparation methods of nanofluids are categorized into two categories:

(a) The one-step way.

This method generally prepares the nanofluid directly with the base fluid, without any other in-between process such as storage or dispersion of nanoparticles in base fluid (Y. Li, 2009). This method simultaneously synthesizes and disperses the nanoparticle into the base fluid. This technique is primarily better than the two-step way to prepare nanofluid stability. This is because of the avoidance of storage, drying, and transportation of particles, limiting the probability of particle aggregation (Samarshi Chakraborty, 2020). This methodology jeopardizes any chance of particle density. This method's production cost is significantly high compared to the two-step way; thus, it makes it impractical for large production.

(b) The two-step way

This is the most common method of nanofluid preparation due to its implementation, cost-effectiveness and particle agglomeration control. In brief, the two-step method of nanofluid synthesis includes two distinct steps (J.C. Joubert, 2017)

(1) Drying of nanoparticles and preparation.

(2) Nanoparticle dispersion in a base fluid using physical (ultra-sonication, magnetic stirrer, and high-pressure homogenizer).

Researchers have developed an exciting synthesis method for nanofluid in recent years at Argonne National Laboratory. The Nano-particle is deionized using multi-beam laser ablation in liquid, meaning the laser parameters control the nanoparticle size and distribution (Mujumdar, 2008). For the experiment, the two-step method used by (J.C. Joubert, 2017) is used to prepare the fluid due to its cost. It is an effective method of preparation if the nanofluid is evaluated carefully before experimentally by using various stability measurement techniques, as discussed in section 4.3 below. Stability evaluation of the HNF is one of the major steps in an experiment; if the fluid is not stable, the properties are compromised, and the enhancement is affected; hence it is crucial to

find a stable fluid without any particle agglomerations or deposits.

(a) Sedimentation and centrifugation

The sedimentation technique is one of the most used techniques for evaluating NF stability. Sediment collection at the bottom of the liquid container is due to the gravitation force, which forms the basis of this technique. Many researchers say that more extended time taken by nanofluid to form a precipitate indicates good stability. The centrifugation technique uses centrifugal force instead of gravitational force. This method requires less time to find stability because the power is more significant. (A.K. Singh, 2008), used the centrifugal method to evaluate the stability of ethanol-based Ag nanofluid with PVP as a stabilizer. The study showed no sedimentation in a time frame equal to 1 month of waiting time in the Sedimentation method.

(b) Zeta potential measurement

In this method, the measurement of the Zeta potential of the fluid is used to find stability. A colloidal suspension is constant with a high zeta potential value. Having less zeta potential value tends to agglomerate faster and is considered unstable. Particles with a zeta potential value more excellent than ±30 mV are considered stable (Samarshi Chakraborty, 2020).

(c) Transmission electron microscopy (TEM)

TEM can measure nanofluid stability by measuring the particle size distribution. High-resolution TEM images provide 2D images of the particle in a fluid. TEM was used by (J.C. Joubert, 2017) to investigate the conventional property of nanofluid. This method was an effective method of checking stability before using the nanofluid for any experiment.

(d) Dynamic light scattering (DLS)

A laser illuminates the suspended nanoparticles in the base fluid in this method. A photon tracer captures the scattering of light caused by the Brownian motion of the fluid. The diffusion coefficient is estimated using the intensity Equation, commonly referred to as the Stoke-Einstein Equation (Bhattacharjee, 2016). The instability causes a cluster in nanofluids and sedimenting. So, DLS analysis indicates a rise in the size of a particle because of clustering. It is an indicator of nanofluid instability (Samarshi Chakraborty, 2020).

From the literature, methods of examining the particle and fluid stability are selected, namely, the TEM analysis, Zeta potential with the DLS method.

2.5 Nanofluid thermo-physical characteristics

Nano-fluids are slightly denser than their base fluid. They have flow properties similar to the base liquid. Properties can be manipulated by changing the particle shape, size, material and concentration. Thermal conductivity, with the unit of W/m.K, is one of the most critical thermal properties of HTF. The fact that solids usually have a high thermal conductivity compared to fluids makes nano-sized solid particles dispersed in liquid increases the conductivity of the fluid effectively. Suspending solid particles of size micrometre or mm into liquids to improve the physical property has been well known for 100 years. The innovation is traced back to James Clerk Maxwell's research (Maxwell, 1873).

$$k_{eff}=k_{bf}+3f\frac{k_p-k_{bf}}{2k_{bf}+k_p-f\left(k_p-k_{bf}\right)}k_{bf} \tag{2.1}$$

Equation (2.1) by (Maxwell, 1873) above can predict the thermal conductivity of a relatively large particle in the base fluid mixture. (R.L Hamilton, 1962) Further widened the Maxwell model by integrating the shape component as Equation (2.2) below.

$$k_{eff}=\frac{k_p+(s-1)k_{bf}+(s-1)\phi\left(k_p+k_{bf}\right)}{k_p+(s-1)k_{bf}-\phi\left(k_p-k_{bf}\right)}k_{bf} \tag{2.2}$$

Here the space factor is used, where $s=\frac{3}{\psi}\Psi$ is the spherical factor of the nanoparticle. Most models were developed for millimetre-sized particles; however, the same analytics and numerical applies to nano-sized particles. (W. Yu, 2003), took into consideration the nano-layer factor of liquid and derived the thermal conductivity of spherical shape mantellic oxide nanoparticles in fluid as shown in Equation (2.3), where α is the thickness ratio of the liquid nanolayer to the oxide nanoparticle radius, which is usually equal to 0.1.:

$$k_{nf}=\frac{k_s+2k_f+2\phi(k_s-k_f)(1+\alpha)^3}{k_s+2k_f-2\phi(k_s-k_f)(1+\alpha)^3}k_s \tag{2.3}$$

(J. Koo, 2004), introduced a new model, Equation (2.4), that considered fluid's static and dynamic state; the model was named the K-K model.

$$k_{eff}=k_{static}+k_{brownian} \tag{2.4}$$

Where:

$$k_{static}=\left\{1+\frac{3\left(\frac{k_p}{k_{bf}}-1\right)\phi}{\left(\frac{k_p}{k_{bf}}+2\right)-\left(\frac{k_p}{k_{bf}}-1\right)\phi}\right\}k_{bf}$$

And

$$k_{brownian}=5\times10^4\sigma\phi\left(\rho C_p\right)_{bf}\sqrt{\frac{C_B T}{\rho_p D_p}}f(T,\phi)$$

Here C_B is the Boltzmann constant and f(T,∅), and σ are experimental functions.

Viscosity is the measurement of the fluid resistance to flow. The viscosity aspect is critical because the synthesis of Nano-fluid involves suspension into the liquid. A relationship for effective viscosity of the fluid to the viscosity of particles was brought up in Equation (2.5) of (Xuan 2000).

$$\mu_{eff}=\left(1+2.5\phi_p\right)\mu_p \tag{2.5}$$

This model applies to the nanofluid, with a nanoparticles' volume fraction less than 1%. (Brinkman, 1952) Suggested the density model of nanofluid of spherical shaped nanoparticles with 4% concentration in the following form Equation (2.6):

$$\mu_{eff}=\frac{\mu_{bf}}{(1-\phi)^{2.5}} \tag{2.6}$$

(I.M. Krieger, 1959), anticipated the viscosity model for a more significant concentration of nanoparticles of spherical shape as Equation (2.7)

$$\mu_{eff}=\mu_{bf}\left(1-\frac{\phi}{\phi_m}\right)^{-[\mu]\phi_m} \quad (2.7)$$

Where μ=2.5 for complex spherical shaped nanoparticles and ϕ_m=0.605 is for maximum volume concentration.

The force acting over the surface of the liquid per length of the surface perpendicular to the point is known as surface tension (Yunus A.Cengel, 2015). The reduction of surface tension leads to a better enhancement in the wettability of the fluid. Due to the wettability factor, surface tension becomes increasingly significant in applying pharmaceutical and paint coating. A surface tension analysis is also performed by (S.M. Mousavi, 2019). A dual hybrid MgO-TiO_2 and DI-water was used for analysis with varying weight ratios (50:50, 80:20, 20:80, 60:40 and 40:60), varying particle concentrations (0.1–0.5 vol%), and temperatures between 15 to 60°C. The HNF achieved the highest Prandtl number with MgO-TiO_2(80:20) dispersed in DI-water at particle concentration 0.3vol%.

(Hemat Ranjbar, 2015), studied the effect of γ-Al_2O_3 and MgO nanoparticles concentration on the surface tension of Tri Ethylene Glycol (TEG). From their results, it was clear the surface tension varies for specific NFs concentrations; in other words, if particle concentration is incremented, the change in surface tension is not necessary following an increasing or a decreasing trend. It is evident from the study of (Deqing Mei, 2021) and (Hemat Ranjbar, 2015), the surface tension of NFs is much better than that of its base fluids. Regarding HNF, the surface tension is seen to be lower than its counterpart mono-particle fluid mixture. Moreover, when a surfactant is added to the fluid, it causes an increase in surface tension. However, it is shown that by increasing surfactant concentration by a large amount, the NFs surface tension would decrease. The pendant drop method is the most used method for calculating surface tension due to its high accuracy and low cost; hence in this experiment, the method will be adopted to calculate the surface tension.

The density of a matter is defined as its mass per unit volume, as shown by Equation (2.8) of (Yunus A.Cengel, 2015). Density is crucial in heat transfer and affects natural convection because of the Buoyancy and Archimedes law. The upward force on a body immersed is called the Buoyancy force. The convectional current in Lakes Ocean and atmosphere is due to Buoyancy

existence (Yunus A.Cengel, 2015).

$$F_{buoyancy}=\rho_{fluid}\times g\times V_{body} \tag{2.8}$$

Volume expansion is better explained with a volume expansion coefficient (Yunus A.Cengel, 2015) as shown in Equation (2.9):

$$\beta=\frac{1}{V}\left(\frac{\partial V}{\partial T}\right)_P=\frac{1}{\rho}\left(\frac{\partial \rho}{\partial T}\right)_P \tag{2.9}$$

When particle volume concentration increases, the nanofluid density rises. The density of the base fluid is reduced by increasing the temperature. The density of the adequate fluid can be calculated with Equation (2.10) below (S. Aminossadati, 2009).

$$\rho_{eff}=\left(\frac{m}{V}\right)_{eff}=\frac{m_{bf}+m_p}{V_{bf}+V_p}=\frac{\rho_{bf}V_{bf}+\rho_p V_p}{V_{bf}+V_p}=\left(1-\phi_P\right)\rho_{bf}+\phi_{bf}\rho_p \tag{2.10}$$

The adequate specific heat of the NFs can be analysed using the following Equation (2.11) (Pak B.C, 1998); therefore, the specific heat can be written as:

$$C_{p_{eff}}=\frac{(1-\phi_p)\left(\rho C_p\right)_{bf}+\phi_p\left(\rho C_p\right)_p}{\left(1-\phi_p\right)\rho_{bf}+\phi_p\rho_p} \tag{2.11}$$

From the literature regarding the thermo-physical property of mono nanofluid, it is clear that mixing formula is used to evaluate the NFs density and specific heat (S. Aminossadati, 2009), (Pak B.C, 1998), and experimental methods are used to evaluate the HNFs viscosity and thermal conductivity with each fluid having different characteristics due to the nanoparticle's physical and thermal properties. Section 4.5 below thoroughly discusses some of the findings in the literature regarding its thermo-physical properties of HNFs.

A new type of NFs called Hybrid-NFs has been recently developed to enhance flow and thermal properties. HNFs comprise hybrid nanoparticles composed of two or more different nano-particles. This section discusses previous relevant experiments and investigations on HNFs and their flow and thermo-physical properties.

(L. Syam Sundar M. K., 2017), examined the thermal and transport properties of HNF graphite oxide Go/CO_3O_4 in ethylene glycol-based fluid. The experiment was carried out at changing volume concentrations and temperatures. It was found that the fluid with the Go/CO_3O_4 nanoparticles present has a better enhancement than GO-only ethylene glycol solution, which is prevalent for all cases. The viscosity is only slightly enhanced by adding the GO/CO_3O_4 nanoparticles. They found that thermal conductivity has more effect than viscosity when adding the CO_3O_4 nanoparticle to Ethylene glycol solution than GO/ethylene glycol solution.

(Afshin Ahmadi Nadooshan, 2018), presented a study of rheological behaviours of Fe_3O_4-MWCNTs/ethylene glycol HNF. This experiment was for various fractions' volumetric (0.1, 0.25, 0.8, 1.25, and 1.8%), including the equal amounts of suspended iron oxide (Fe_3O_4) and MWCNTs nanoparticles. Temperature is between 25 to 50°C, and shear ranges are 12.24 to 73.44 s−1. They concluded that the nanofluid, resembling its base fluid, exhibits a Newtonian behaviour at a concentration of 0.1, 0.25, 0.45, and 0.8vol%. It means rising temperature reduces viscosity, and advancing the volume fraction increases it. The fluid shows a non-Newtonian behaviour at 1.25 and 1.8% volume fractions; hence a power-law model (m and n) was experimentally developed for the nanofluids at volume fractions of 1.25 and 1.8% of any temperature. A new Equation (2.12) was held to estimate and foretell the viscosity of Fe_3O_4-MWCNT/ethylene glycol HNF. Pressure drop and HTC are raised in nanotubes and nanoparticles.

$$\frac{\mu_{eff}}{\mu_{bf}}=\frac{-2.0987+(4.65\varphi)^{0.0969}+(0.8702T)^{0.2633}+(62323.1365\varphi^2)}{(143.1076T^2)} \tag{2.12}$$

According to the principles governing two-phase mixtures of equal particle volume, nanofluid properties Cρ and ρ were estimated as Equations (2.13) and (2.14) (Afshin Ahmadi Nadooshan, 2018),

$$\rho_{eff}=(1-\varphi)\rho_f+\left(\frac{\varphi}{2}\rho\right)_{Fe_3O_4}+\left(\frac{\varphi}{2}\rho\right)_{MWCNT} \tag{2.13}$$

$$C_p=\frac{(1-\varphi)(\rho C_p)_f+\left(\frac{\varphi}{2}\rho\right)_{Fe_3O_4}+\left(\frac{\varphi}{2}\rho\right)_{MWCNT}}{\rho_{eff}} \tag{2.14}$$

(Amir Kakavandi, 2018), experimentally studied the stability and thermal conductivity of MWCNT-SiC/water-EG HNF under temperatures range (25- 50°C) and particle volume fraction up to 0.75%. The two-step method for preparation was followed. A stability test was conducted using DLS to assure that the stability of the fluid was acceptable before commencing the experiment. From the results, it was deduced that by increasing the concentration, the thermal conductivity of HNF is improved. They measured the effect of temperature to have a higher impact at higher temperatures and achieved a 33% enhancement in the fluid compared to the base fluid. It was performed at the highest temperature of 50°C. The curve fitting method obtained an empirical correlation for the thermal conductivity coefficient. (Amir Kakavandi, 2018) given its acceptable accuracy, this correlation is suggested as Equation (2.15) and is used to calculate the HNFs thermal conductivity.

$$\frac{k_{eff}}{k_{bf}} = 0.0017 * \varphi^{0.698} * T^{1.386} + 0.981 \qquad (2.15)$$

(Eric C. Okonkwo, 2019), performed a comparison study between the experiment and theoretical approach for obtaining the thermal properties of Al_2O_3-water mono and $Al_2 0_3 - Fe$ –water HNF. The thermo-physical properties measurements are carried out over five temperature ranges from 25°C to –65°C, at three varying nanoparticle concentrations of 0.05%, 0.1%, and 0.2%. They found that the HNF experiences the most significant reduction in specific heat than the mono nanofluid and water. The thermal conductivity in the HNF was significantly improved compared to mono and base fluid, especially when the volume concentration was increased. Furthermore, it was observed that thermal conductivity could further be more accurately predicted when considering the multivalent Nano layers in the thermal transportation of fluid. The size of the fluid also influences the thermal conductivity; hence this study should be repeated with different size nanoparticles. The smaller particles move faster and have a higher collision rate leading to a more remarkable improvement in thermal conductivity. They also compared many theoretical modules to the experiment. They did not find any previous studies to match their results, and the reason is that most previous studies use temperature and volume concentration to establish correlation. More study would be needed to correctly understand the heat transfer properties of the HNF, such as considering the interfacial interaction in the nanofluid.

(Ravikiran Balaga, 2019), investigated the temperature, concentration, and ratio of the two solid particles that make up the HNF. They considered nanoparticles Fe_2O_3 and f-MWCNT and water as base-fluid, with a concentration of 0.01vol% to 0.03vol% at different ratios and temperatures (30°C to 60°C). The thermal conductivity was dependent on the temperature and total weight fraction. As the incremental concentration increases, the thermal conductivity is said to increase, but for 2:3 ratios, the thermal conductivity is negatively affected if the ratio increases. They showed that HNF needs to be used correctly or the heat transfer enhancement negatively impacted.

(Neeshoun Asokan, 2020), investigated flow and thermal properties behaviour such as density, specific heat, viscosity and thermal conductivity of low concentration HNF. The HNF used is $Al_2O_3{-}CuO_3$ and compared to just $Al_2O_3$and Cu0 nanoparticles are all based on a 60:40 ratio of DI water and ethylene glycol solution. The concentration range considered for this investigation was 0.02-0.06%. The experiment concluded that the fluid and thermal properties are significantly enhanced even at this low concentration. An increase of 2.3% and 3.6% was seen in the thermal conductivity of HNF when compared to CuO and Al_2O_3 NFs respectively. They also studied the flow properties by running the fluid in a heat exchanger (rig radiator). It seemed to enhance the Nu number and OHTC by 6.7 % and 7.2 %, respectively, compared with CuO and 17.9% and 12.1% when compared with Al_2O_3. This experiment confirmed that the HNF has a better performance than monotype NFs, even at a low concentration.

(Farid Soltani, 2020), experimentally studied the measurement of thermal conductivity of WO_3-MWCNT/ engine oil HNF. A correlation was derived as shown in Equations (2.16) for the HNFs thermal conductivity in two parameters; temperature and vol% concentration of HNF. The fluid was prepared using the two-step method. The correlation was found by entering the data in the Sigma plot software to obtain an Equation (2.16).

$$\frac{k_{eff}}{k_{bf}} = \frac{0.9714+(1.3974\varphi^{0.3681})(0.00771^{0.7787})}{\exp\left((-310.0683\varphi^{2})\left(T^{-1.9772}\right)\right)} \tag{2.16}$$

The results showed that an increase in volume concentration raises the thermal conductivity of HNF; however, agglomerations or deposits occur at very high concentrations. At constant attention, increased temperature led to better thermal conductivity, but the HNF concentration has a more significant impact on thermal conductivity than the temperature change. However, this experiment was only carried out from 20- 60°C and volume concentration up to 0.2%.

Thermal conductivity was investigated for HNFs made of Al_2O_3 –SiO_2/ pure water-based fluid, (Georgiana Madalina Moldoveanu, 2018). They investigated the effect of various concentrations and temperatures. The concentration regraded ranged from 1-3%, and temperature ranged between 20-50°C. The volume fraction of SiO_2 nanoparticles placed in the HNF directly affected the thermal conductivity of HNF. A thermal conductivity enhancement correlation for alumina and silica NFs based on volume fraction variation is proposed as Equation (2.17);

$$k_{eff}=0.607-0.005\varphi_1+0.009\varphi_1^2+0.109\varphi_2-0.059\varphi_2^2+0.013\varphi_2^3 \quad (2.17)$$

A proposed correlation for estimating the thermal conductivity of alumina-silica HNF is based on varying volume fractions, and temperature is shown below in Equation (2.18). φ_{tot} is the total volume fraction.

$$k_{eff}=0.474+0.006T-0.00005T^2+0.041\varphi_{tot} \quad (2.18)$$

(Wajiha Tasnim Urmia, 2020) experimentally studied the thermo-physical properties of TiO_2-Al_2O_3(60:40) / water ethylene glycol HNF. The thermal conductivity is studied at varying concentrations 0.02-0.1vol% and temperature range between 30-80°C. The Newtonian behaviour of HNF was analysed by performing a rheological test. The HNF viscosity is increased as the particle concentration in the fluid is increased, while the viscosity value decreases with increasing temperature. With the fluid vol% concentration constant, the viscosity variations are greater at lower than higher temperatures. The thermal conductivity increases in both instances with the rise in volume concentration and temperature. The results indicated that the temperature effect is more remarkable for higher concentration fluid than low concentration fluids. The thermal conductivity of HNF is higher than its counterpart mono NFs. The HNFs viscosity is not significantly better than mono NFs, and it falls between TiO_2 and Al_2O_3 mono NF viscosity Correlations for the viscosity and thermal conductivity of HNF was established experimentally, and both viscosity and thermal conductivity models. Both thermal conductivity and viscosity correlation showed good accuracy for the range of concentrations and temperatures studied. The correlation between experimental viscosity and thermal conductivity is shown in Equations (2.19) and (2.20).

$$\mu_{hnf}=7.1074+3.65\varphi-0.14097T+0.05176\varphi T+0.0907\varphi^2+0.00092T^2 \quad (2.19)$$

$$k_{hnf}=0.386\ \exp(2.27\varphi+0.02939T) \quad (2.20)$$

(Munish Guptaa, 2020), presented an experimental study of heat transfer properties of aqueous zinc Ferrite/water $ZnFe_2O_4$/water HNF. The HNF was prepared at a different concentration ranging from 0-0.5% volume. They created a laminar flow in a circular tube experiment, and in particular, the viscosity, convective HTC and thermal conductivity were examined. The observed thermal conductivity and HTC enhancement increased as the volume concentration increased. The maximum thermal conductivity enhancement of 11.8 % and 42.99% in HTC was achieved using the highest volume concentration NF. Although the increase in volume concentration enhances the thermal properties, they noticed that pressure drop also increased significantly; it is crucial to find the balance between volume concentration and pressure drop to minimize cost for application purposes. Based on the experimental data, the following correlations were proposed for water $ZnFe_2O_4$/water HNFs, as shown below in Equations (2.21 and 2.22).

$$\mu_{eff}=0.39077*(T)^{-0.79359}*(\psi)^{0.0369} \quad (2.21)$$

$$k_{eff}=0.39077*(T)^{0.14566}*(\psi)^{0.02175} \quad (2.22)$$

(Gabriela Huminic, 2020), used iron-based silicon nanophases to improve the thermal conductivity of the base solution. In the experiment, the volume concentration ranged between 0.25-1vol%, and temperatures ranged between 20-50°C. An experimental based correlation was presented for thermal conductivity at varying concentrations and temperatures. The conclusion was that as the mass concentration of particles and the overall temperature of the fluid is increased, the thermal conductivity is seen to increase. The 1.0% fluid showed the maximum enhancement in thermal conductivity. The thermal conductivity Equation was correlated for varying particle volume concentrations and temperatures and is shown in Equations (2.23) below. The deviation, R^2 =0.9386.

$$k_{eff}=-0.1989+0.002661T+7.243\varphi \quad (2.23)$$

(KeNan Liu, 2021), experimentally studied the efficacy of loading MWCNT−TiO_2 into SAE 20 W −40 HNF on its thermal conductivity. They used a two-step preparation method for the manufacturing of HNF and used the concentration of NF between 0.1 to 0.8 vol% for the experiment. In all the experiments performed using the different concentrations, the addition of

the HNFs positively affected thermal conductivity compared to mono NFs only. They also found that the temperature of SAE 20W −40 significantly affects the thermal conductivity of NF. Higher temperature resulted in higher enhancement, implying that high-temperature applications can benefit more from the HNF.

(Yanfang Zhu, 2021), used MWCNT-WO_3/water –ethylene (80:20) HNF to evaluate the effect of temperature and volume fraction on dynamic viscosity. The volume fraction and temperature ranges are 0.1-0.6vol% and 25 -50°C, respectively. The results show that as volume concentration is increased with constant temperature, the dynamic viscosity increases. As the temperature is increased with continual volume concentration, the active viscosity decreases. The increase in dynamic viscosity with a change in volume concentration is due to particle aggregation and settling. A mathematical relationship Equation (2.24) is proposed as a temperature and volume concentration function based on the experiment.

$$\frac{\mu_{eff}}{\mu_{bf}} = \frac{0.1708+(-0.0131\varphi T)+(0.0003\varphi)^{0.1443}}{\mathrm{Exp}((-1.5776\varphi^2)+\left(-0.6442T^{0.1443}\right)+\left(-0.1882\left(\frac{T}{\varphi}\right)^{0.1443}\right))} \tag{2.24}$$

(S.O Giwa, 2020), investigated the thermo-convection performance of HNFs by using Al_2O_3 - MWCNT/water in a differentially heated square cavity. The published article is essential for comparison with the value calculated in the experiment for thermal properties as it deals with the same HNFs used for investigation in this research. The nanoparticles with different weight ratios (80:20, 60:40, 40:60 and 20:80) of 0.1% volume concentration were investigated at varying temperature gradients (20 -50°C). The HTC and heat transfer rate and two non-dimensional constants, Nu and Rayleigh numbers, were considered for investigation. Once they found the fluid to be stable, they measured the viscosity and thermal conductivity of the stable fluid. A relationship between the Rayleigh number and the average Nu number is observed between 1.65×108−3.8 ×108, Rayleigh numbers. The 60:40 ratio HNFs were the best-performing fluid at various temperature gradients in terms of its Rayleigh, average Nu number, and HTC rate. Maximum enhancements of 16.2%, 20.5%, and 19.4% were seen for the average Nu number, average HTC, and heat transfer rate, respectively, at T = 50°C, about the base fluid. The use of Al_2O_3−MWCNT/water HNFs in a square cavity has improved natural convection performance

compared to water only. A correlation for viscosity is found as Equation (2.25) using experimental correlation.

$$\mu_{eff}=1.41467+5.197\times10^{-3}R-1.37\times10^{-2}T(R^2=97.81\%) \quad (2.25)$$

(Dan Huang, 2016), experimentally investigated the HNFs heat transfer and pressure drop characteristics in a plate heat exchanger. The HNF was made of Alumina/ MWCNT (1:2.5) nanoparticles and water base solution with a constant volume fraction of 1.89%. The HTC is increased by using HNF compared to base fluid with constant velocity in the heat exchanger. It is caused by an increase in the overall thermal conductivity in the fluid when considering HNF. The HNF mixture exhibited the highest HTC at pumping power. Besides, the pressure drop of the HNF mixture is only slightly higher than that of water. Therefore, HNF combinations can be promising in many heat transfer applications.

(Essam M. Elsaid, 2021), investigated the mixed convection properties of (H_20-Cu/Al_2O_3) HNF through a vertical channel. The channel sides are subjected to thermal radiative flux and variable temperatures. The Nu number is analysed under various changing parameters. The addition of hybrid nano-particles reduces the velocity at the channel's centreline. When adding Hybrid nanoparticles to the system, the system is changed from thermal conduction to thermal convection heat transfer. The Nu number is decreased when increasing particle concentration of HNF in the absence of thermal radiation flux. Using dual types of nanoparticles raised these reductions. This relation reverses the thermal radiation presence.

The fact that solids usually have a high thermal conductivity compared to fluids makes nano-sized solid particles dispersed in liquid a very effective way of increasing the conductivity of the fluid. Almost all experiments conducted in the literature study concluded that the addition of hybrid nanoparticles positively impacted heat transfer more than its counterpart mono nanofluids. Therefore, the relation proposed for effective thermal conductivity by (Georgiana Madalina Moldoveanu, 2018), (Munish Guptaa, 2020) and (Gabriela Huminic, 2020), is used for comparing to the experimental correlation obtained for thermal conductivity.

It was found that the HNF experiences the most significant reduction in specific heat than the mono nanofluid and water (Eric C. Okonkwo, 2019). The density increases as particle concentration increases due to a much denser material being added to less dense material. The equations (S.O.

Giwa, 2019) and (Tahar Tayebi, 2016) for density and specific heat are used for experimental and CFD study calculations. The material, concentration, size/shape, type of particle, and additives used have a significant effect on the heat transfer property of the nanofluid, which many researchers studied. The viscosity nanofluids increase exponentially with particle volume concentrations (L. Syam Sundara, 2020). Using equations found by (Wajiha Tasnim Urmia, 2020) and (S.O Giwa, 2020), the viscosity equation correlated in the experiment was checked for its deviation. Similarly, using equations found by (Georgiana Madalina Moldoveanu, 2018), (Munish Guptaa, 2020) and (Gabriela Huminic, 2020), the thermal conductivity equation used for the work was checked for its deviation.

2.6 Conclusion

The fact that solids usually have a high thermal conductivity compared to fluids makes nano-sized solid particles dispersed in liquid a very effective way of increasing the conductivity of the fluid. Almost all experiments conducted in the literature study concluded that the addition of hybrid nanoparticles positively impacted heat transfer more than its counterpart mono nanofluids.

In the Jet cooling literature study, it was found that metals with high thermal conductivity have more prominent cooling regions than other materials, and the regions increase in size with the decrease in speed (Kulkarni G.A, 2018). Generally, metals with high conductivity are suitable for industrial applications, but one should consider the stress that the maximum temperature during quenching causes on the metal. For a non-uniform temperature, there is a decrease in convective heat transfer, which becomes higher with an increase in jet distance (Bin Sun, 2019).

The nanoparticles form nuclei on the surface, increasing the wettability and improving the cooling performance. Optimal heat flux was also found at specific low concentrations and decreased due to the coating of nanoparticles on the plate. The cooling rate was enhanced significantly (O. Zeitoun, 2013), but it was shown to decrease slightly at high concentrations—the HTC increases with reduced surface temperature.

Most of the studies done in high Re number all show a positive outcome in heat transfer improvement in the jet cooling process. All past studies concluded that the average and local Nu number increases as particle concentration increases, indicating convective heat transfer improvement. (Oronzio Manca, 2011), concluded that the power required to carry the nanofluid to

reach the same Re number is more significant than its base fluid, which increased as the particle concentration increased. All studies reveal that the highest heat transfer occurs at the centre of the stagnation point and is the lowest at its surface edges.

The SST κ-ω turbulence model and the Eulerian-Eulerian multiphase model is more suitable to impinge nanofluids' jet cooling. Not much research was done on the shape or state of the surface. The SST k–ω turbulence model form part of the Reynolds-Averaged Navier Stokes (RANS) models; this approach solves ensemble-averaged (or time average) Navier stoke equations. The RANS models are the most widely used approach in the industry, and all turbulent lengths scales are modelled in RANS. The other two, namely Large Eddy Simulation (LES) and Direct Numerical Simulations (DNS), are not appropriate for turbulence flow modelling (Wang Peng, 2014). The SST k–ω turbulence model is one of the better approaches than the other RANS model, although the cost is significantly higher per iteration than different standard and realizable RANS models. The k–ω family of turbulence models is most widely used because all terms are defined in an equation at the wall, and they can be integrated into the wall without using wall functions.

3 Objective and methodology:

Based on the existing gaps in the literature, the following objectives have been defined.

a. Formulate, Synthesize, and characterize hybrid nanofluids at different particle volume concentrations
b. Confirm the stability of the nanofluids differentiated as conventional and popular evaluation methods
c. Quantify the properties of the nanofluid required to evaluate the thermal performance of cooling the free surface by jet impingement
d. Evaluate the effect of flow rate, advection and surface tension on the heat transfer performance of jet impingement cooling under steady-state conditions
e. Perform the numerical investigation to study the heat transfer by modelling it using the Eulerian-Eulerian approach
f. Effectuate the study to understand the thermal performance of nanofluids under transient conditions

To accomplish these prime objectives, the following research methodology is developed and followed.

a. Synthesize the nanofluids by two-step method at different volume concentrations of 0.025, 0.05, 0.1 and 0.15%
b. Evaluate the stability of the nanofluid by visual inspection every week, by transient viscosity method for a few hours, and by zeta potential measurement
c. Characterize the particle distribution within the fluid through Transmission Electron Microscope (TEM)
d. Measure the hydrodynamic size of the particle by Dynamic Light Scattering (DLS) approach
e. Calibrate the property equipment such as Thermal conductivity meter, Viscometer and Surface Tensiometer using the standard liquids
f. Measure the nanofluid properties of all the volume concentrated nanofluid samples at different temperatures between 10 and 60°C

g. Validate the jet impingement experimental setup by running it with base fluid and comparing them with existing and published results
h. Perform the heat transfer experiment on different fluid samples under a single-phase turbulent flow regime at a transient state
i. Enact the thermal experiments on the nanofluid samples under a single-phase turbulent flow regime at a steady-state
j. Develop correlations for nanofluid properties and Nusselt numbers based on the design parameters and derived outcomes
k. Perform numerical investigation to study the thermal performance of jet impingement cooling under the above-said conditions

4 Experiment and Numerical Analysis

4.1 Introduction

This section reports an experimental and numerical aspect of the research work. HNF formation and testing jet impingement with HNF MWCNT-Al_2O_3(90:10)-DI water at varying particle vol% concentration (0.025,0.05,0.1,0.15%). Detailed stability analysis and the steps are taken to prepare MWCNT-Al_2O_3(90:10)-DI HNFs are presented. The thermal conductivity and viscosity measurements of the HNF are done by (SV-10 device -sine wave viscometer) and thermal meter (KD2 pro meter), respectively. The specific heat and density Equations are used from past literature. The data captured by the SCXI-1303 data logger (National Instruments, USA) is used to investigate the HTC, Nu Number, and the non-dimension cooling rate at jet-surface region and impingement surface only. The data is captured for temperature readings from the k-type thermal couples (placed axially on the testing specimen) and the T-type connected at the surface exit, volume flow readings from the ultrasonic flow meter. The calibrated setup is validated with other literature studies before commencing with MWCNT-Al_2O_3 DI water HNF testing. For steady-state analysis, a Nu number is represented as a function of vol% concentration nanoparticle in HNF, and varying Re numbers, the detailed analysis of the correlation method used is described and checked for its fitness. The transient cooling rate was investigated at the highest Re number, calculated using the highest flow rate number achieved in the steady-state analysis. Numerical studies by the Eulerian-Eulerian approach were also carried out by assuming that both gas and solid phases are at interpenetrating continua with the k-w SST model evaluating the changing velocity and turbulent viscosity.

4.2 Materials and Methods

The two nanoparticles used to form the HNF is γ-Al_2O_3 7 nm diameter and ~98% pure as indicated by the manufacturer; the nanoparticles are supplied by (USA - Houston, Texas, Nanostructured and Amorphous Materials Inc.) and MWCNT (inner 3-5 nm, and outer 10-20 nm and lengths of 10-30 μm), supplied by (MKnano Company, Ontario, Canada). The surfactant or dispersant used for the HNFs is Sodium Dodecyl Sulphate (SDS) with a purity of greater than 98.5% and was sourced from (Sigma-Aldrich Germany). Deionised water is used for the base solution of the MWCNT-AL_2O_3(90:10)-DI water HNFs.

The innovative part of this study is that hybrid nanofluids are incorporated as jet impingement coolants as there are no studies yet reported on such types of fluids. Thus the choice of nanoparticles was decided based on the nanopowders that have higher thermal conductivity for rapid and higher heat transfer capability. Moreover, the fluid flow should be associated with ease of handling, and thus density plays a role while spraying it through the nozzle. Hence MWCNT of very small size (5 nm) is chosen. However, these particles are hydrophobic in nature. Hence affiliating its external surfaces with a hydrophilic powder aided in the selection of Al_2O_3 nanopowders of size < 7 nm.

Surfactants containing aromatic groups, such as Triton X-100 and Sodium dodecylbenzene sulphonate, may be used to distribute and stabilise MWCNTs. However, aromatic groups tend to increase the viscosity of these fluids, which may seem to be ideal for stabilisation but has a detrimental effect on the fluid's thermo-convective behaviour. As a result, sodium dodecyl sulphate was chosen above other alternatives to act as a surfactant for this study. The volume fraction of the sample fluid is calculated using Equation (4.1) used by (S.O Giwa, 2020) in the study of thermo-physical properties of MWCNT/Al_2O_3-DI water.

$$\varphi = \frac{X_{Al_2O_3}\left(\frac{M}{\rho}\right)_{Al_2O_3} + X_{MWCNT}\left(\frac{M}{\rho}\right)_{MWCNT}}{X_{Al_2O_3}\left(\frac{M}{\rho}\right)_{Al_2O_3} + X_{MWCNT}\left(\frac{M}{\rho}\right)_{MWCNT} + \left(\frac{M}{\rho}\right)_{bf}} \quad (4.1)$$

A 0.15 vol% nanoparticle in base fluid DI water was formulated by a specific amount of nanoparticles and tubes dispersion into the base fluid for a start. In the next step, the powder Al_2O_3 nanoparticles and MWCNT nanotubes have been dispersed into water base fluid using a magnetic stirrer for 30 min with a magnetic agitator. The moving process is followed by a sonication procedure using an ultrasonic device. The idea behind using an ultrasonic processor is to attain an excellent distribution and eliminate the phenomenon of nanoparticle clustering and, thus, prevent sedimentation and make a stable suspension of HNFs (Samarshi Chakraborty, 2020). The ultra-sonication period is approximately 2 hours with amplitude ranging from 70 to 85, and the dispersion fraction of surfactant is between 0.5-1.2 to optimise the stability of the HNFs. The sonication factors (sonication period and amplitude) and the amounts of surfactants required to HNFs weight were adjusted at the room temperature for all particle vol%. After obtaining the

optimum sonicating adjustment (period and amplitude values) and amounts of surfactants required, the HNFs with particle vol% concentrations of (0.025, 0.05, 0.10, and 0.15%) were prepared.

4.3 Instrumentation facilities

Two steps were taken to homogenise the nanoparticles together into DI water properly. Firstly, a magnetic stirrer (hot plate stirrer) was used, followed by an ultra-sonication (Model Q-700; 700W and 20 kHz USA) mixer. The mixture's temperature was kept constant at 20°C using a thermal bath (LAUDA ECO RE1225). A Transmission Electron Microscope (JEOL JEM-2100F) was used to confirm the size and shape of Al_2O_3 and MWCNT nanoparticles and their morphology in the base fluid. To measure the HNF's viscosity at various temperatures and particle vol% concentration, a viscometer SV-10 device (sine wave viscometer with ±3% accuracy, A&D, Japan) is used. Jenway 3510 pH meter (± 0.003 accuracy and 2 to 19.999 range) was utilised to measure the pH value to validate the stability between the fluid and nanoparticles. All Weight-related measurement was done by a 10 mg – 220 g - Radwag AS 220.R2 (Poland)) digital scale. The following Table 2 lists all other instruments used in the experiment together with their specification:

Table 2 Specifications of devices and equipment's used for MWCNT/AlO_3(90:10)- DI water HNF thermo-physical property reading

Equipment	Manufacturer and specifications
Electrical conductivity meter	EUTECH-CON700 (± 1% accuracy)
pH meter	Jenway 3510 (± 0.003 accuracies and 2 to 19.999 range
Digitally weighing scale	Accuracy of ± 0.01 g and measurement variety of 10 mg – 220 g - Radwag AS 220.R2 (Poland))
Electron scanner	Crossbeam 540 Scanning Electron Microscopy (SEM), Transmission Electron Microscope (TEM) (JEOL JEM-2100F)
Thermal conductivity meter	KD2 Pro device (Decagon devices, US; ± 10%% accuracy for k = 0.2 – 2.0 W/m K)
Viscosity meter	SV-10 device (sine wave viscometer with ± 3% accuracy, A&D, Japan).

4.4 Quantifying the fluid stability

Morphology and dispersion of nanoparticles in the HNFs were observed via various analyses and techniques. The stability of the nanofluid was observed, evaluated and quantified by means of visual inspection to check for the sedimentation of nanoparticles at the basement of the storage containers. It was evaluated by visualising the size of the particles through a Transmission Electron Microscope. A conventional way of checking the overall consistency of the fluid was also done by measuring the viscosity over a certain period of time. However, the perfect way of quantifying the stability is through zeta potential measurements, and the same was also carried out.

4.5 Measurands and methods

4.5.1 Viscosity

The sine wave viscous meter SV-10 was used to measure the viscous behaviour of the base fluid between 10 – 60 °. During the evaluation, the temperature was controlled utilising a circulating water bath (LAUDA ECO RE1225) after adjustment with the base fluids. A contrast of the measured viscosity of the DI-water and (SAHEED A ADIO, 2015)viscosity values was shown to confirm the viscous behaviour after adjusting the SV-10 device. Relative viscosity and enhancement of the HNFs related to base fluids were estimated by Equations (4.2) and (4.3), respectively.

$$\mu_{rel} = \frac{\mu_{hnf}}{\mu_{bf}} \tag{4.2}$$

$$\mu_{enhance}(\%) = \left(\frac{\mu_{hnf} - \mu_{bf}}{\mu_{bf}}\right) \times 100 \tag{4.3}$$

Where μ_{hnf} and μ_{bf} are the viscosity of HNFs and the DI-water, respectively, the margin of deviancy (MOD) for both thermal conductivity and viscosity of the HNFs is stated in Equation (4.4).

$$\text{MOD} = \left(\frac{\text{Exp.} - \text{Pred.}}{\text{Exp.}}\right) \times 100\% \tag{4.4}$$

Where, Exp.. and Pred.. are experimental, and correlation predicted values of the specific property.

4.5.2 Thermal conductivity

Once the fluid was prepared, its thermal conductivity was tested using a KD2 pro thermal meter. The measurement was taken between 10 and 60°C. The prepared HNFs were kept at a constant temperature of 20°C by placing them in a thermal bath while testing for thermal conductivity by measuring the thermal conductivity of relative standard fluid glycerine provided by the manufacturer. The measurement was redone eight times, and the average value was considered for calculation data. The relative and enhanced thermal conductivity of the HNFs were calculated using Equations (4.5) and (4.6) concerning the base fluid.

$$k_{rel} = \frac{k_{hnf}}{k_{bf}} \tag{4.5}$$

$$k_{enhance}(\%) = \left(\frac{k_{hnf} - k_{bf}}{k_{bf}}\right) \times 100 \tag{4.6}$$

Where k_{rel}, k_{hnf}, k_{bf} and $k_{enhance}$ are the relative HNFs, based fluids, and the improvement of the thermal conductivity. The thermal conductivity margin of deviation (MOD) for the HNF is also calculated using Equation (4.4).

4.5.3 Surface Tension

Aiding with the use of a platinum du Nuoy ring probe, 0.1mN/m accurate GBX 3S tensiometer (France) was calibrated with milli-Q water by detecting its surface tension. A Lauda thermal bath was used to keep the fluid samples at a constant 25±0.1 °C. Details of the experimental methodologies are available elsewhere. It is made clear during all of these studies that the nanosuspensions reached equilibrium surface tension within a few seconds, after which the measurements were taken. The samples' constant surface tension values over a minimum of 30 minutes confirmed this. Repeated measurements with fresh samples were used to verify the repeatability of the experimental results.

4.6 Experimental test facility

For the fluid delivery system, the two reservoirs were manufactured using polypropylene plastic, and the reservoirs were used for storing the fluid. One was created to store the fluid before we cooled down the fluid through the heat exchanger; one was created to keep the cold fluid after it had passed through the heat exchanger and it is well insulated to get a constant temperature of fluid

before being released by jet. The heat exchange was manufactured using a helical copper (ASTMB280) tube of 6.35 mm inner diameter and 0.61 mm thickness. A total of 15.24m length of tubes was used to reduce the temperature of the HNF to the desired 10°C. For the fluid delivery system to achieve high jet speed, a centrifugal pump BADU 45/16 (supplied by the Speck pump) was used. A small Orifice jet nozzle of diameter 1.65mm was used for fluid release, and Lechler supplied the jet nozzle. The flow rate of the fluid delivery system is calculated using a Burkert ultrasonic flow meter (Type 8081) with 2% and 0.01% measured and full-range accuracy, respectively. The flow meter was compared to volumetric reading and configured with the pump setting. Six cartridge type heaters achieved the heating of the copper surface with 220V and 100 W power rating manufactured by (Marathon heater INC, USA). A solid-state relay controls the heating element's electric power. A type 2053-amp meter (Yokohama, Japan) and type 2052-volt meter is used for reading the voltage, and current supplied to the heating elements. The test surface is created using a round copper bar, is tapered down to 42mm from 62.45 mm at the top and has a total length of 100mm. Holes of diameter 10mm are drilled on the copper bar to press-fit the heating onto the copper bar in a polygon shape layout, as shown in Figure 3.

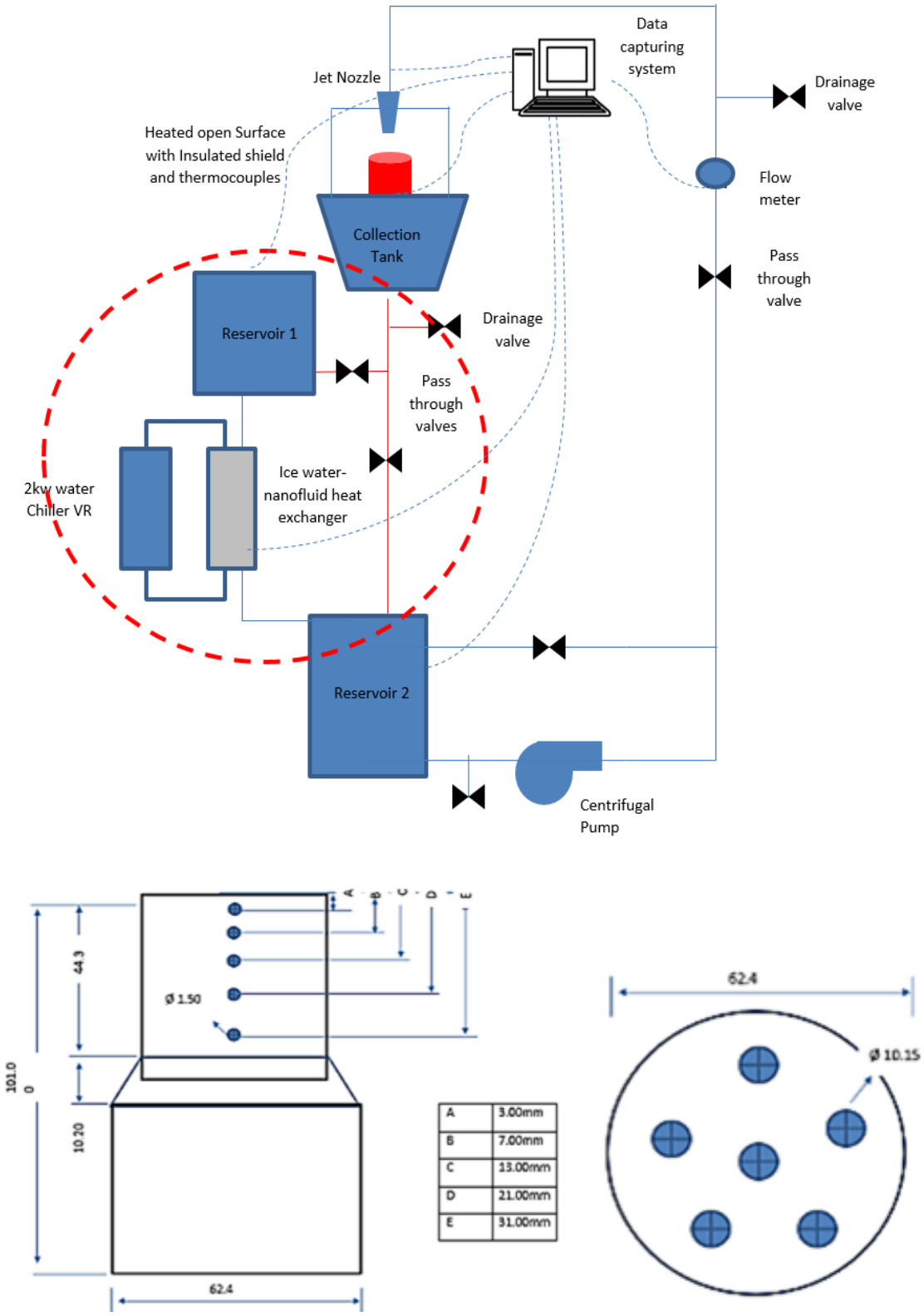

Figure 3 Jet cooling experimental setup layout used for testing of MWCNT/Al_2O_3 (90:10)-water HNFs

The tapered top section of the copper bar is drilled with 1.5mm diameter holes at a depth of 15mm in different axial points to insert thermocouples. The thermocouples are placed in sequential locations to the target surface to get a temperature difference curve. The thermocouple holes were filled with silicone heat-transfer thermal paste to prevent any air gaps from tampering with the temperature readings. The thermal paste was supplied (Unick Chemical Corp.) and is rated to have 0.026W/mK thermal conductivity. There are eleven thermocouples used for critical data in the experiment; five on the copper bar and five for the exit temperature of the fluids, and one for inlet jet temperature. The RS Pro K-type thermocouple of 1.5mm diameter is used, RS Components supplied the thermocouples. For the exit temperature, Type-T thermocouples were used and placed equidistant from one another around the exit point of the circular copper surface. These thermocouples have an accuracy of 0.12°C. Additional thermocouples were also used to monitor the HNF temperature of fluid before heat exchanger and after; however, these were not calibrated due to their values not being used directly in calculations. Polytetrafluoroethylene (PTFE) cases were manufactured to cover the copper bar from the sides and bottom to reduce thermal losses. The SCXI-1303 data logger (National Instruments, USA) was used to capture all current and thermal reading outputs from the ultrasonic flow meter and thermocouples, respectively. We connected the data logger with 32-channels input to a computer. The data was sampled through the Labview program and predetermined frequency. All investigated calculation operations were done on Microsoft Excel except for uncertainty calculations, which was performed using MATLAB. The initial data captured from the SCXI-1303 data logger were adjusted depending on the calibration before using it in experimental calculations. Table 3 lists all specifications of the parts or equipment used in the experiment.

Table 3 Experiment pieces of equipment and components specification

Component	Specification
Reservoir Tank	Max capacity : 10lt
Pump	Type: Centrifugal Specs : BADU 45/16 Spa pump Manufacturer: Speck Pumps
Flowmeter	Type: 8081 Manufacturer: Bürkertuere
Nozzle	Type: Orfice jet nozzle Specs: 1.65 mm diameter Nozzle Manufacturer: Lechler
Thermocouples	Type: k-type thermal couple Specs: 1.5mm Manufacturer: RS Components
Testing section	Material: Copper Surface type: Open circular surface
Heating elements	220V, 100W Manufacturer: Marathon Heaters INC
DATA capturing system	SCXI-1303 data logger (National Instruments, USA) 32 channels

4.7 Experimental Procedure

In this experiment, we aim to perform a cooling analysis of the copper cylinder described above in the experiment setup. The investigation will be carried out at both steady-state and transient states for water and varying volume fraction of MWCNT-AL_2O_3(90:10) –DI water HNF (0.025, 0.05, 0.1, 0.15 vol%).

4.7.1 Steady-state analysis

(1) Firstly, hot reservoir 1 is filled with fluid using deionized water.

(2) The hot or normal temperature fluid is then pumped through the heat exchanger to cool the fluid to the desired temperature of 10°C.

(3) The heating elements are turned on by adjusting the steady-state relay power input knob.

(4) Thermocouples are placed on the target surface, the temperature is observed, and the power input to the specimen is kept at a specific rate of 145 W once the desired temperature is reached.

(5) Once the fluid and surface temperature of 10°C and 50°C, respectively, is achieved, the next step is to create a flow of fluid; this is done by turning the power dial on the centrifugal pump. The flow meter connected to the Lab view is used to observe the flow rate of the fluid. The flow rate should be adjusted to investigate Re numbers of 6 000- 16500 approximately.

(6) As the pump is turned on, the cooling data is recorded for 4 minutes, and an average result is found. Note that one should use the final minutes of the reading to find the average.

(7) Upon completion of one nanofluid type, the fluid is allowed back in the hot reservoir 1 and sits there until the next experiment. The thermocouple placed in the two reservoirs can be used to check the temperature fluid at the reservoirs.

(8) Repeat the same test at least three times to get an accurate result.

(9) Repeat the entire process for different concentrations of MWCNT-Al_2O_3(90:10) -DI water HNFs.

4.7.2 Transient analysis

(1) Firstly, the reservoir is filled with fluid using deionized water.

(2) The hot or normal temperature fluid is then pumped through the heat exchanger to cool the fluid to the desired temperature of 10°C.

(3) The heating elements are turned on by adjusting the steady-state relay power input knob.

(4) Thermocouples are placed on the target surface, the temperature is observed, and the power input to the specimen is switched off once the desired temperature of 105°C is

reached. The temperature should be higher than steady-state to allow for a more significant drop in temperature with time.

(5) Once the fluid and surface temperature are achieved, the next step is to create a flow of fluid. It is done by turning the power dial on the centrifugal pump. It should be done in conjunction with switching the power input off. The flow meter connected to the Lab view is used to observe the flow rate of the fluid. The flow rate should be adjusted to the max to achieve the high Re number.

(6) Soon as the pump is turned on, the cooling data is recorded for a duration till the temperature has dropped by a specific temperature or when the temperature change is very little compared to the initial drop.

(7) Upon completion of one fluid type, the fluid is allowed back in the hot reservoir 1 and sits there until the next experiment. The thermocouple placed in the two reservoirs can be used to check the temperature fluid at the reservoirs.

(8) Repeat the same test at least three times to get an accurate result.

(9) Repeat the entire process for different concentrations of MWCNT-Al_2O_3(90:10) -DI water HNFs.

It is essential to dispose and drain the fluid being worked for the setup to not effects its measurement during the following experiment being performed on it. Once steady and transient state experiments were performed for a specific volume concentration of HNFs, the setup was cleaned and rinsed so that any remaining deposit would not affect the subsequent investigation. The fluid was drained using a drainage valve connected to the design, as shown in Figure 3. Once all the nanofluid is exhausted, the system is run with water until no deposits or contaminations remain. The checking was done by visually evaluating the drained water transparency. In addition, the copper surface was also eliminated of all impurities, which could hinder the following experimental results.

4.8 Data reduction and Uncertainty

All properties were calculated using the bulk fluid temperature using Equation (4.7)

$$T_b = \frac{T_j + T_e}{2} \tag{4.7}$$

Where T_j is the exit temperature of the jet fluid and T_e is the exit temperature of fluid just after it has left the target surface. Reynolds Number is calculated using Equation (4.8):

$$Re=\frac{\rho v_j D_j}{\mu} \tag{4.8}$$

Where ρ is the density at bulk temperature, v_j is the jet exit velocity, D_j is the jet diameter and μ is the viscosity at bulk fluid temperature. For fully developed turbulent flow Re>3000, Nu Number is calculated using Equation (4.9) shown below:

$$Nu=\frac{hD_j}{k} \tag{4.9}$$

Where h the HTC of the surface and k represent the fluid thermal conductivity at bulk mean temperature. The HTC of the surface can be calculated using Equation (4.10) shown below:

$$h=\frac{\dot{q}}{T_s-T_j} \tag{4.10}$$

Where $\dot{q}$ is the heat transfer rate from the target surface using method two below, T_s represents the temperature of the surface and T_j is the jet temperature. Three Different methods can be used to calculate the heat transfer in the copper surface, as discussed below.

Method 1: Using the fluid properties

$$\dot{q}=\frac{\dot{m}C_p(T_j-T_e)}{A_s} \tag{4.11}$$

In the Equation (4.11) above $\dot{m}$ is the mass flow rate of the HNF fluid, C_p is the specific heat of HNF at bulk mean temperature and A_s is the target surface area.

Method 2: Using the electric readings of the heated copper bar

$$\dot{q}=\frac{\dot{Q}_{electric}}{A_s} \tag{4.12}$$

$$\dot{Q}_{electric}=VI \tag{4.13}$$

In the power Equation (4.13) above, V and I are voltage and ampere meter readings, respectively.

Method 3: Fourier law using material conductivity

$$\dot{q}=-k_s \frac{\Delta T}{\Delta x} \tag{4.14}$$

In general, the Fourier law as in Equation (4.14) is considered to solve the conduction in the heated surface, based on which by using the thermocouple placement in the copper bar, we can get the heat transfer rate of the whole bar.

$$\dot{q}_{bar}=\frac{\sum_{i=1}^{n}(\Delta x \cdot \dot{q})_{i,i+1}}{\sum_{i=1}^{n}\Delta x_{i,i+1}} \tag{4.15}$$

In the above Equation (4.15) k_s is the thermal conductivity of the target surface material. ΔT is the temperature difference between the target surface and thermocouple reading, Δx is the distance from target surface and thermocouple, and n is the number of thermo-couples. The surface temperature used in the Equation of HTC is calculated using the Fourier law Equation shown in Equation (4.16) below.

$$T_{s,\,i}=T_{TC,\,i}-\frac{\dot{q}_{bar}\Delta x_{s,\,i}}{k_c} \tag{4.16}$$

Where T_{TC} is the thermocouple temperature and k_c is the thermal conductivity of the copper bar. With respect to evaluating the problem at the impingement surface rather than from the jet inlet, the following Equation (4.17) of the adjusted impingement Re number and Equation (4.18) of Nu number at impingement is calculated. Further analysis is done with respect to Weber number for deformity and stability forces in the HNF and Péclet number for the advection and diffusion between the different modes of fluid. The Re number at impinge surface can be calculated using Equation (4.17) below.

$$Re_{ip}=\frac{\rho V_{ip} D_{ip}}{\mu} \tag{4.17}$$

The impinging diameter is calculated considering the jet and impingement velocity, which is calculated considering the gravitational acceleration over the total jet to the surface area.

$$D_{ip}=D_j\left(\frac{V_j}{V_{ip}}\right)^{0.5};\ V_{ip}=\sqrt{V_j^2+2gH}$$

The Nusselt number correlation for imping surface becomes as Equation (4.18);

$$Nu_{ip}=\frac{hD_{surf}}{k} \tag{4.18}$$

Weber number at the impingement surface can be calculated using the following Equation (4.19) to evaluate the stability and deformability of the fluid at the surface.

$$We_{ip}=\frac{\rho D_{ip} V_{ip}^2}{\sigma} \tag{4.19}$$

To study the interactions between different modes of fluid, the Péclet number was evaluated at the impingement surface using the following Equation (4.20);

$$Pe_{ip}=Re_{ip}*Pr \tag{4.20}$$

In the trainset cooling study, a cooling curve of the surface temperature against time was analysed. A non-dimensional Equation (4.21) was formed to remove any effect of jet-exit fluid temperature.

$$\theta=\frac{T_s-T_j}{T_j} \tag{4.21}$$

Energy balance:

$$EB\%=\left|\frac{\dot{Q}_{elec}-\dot{Q}_{Cu}}{\dot{Q}_{elec}}\right|\times 100 \tag{4.22}$$

$$EB\%=\left|\frac{\dot{Q}_{Cu}-\dot{Q}_{fluid}}{\dot{Q}_{Cu}}\right|\times 100 \tag{4.23}$$

Equations (4.13) and (4.15) discussed above were used to get the copper surface and jet fluid's heat transfer rate and the cartridge heater electric power. The fluid heat transfer is calculated using Equations (4.11). The average energy balance in the electric and the copper surface was estimated to be 39.5% and is calculated using Equation (4.22). The average energy balance between the copper surface and fluid is 11.98% and is calculated using Equation (4.23) above.

A simple mass flow study is done using the flow curve of the varying particle vol% at the constant power input to the centrifugal pump. The flow rate was captured at continual power supply by keeping the centrifugal pump voltage at continuous 161 V and current at a steady 1.76 Amp. The relative flow rate loss percentage to DI -water was calculated using the following equation (4.24):

$$\dot{V}_{loss\%}=\frac{\dot{V}_{hnf}}{\dot{V}_{DI\text{-}water}}\times 100 \quad (4.24)$$

Numerous measuring instruments, tables, and Equations (including its parameters) are used for the calculation of results. In this section, all uncertainty relating to the Instruments, Equations, and thermal properties used for MWCNT/ Al_2 O_3 (90:10)-DI water HNFs investigation is evaluated. The uncertainty was divided into two sections on for the measuring instruments uncertainly and other for thermal property uncertainty of MWCNT/Al_2O_3(90:10)-DI water HNF. For a single observation, the following Equation by (Everts, 2014) and (Dunn, 2014) was used to calculate the uncertainty.

$$\delta x_i=\sqrt{b_i^2+p_i^2} \quad (4.25)$$

Where the single observation is represented by x_i and δx_i represents the standard deviation of time variables. Using the root square method, this in case of a multiple observation(R) becomes:

$$\delta R=\sqrt{\left(\frac{\partial R}{\partial x_1}\right)^2\delta x_1+\left(\frac{\partial R}{\partial x_2}\right)^2\delta x_2+\left(\frac{\partial R}{\partial x_3}\right)^2\delta x_3+\ldots+\left(\frac{\partial R}{\partial x_n}\right)^2\delta x_n} \quad (4.26)$$

Where $R=R(x_1,x_2,x_3,\ldots,x_n)$. According to (Dunn 2014), regression analysis is utilized to define the relation of two or more variables. They try to test the effects of more than one independent variable on a dependent variable despite multiple forms of regression analysis. The Linear Regression analysis is carried out when one- variable is known. The known variable is known as the independent variable, and the gained variables are known as the dependent variable. Due to that, uncertainty arose. After completing the calibration process, A linear regression analysis method was utilized to determine the uncertainty of various thermocouples.

4.9 Numerical Analysis

Besides experimental investigation, a numerical simulation has been performed to gain more understanding of the HNF. In the numerical simulation, the researcher can extract data from every point of the setup they cannot access in the experiment. To accurately estimate the results, all governing Equations must be solved correctly. To reduce numerical simulation error compared to experimental, they must consider some keys. Some assumptions have been applied to the model in this section of the study.

1. 2-Dimensional computational domain
2. There is no heat loss from
3. Eulerian Two-phase model for interaction between air and water
4. HNF is single-phase
5. Time is transient for some cases to see impingement of the jet

Each of the above assumptions is a source of an error.

4.9.1 Geometrical model

The jet impingement setup from the experimental section is analysed as a two-dimensional model for the CFD analysis. The geometry is used to evaluate the thermal and fluid dynamic performance of the HNF on a jet-surface setup. The two-dimensional model has a length (wall diameter) equal to 42 mm while the height (distance of inlet to the wall) is 6.6mm, and the jet orifice width (inlet diameter) is 1.65 mm. For validation, a constant heat flux value of 145W is applied on the impingement bottom surface; this value was used in the experiment, and it is assumed that no heat loss occurs on the insulation walls. Then for transient simulation, an initial temperature equal to 373 K was applied on this surface. The working fluid is water or a mixture of water and nanoparticles, at different volume fractions equal to 0.025, 0.05, 0.1, and 0.15vol%.

4.9.2 Material properties

The HNF is used as jet heat transfer fluid (HTF), solid is used for the copper surface, and air for initial air space. The fluid properties are used according to the HNFs properties found by either experiment or literature. The values are edited fluently accordingly. The wall material was considered to be copper with a density of 8978 g/m^3 Specific heat of 381 j/kgK and thermal conductivity of 387.6 w/m.K. HNFs can be considered as Newtonian fluids for low volume fractions.

4.9.3 Governing Equations

There are air and liquid interactions in the computational domain of jet surface. The multiphase Eulerian model has a solid approach for mathematically tracking the shared accessible interface between two phases with the assumption of no interference in each other medium. This approach is known to produce the best estimates compared to other models (Wang Peng, 2014). According to this approach, only momentum and energy Equations are solved. In this numerical modelling,

the flow is thought incompressible. It is because there is no mass exchange between phases. Based on the reality of the continuity Equation, it is applied to both phases, and the Equation must be satisfied. Since the Re number is in the turbulent flow region, a turbulence model is required for calculation. We chose the k-w SST model to estimate the fluctuating velocity and turbulent viscosity that other researchers have successfully used. This study employs the Eulerian-Eulerian approach to model jet impingement. As mentioned before, in this approach, it is assumed that both gas and solid phases are interpenetrating continua. The Navier-Stokes equations are used to represent the gas-liquid interactions. The continuity equations can be written for the gas and particle phases as follows:

$$\frac{\partial}{\partial t}\left(\varepsilon_g \rho_g\right)+\nabla.\left(\varepsilon_g \rho_g \vec{v}\right)=0 \tag{4.27}$$

$$\frac{\partial}{\partial t}\left(\varepsilon_l \rho_l\right)+\nabla.\left(\varepsilon_l \rho_l \vec{v}\right)=0 \tag{4.28}$$

and momentum Equations for both phases are:

$$\frac{\partial}{\partial t}\left(\varepsilon_g \rho_g \vec{v}_g\right)+\nabla.\left(\varepsilon_g \rho_g \vec{v}_g \vec{v}_g\right)=-\varepsilon_g \nabla P_g+\nabla.\tau_g+F_{gl} \tag{4.29}$$

$$\frac{\partial}{\partial t}\left(\varepsilon_l \rho_l \vec{v}_l\right)+\nabla.\left(\varepsilon_l \rho_l \vec{v}_l \vec{v}_l\right)=-\varepsilon_l \nabla P_l+\nabla.\tau_l-F_{gl} \tag{4.30}$$

Where ε, ρ, and $\vec{v}_l$ is the volume fraction, density, and velocity, respectively. *P* is the pressure, τ denotes stress tensor, and F_{gl} represents the exchange of momentum between phases. As mentioned in Equations (4.29) and (4.30), F_{gl} represents the exchange of the momentum between phases and can be calculated as $F_{gl}=\beta_{gl}\,(v_g-v_l)$. The parameter of β_{gl} is known as a drag function which is assumed that be 1.

4.9.4 Boundary Conditions:

The boundary conditions used for the modelling of the jet cooling are as follows: At first, the volume fraction of water inside the domain is zero. It means the environment is full of air. Velocity for liquid at the nozzle boundary has been set based on the Re number. An interface between the solid and fluid domain converts conduction heat transfer from the solid body to convection heat

transfer to the jet fluid. Finally, a pressure outlet boundary condition is set for the outlet. Figure 4 shows the location of boundary conditions.

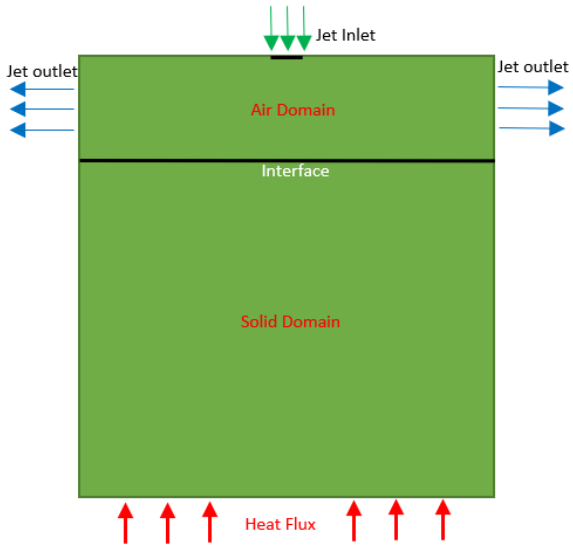

Figure 4 Geometry and BC location of the CFD domain

Table 4 shows the initial and boundary condition of the problem. According to this table, at the initial time, the volume fraction of the liquid phase in the domain is equal to 0. It means the liquid phase will come in the field from the nozzle. About the heat flux is apparent that there is no heat in the solid domain at the initial time. As time goes by, the heat flux will penetrate the solid part, and the jet will extract it from the interface. The heat flux is approximated to be 145W, similar to the heater setting in the experiment conducted, assuming no heat loss occurs through the sidewalls of the sample.

Table 4 Initial Conditions & Boundary Conditions

Gas-Phase (g)	Liquid Phase (l)	Solid Domain
$\varepsilon_g=1$ at domain (t=0 s)	$\varepsilon_l=1$ at the inlet	Q = (W) at bottom (Fig. 26)
$v_{g,x}=0, v_{g,y}=0, v_{g,z}=0$	$v_{l,x}=0, v_{l,y}=v, v_{l,z}=0$	$\frac{\partial q}{\partial n}=0$ for the rest of the walls

4.9.5 Geometry, Mesh Independence, and validation:

Computational Fluid Dynamics (CFD) is a way to solve partial differential equations numerically. It means all Equations must be discretized on a computational domain called mesh. The question is, what is the optimum number of meshes that have low computational costs and high accuracy

simultaneously. The mesh independence method has been utilized to answer this question. In this study, several meshes are generated and applied to the model. The velocity of the jet at a particular time and section shown by the sample line in Figure 6 is captured during the solving process and compared with other meshes.

Figure 7 shows the results of mesh independence. According to figure 7, 65400 number of nodes is optimum, and a part of the final mesh has been shown in Figure 5. These nodes are generated on the geometry, which is shown in Figure 4. The dimensions of the geometry are precisely like the experimental setup.

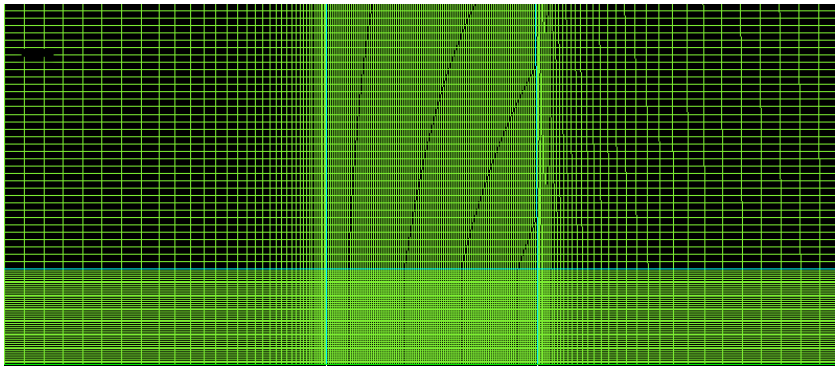

Figure 5 A zoomed section of the mesh

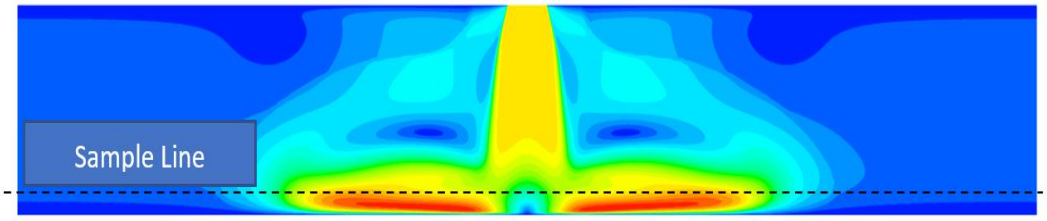

Figure 6 Contour of velocity at the time of 0.01 s and the sample line for mesh independence

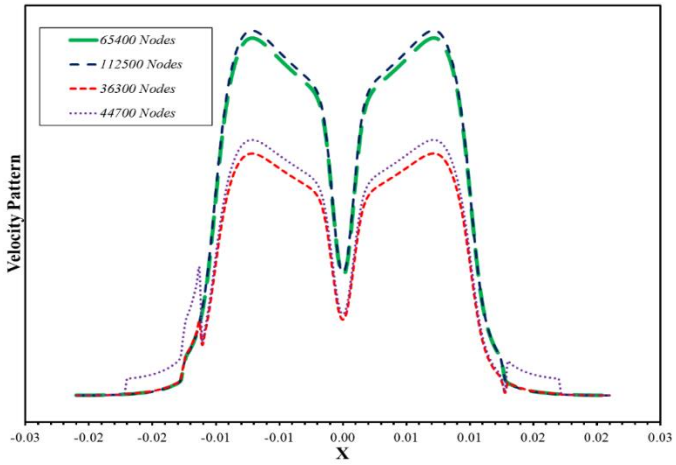

Figure 7 Mesh independence results based on velocity pattern for four different numbers of meshes

5 Results and Discussion

5.1 Particle and fluid characterization

A TEM analysis of the MWCNT and Al_2O_3 nanoparticles are performed to investigate the actual size of the nanoparticle. The majority of the nanoparticles were found to show a good correlation with the information provided by the supplier (USA - Houston, Texas, Nanostructured and Amorphous Materials Inc.). The TEM in Figure 8 shows good morphology in the fluid. Both the cylindrical tube-shaped MWCNT and spherical Al_2O_3 can be seen to keep their shape and size when mixed with base-solution. The TEM image is also evidence of the fact that particle of similar sizes has acquainted themselves with each other with a difference of sizes. The particles have their sizes much enhanced due to their bonding with the water and surfactant molecules ensuring the formation of the hydrodynamic boundary formed around the involved constituents. The evidence of such layers, if needed for analysis, can be inferred from the data obtained from the DLS method. The size of the nanoparticle is 38 nm in diameter when mixed in the base fluid, and the diameter is bigger than the manufacturer's specifications due to their bonding with the water and surfactant molecules ensuring the formation of the hydrodynamic boundary formed around the involved constituents.

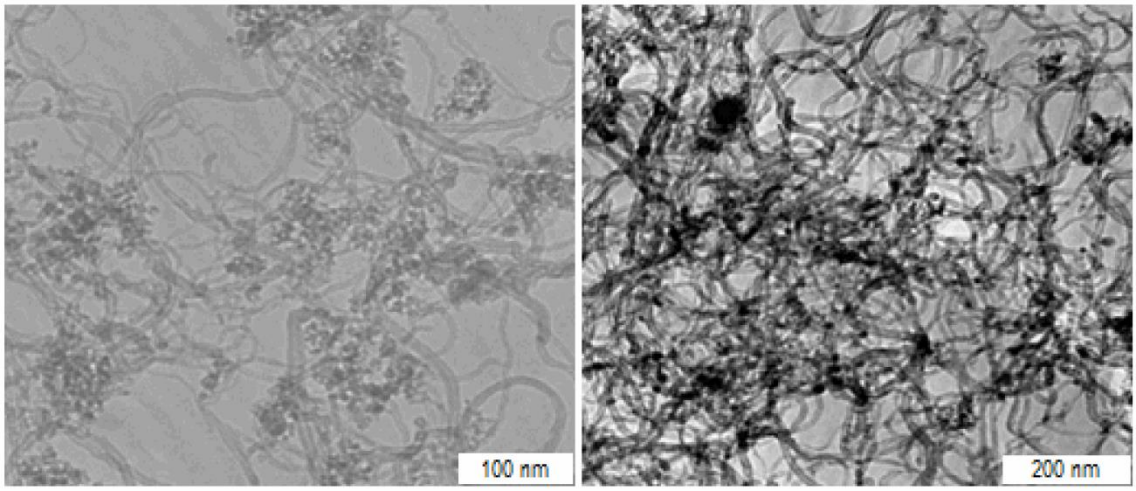

Figure 8 TEM image of dispersed powder within the nanosuspension at 100nm scale

The size of the nanoparticle is 38 nm in diameter when mixed to form in NF as seen in figure (9) of the DLS results, and the diameter is bigger than the manufacturer's specifications of 7 nm diameter for is γ-Al_2O_3 and MWCNT (inner 3-5 nm, and outer 10-20 nm and lengths of 10-30 μm) due to their bonding with the water and surfactant molecules ensuring the formation of the hydrodynamic boundary formed around the involved constituents.

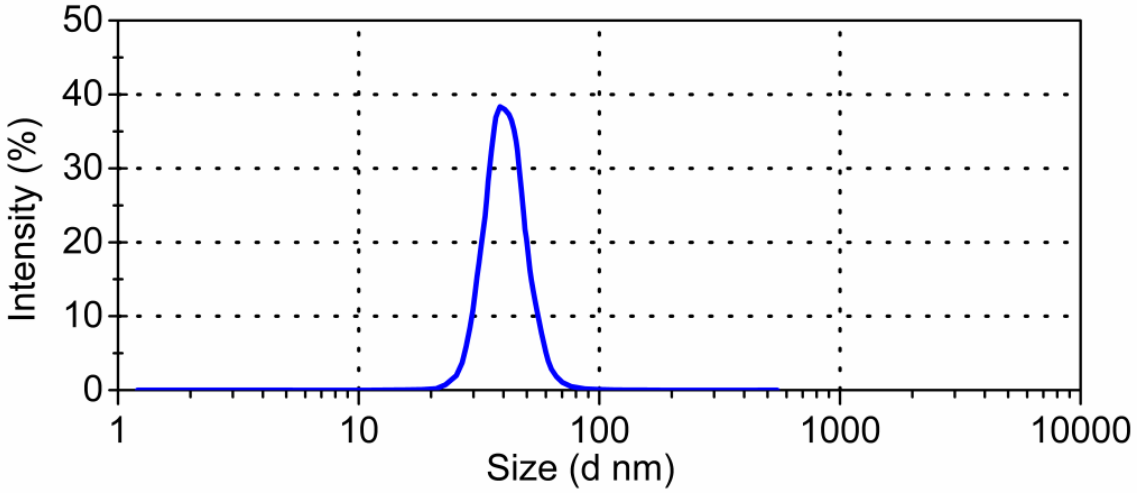

Figure 9 DLS size graph of the MWCNT-Al_2O_3 nanofluid confirming nanoparticle size of the prepared liquid

5.2 Stability of the nanofluid

Zeta Potential provides an estimate of a repulsive force between the nanoparticle (MWCNT and Al_2O_3) fluid layer and the bulk phase of the DI water fluid. The higher the repulsive force, the

better the stability of the NF. A value of ± 30mV is considered to be a stable fluid (Samarshi Chakraborty, 2020). Jenway 3510 pH meter (± 0.003 accuracy and 2 to 19.999 range) was utilised to pH values. The pH meter was calibrated using fluid supplied by the producer of pH values of 10, 7 and 4 before measuring the pH values of the HNFs. The negative value of -37 mV of the zeta potential on MWCNT and Al_2O_3 nanoparticles show the negative charge present on the MWCNT and Al_2O_3 nanoparticles as seen by zeta potential in Figure 10. The value is also above the value of stable NFs of ±30mV, stating better stability in the HNFs than conventional mono NFs. Another stability test was done every hour for 6 hours within 12 hours of testing the fluid. The viscosity stayed constant over the period tested for all vol% concentrations; however, there was a slight variation in the highest concentration, 0.15vol%.

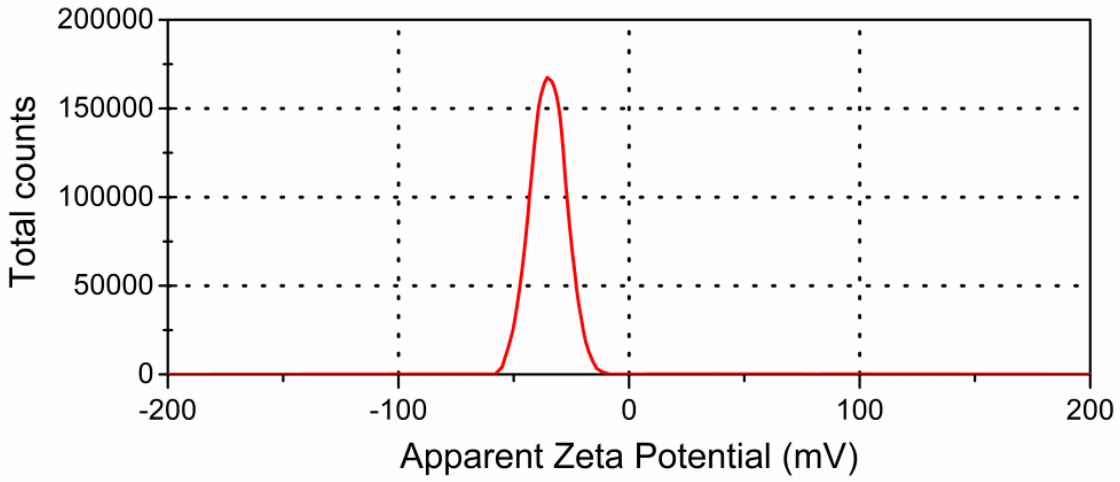

Figure 10 Zeta-potential of 0.1% concentrated MWCNT-Al_2O_3 nanofluid

The particle needs to be stable in fluid for several hours before the HNFs are used for any thermal study. A visual inspection was conducted after a week since the HNF was prepared. The results are shown below. It can be seen that the fluid is relatively stable for all three concentrations by looking at the fluid colour change from the bottom, which should be evenly distributed. More analysis can be done to provide a better stability inspection to visual inspection such as time depended on viscosity reading. Below in Figure 12 is a graph for viscosity reading which was done every hour for 6 hours within 12 hours of testing the fluid. Figure 11 displays the means of visual inspection to demonstrate that there was no sedimentation found even after two months.

Figure 11 A visual image of MWCNT/Al_2O_3(90:10)-DI water HNFs at varying particle vol% concentration (0.025, 0.05, 0.1 and 0.15%)

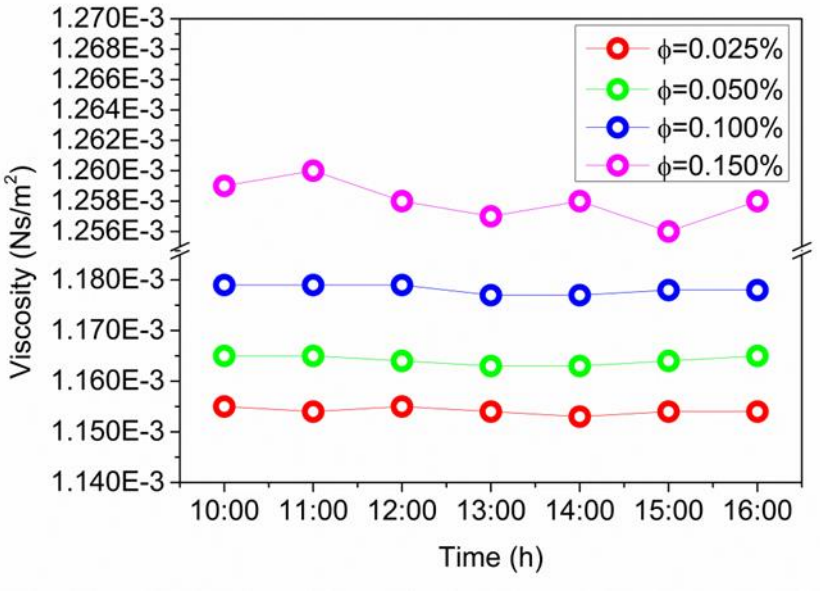

Figure 12 Dynamic viscosity of MWCNT/Al_2O_3(90:10)-water HNFs at varying particle vol% concentration (0.025, 0.05, 0.1 and 0.15%) over time

5.3 Properties of the nanofluid

Nanofluids' thermal conductivity increases as particle loading and temperature rise. Particle loading has a much greater impact on performance than temperature. In order to increase thermal conductivity, a thermal link is formed between the fluid molecules and the particle molecules by encapsulating them around their surfaces. In the fluid, the Brownian motion of the particles causes micro convection processes, which move energy. Temperature rise causes Brownian convection,

which in turn promotes random movement of particles, resulting in an increase in thermal conductivity. In spite of their 2000 W/mK thermal conductivity, MWCNTs are less dense and hydrophobic, resulting in a lower particle Reynolds number. This results in poorer thermal conductivity. Since dense alumina combines with surfactant and holds the MWCNTs together, the increase in thermal conductivity can't be explained only by MWCNTs' superior thermal characteristics. As a result, the Brownian motion of the denser particle, which is responsible for the movement of MWCNTs around the fluid molecules that promote excess thermal conductivity, must be the dominant influence.

When observing the experimental data is clear that there was a relationship between the particle vol% and the thermal conductivity, as seen by Figure 13. The thermal conductivity was relatively increasing when adding particles to the base fluid. The 0.15vol% HNF saw the most significant change in thermal conductivity. The difference in thermal conductivity increased linearly as particle vol% increases in the HNF. The relative and enhanced thermal conductivity results provided an increasing linear rate; both values were examined at 10°C and 20°C. Both showed that as the particle vol% concentration is increased, the relative thermal conductivity of HNF has a better ratio. Hence thermal conductivity is highly enhanced when using high concentration HNFs. At higher temperatures, the enhancement of thermal conductivity was much more significant. The average MOD between the correlation predicted value and experimental data values is less than 2%.

As the density of the involved nanoparticles is much higher than that of the water, the viscosity of the hybrid nanofluids is much higher than that of DI water. Hybrid nanoparticles enhanced the intermolecular forces amidst the liquid-particle interaction and particle-particle interaction, as well as decreased the impacts of DIW molecules owing to Brownian motion, raising the resistance to the flow of hybrid nanofluid. Flow resistance decreases when the temperature rises, owing to the weakening of intermolecular interactions and higher turbulence of molecules (particle-particle and particle–water) due to Brownian motion. Significantly, the viscosity of a fluid may be improved or harmed by the dissemination of two distinct types of nanopowders, one of which is water-phobic and the other is water-philic. In contrast to alumina, which reacts rapidly with water, MWCNT requires a second interaction with surfactant molecules in order to maintain a stable nanofluid. As a result, the more MWCNT that is added, the stronger the viscosity. The fluid's viscosity is meant to increase as a solid is added to liquid is a general phenomenon; this was also observed for the

viscosity measurement of the HNF in Figure 14, the highest particle vol% concentration fluid has the highest viscosity due to the addition of particle and surfactant to the base fluid. NFs and HNFs could be considered as Newtonian fluids for low volume fractions. The viscosity, as well as thermal conductivity, Equations (5.1) and (5.2) are correlated experimentally using the curve fitting method: The viscosity relative ratio was seen to increase as the particle vol% concentration in HFNs was raised. It showed a positive enhancement percentage in the viscosity of HNFs compared to water. Both enhancement and relative viscosity ratios are much higher at a lower temperature than at a higher temperature, and this is prevalent for all particle vol% concentrations of HNFs. The average MOD between the correlation predicted value and experimental data values is less than 2%. The two-phase mixing formula used by (S.O Giwa, 2020) is used to calculate the density and Specific heat according to the nanoparticle ratio used during preparation and are shown in Equation (5.3) and Equation (5.4), respectively.

$$\mu_{hnf}=\mu_{bf}(1.099055-0.00166T_{hnf}+1{,}0855\phi) \tag{5.1}$$

$$k_{hnf}=k_{bf}(0.940688+0.00428T_{hnf}+0.4696\phi) \tag{5.2}$$

$$\rho_{hnf}=(1-\varphi)\rho_{bf}+\rho_{hnp}\varphi \tag{5.3}$$

$$C_p=\frac{(1-\varphi)(\rho C_p)_{bf}+\varphi C_{p,hnp}\rho_{hnp}}{\rho_{hnf}} \tag{5.4}$$

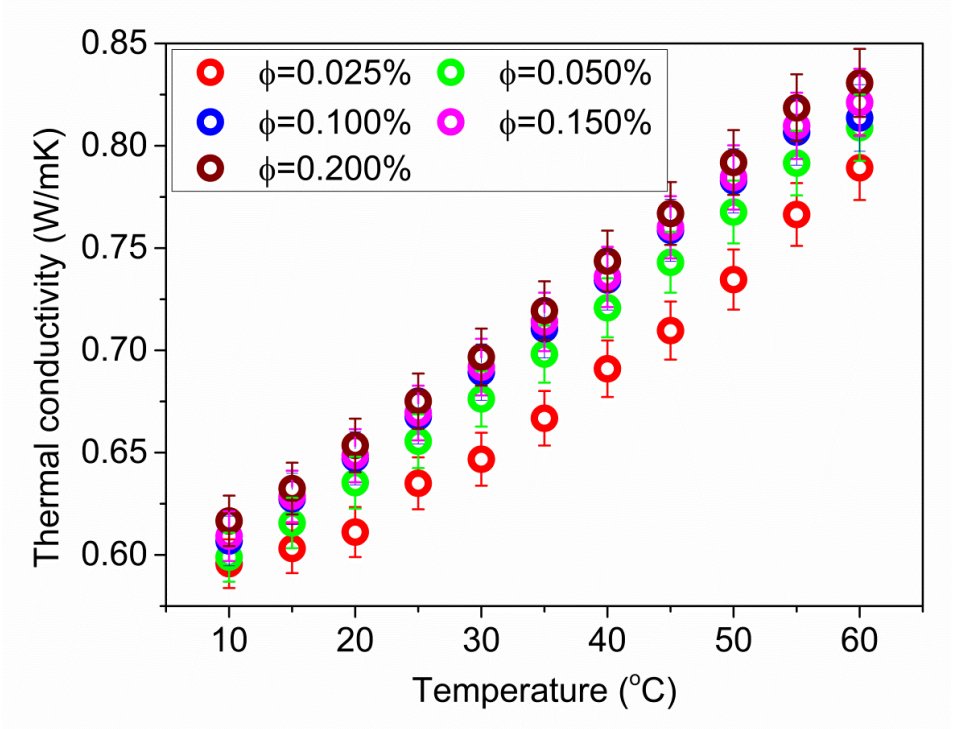

Figure 13 Thermal Conductivity plot of MWCNT/Al_2O_3(90:10) –DI water at varying particle vol% concentration and temperature

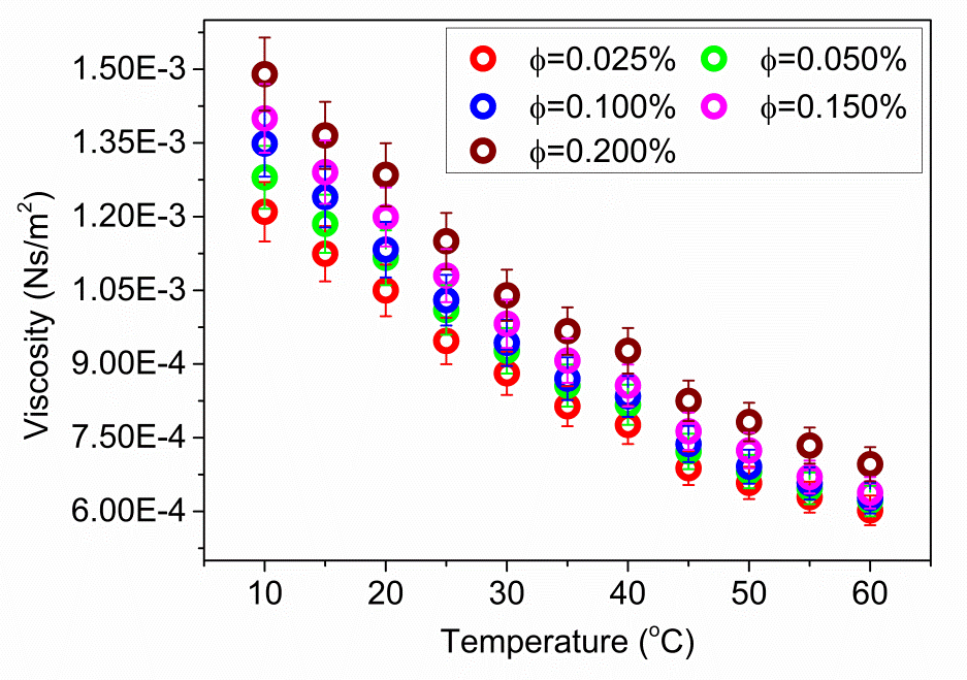

Figure 14 Viscosity plot of MWCNT/Al_2O_3(90:10) –DI water at varying particle vol% concentration and temperature

The pendant drop method to calculate surface tension is most widely used for calculating surface tension due to its high accuracy and low cost; hence in this experiment, the method I used to investigate the surface tension. The surface tension correlation for 90:10 MWCNT-Al_2O_3 HNF is as Equation (5.5) and is given in temperature and particle volume fraction.

$$\sigma_{hnf}=(0.075998-1.59\times10^{-4}T)\ (0.99145+9.32\times10^{-6}T-3.275\times10^{-2}\phi) \quad (5.5)$$

The experimental results clearly show that the surface tension will decrease with particle concentration increasing for all cases except for the lowest concentration HNF; this can be due to attractive forces (van der Waal's forces) between the dominant H_2O molecules. The 0.05 vol% does the slightest change in average surface tension. In the synthesis of the HNF, to get a stable fluid, a surfactant was added to the mixture. In the steric stabilisation process, long-chain surfactant forms a layer between the nanoparticles and the surrounding. The potential between particles is increased by this process; hence repulsive force (electrostatic) between them also increases. This, in turn, can reduce the surface energy and thus surface tension, as seen by the decrease in surface tension in Figure 15. At low particle concentrations, the surface tension of DI water containing nanoparticles is almost unaffected. Because the distance between particles is significantly bigger than the particle size, the forces and collisions amongst nanoparticles at/near the fluid interface have minimal influence on the surface energy of such dilute suspensions. The van der Waals force, on the other hand, rises as the number of particles in a given area grows. This will result in greater surface tension as a consequence of an increase in the free energy at the surface. However, Figure 15 shows a drop in surface tension for DI water that contains MWCNTs and Al_2O_3. The dispersible MWCNTs employed in this work have a length of 10–30 nm and a diameter of 3–5 nm, as previously stated. In addition to carbon nanotubes, they include surfactants, which contribute to the creation of stable nanofluids. There is a possibility that the long-chain groups of the MWCNTs, which provide excellent dispersion, reduced surface energy at the interface, leading to a decrease in surface tension. Increasing the concentration of MWCNTs may lead to a rise in surface energy and surface tension since Van der Waals forces may outweigh electrostatic repulsion.

In our case, the concentration of MWCNTs is more than Al_2O_3, which prompts to increase in the concentration of surfactants proportionately. Thus, when particles are further coated with layers of long-chain surfactant molecules, they function as a barrier between them and the encapsulating fluid molecules. This leads to particle repulsion, and as a result, the surface tension and energy at

the surface gets reduced. The fluid's interfacial tension may be altered if the particles are surface activated and pile up near the interface. This is a well-known property of colloidal particles. If surfaces are engaged in the heat exchange, changes in interfacial tension may alter the wetting characteristics of the fluid, which can affect heat transmission. The results could be compared with the data of Tanvir and (Saad Tanvir, 2012).

Table 5 Surface tension of MWCNT and Al_2O_3 in mN/m (Saad Tanvir, 2012)

Vol. conc.(%)	MWCNT	Vol. conc.(%)	Al_2O_3
0.045	71.45	0.085	72.21
0.064	71.25	0.50	72.33
0.52	71.33	0.998	72.71

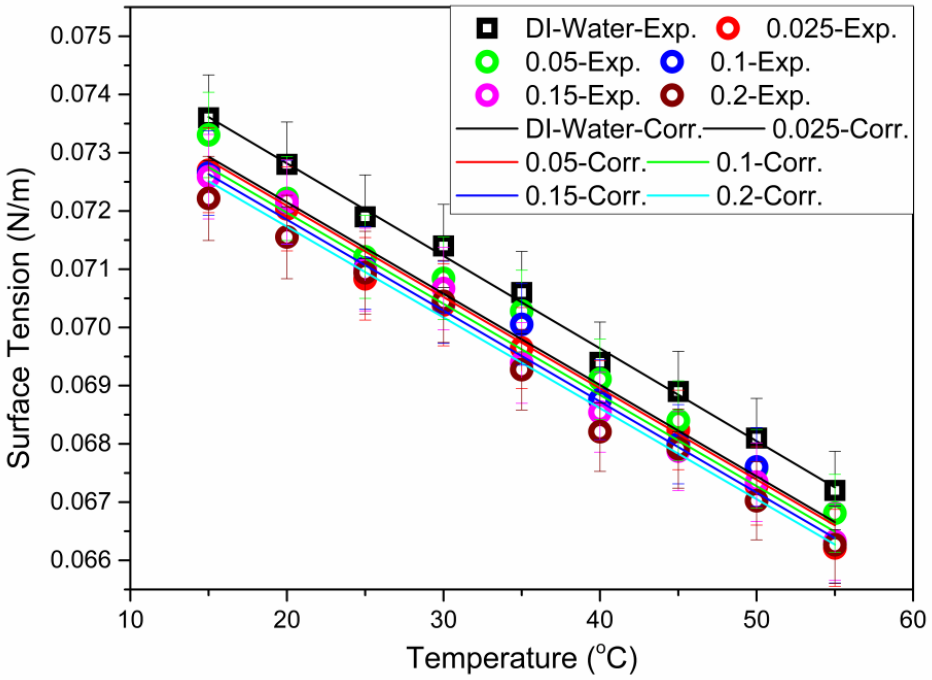

Figure 15 Surface tension plot of MWCNT/Al_2O_3(90:10) –DI water at varying particle vol% concentration and temperatures\

5.4 Comparison and Validation

The jet impingement setup calibrated needs to validate with other literature studies before commencing with any HNF testing. Two studies (Webb, 1995) and (Wilken, 2019) were used to validate the experimental setup. (Webb, 1995), Analytical research into local HTCs for round, single-phase free liquid jets impinging normally against a flat constant heat flux surface —an equation for Nu numbers were obtained in stagnation and boundary layer regions. The heat transfer between the surface wall and the water jet was examined and calculated using the experiment results. The considered factor, nozzle diameter, was examined for 2.2mm and 8.8mm diameter. Re numbers were between 4 000 and 52 000. The resulting Nu number correlation is given as a Reynolds and Prandtl numbers function, as shown in Equation (5.6) below. The smallest nozzle diameter of 2.2mm was chosen for comparison. The value for the coefficients A, q, s for the 2.2mm diameter nozzle is 5.36,0.27, -0.052, respectively.

$$Nu_0 = A Re^q \left(\frac{z}{d}\right)^s (Pr)^{0.4} \tag{5.6}$$

Another free-surface jet impingement cooling experiment was done by (Wilken, 2019) using $TiO_2 - water$ NFs. The general conclusion was that $TiO_2 - water$ NFs in jet-impingement cooling applications create thermal enhancement, which depends on the relevant particle concentrations. Regarding the considered parameters, nozzle diameter was 1.65 mm, and Re numbers were between 9 000 and 28 000. The Nu number in terms of Re number and vol% concentration of particles was experimentally correlated with R^2 0.98%, shown below in Equation (5.7).

$$Nu = \begin{cases} 0.1263 \cdot Re^{0.705} \varphi^{0.235}, & \varphi < 0.1\% \\ 0.0669 \cdot Re^{0.67} \varphi^{-0.1}, & \varphi \geq 0.1\% \end{cases} \tag{5.7}$$

The validation showed a good correlation between the experimental values calculated for DI-water and the values calculated by Equation 5.6 and Equation 5.7, as shown in Figure 16 below. From Figure 16 below, the correlation proposed by (Webb, 1995) showed low accuracy; however, the average accuracy was 7.9% when using the equation proposed by (Wilken, 2019) and showed a much better similarity than of (Webb, 1995) ; this is due to the nozzle and surface geometry being different and not accounted for.

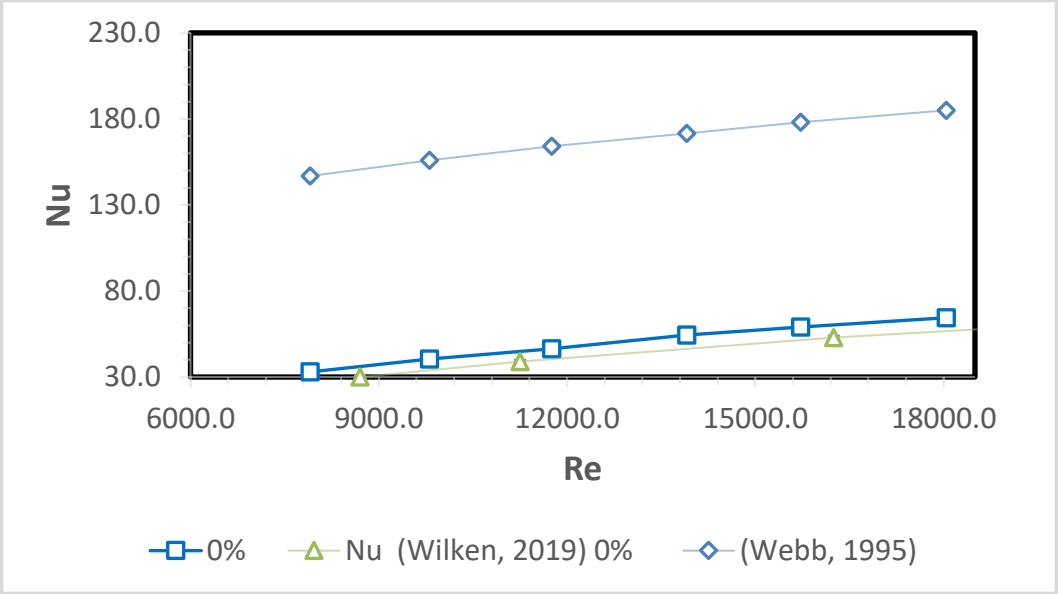

Figure 16 Jet impingement Nusselt numbers against Reynolds number validation plot for steady-state DI water.

5.5 Experimental Cooling performance results

Figure 17 (b) indicates the relationship between HTC of different particle concentration MWCNT/AL_2O_3(90:10)-DI water HNFs and varying Re numbers. The average HTC for varying particle concentrations MWCNT/Al_2O_3(90:10)-DI water HNFs increased as the Re number was increased for all experiments showing linear behaviour. This behaviour is due to higher convective heat transfer achieved because of the high speed of the fluid at high Re numbers. The HTC was seen to increase as particle vol% concentration was increased; however, after the 0.05vol%, the HTC started to have a decreasing trend. However, the 0.15vol% and 0.1vol% are almost evenly enhanced. The decreasing enhancement could be due to the increase in thickness of the boundary layer and viscosity of the fluid and the more significant impact of these parameters over the thermal conductivity. From Figure 17 (b), it is evident that all the volume concentrations of the nanofluids have fared better than the base fluid. The following reasons could be attributed to such behaviour. The first explanation is that nanofluids have better thermal conductivity than DI water, as discussed earlier. The second is that the heat transmission between heated surfaces and fluids is facilitated by intensive bombardment from the thermally superior nanoparticles. Such an extreme impact causes the working fluid to become more turbulent, thus reducing its boundary layer thickness close to the impinging surfaces. Naturally, the convective heat transfer coefficient increases with

increasing particle volume concentration. When the H/ is the same, the convective heat transfer coefficient of nanofluid rises linearly with the Reynolds number. Higher Reynolds number results in an increase in jet velocity and a decrease in wall boundary layer thickness, both of which augments heat transfer. A greater heat transfer effect may be achieved at high Reynolds numbers due to increased turbulence at the free interface caused by the jet and surrounding gas mixing intensely. However, it must be noted that more particle concentration can also cause accumulation of particles over the surface causing heat transfer resistance, thus reducing the heat transfer coefficient. This is the reason behind the lowering of the heat transfer coefficient when the particle concentration is increased beyond 0.05%.

From Figure 17 (a), it is shown that 0.05vol% fluid is the best performing fluid in terms of heat transfer. Beyond this vol% concentration, the enhancement is known to decrease as the Re number is increased. The Nu number is seen to increase due to the mass flow rate increases, which causes an increase in the fluid advection. The 0.05vol% HNF has the most outstanding Nu number value due to the relatively increased Brownian motion, which results in better heat transfer. The 0.05vol% nanofluid at Re= 15000, for instance, depicts a 17% rise in Nu number by comparison with distilled water. On the other hand, higher volume concentration reduces Nu number; in this case, secondary flows become less intense, and thus Nu number is more degraded. It is noteworthy that maximum improvements (in comparison with distilled water) of 17% and 14% in Nu number are achieved using 0.05vol% and 0.1vol% HNFs, respectively.

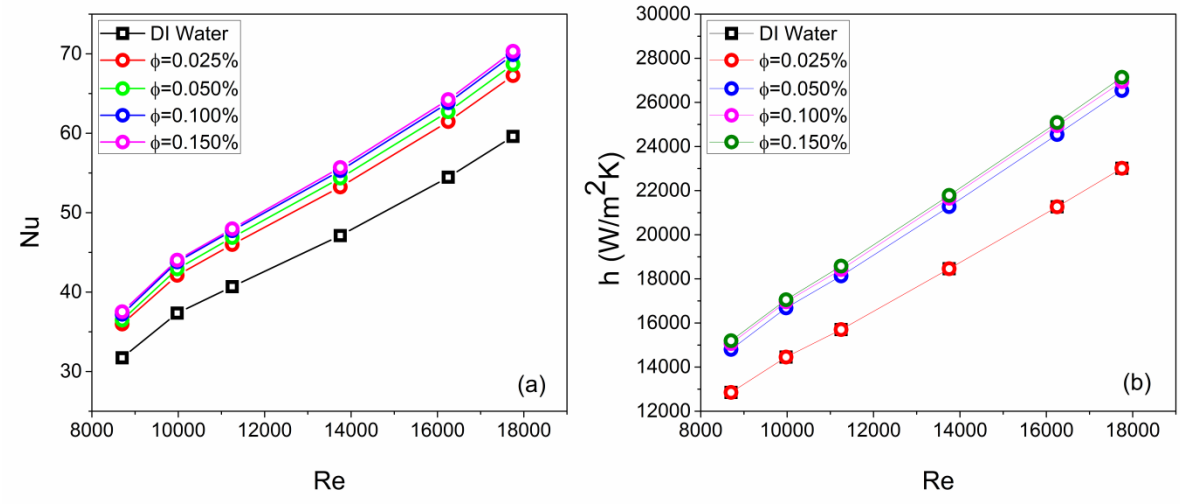

Figure 17 (a) Average Nusselt Average and (b) Heat Transfer coefficient plots for changing volume fractions of MWCNT/Al_2O_3(90:10)–DI water HNFs at changing Reynolds numbers

Figure 18 illustrates the Nu number and Re number at the impinged surface at varying volume concentrations percentage of HNFs (0.025, 0.05, 0.1, and 0.15vol%). Using HNFs, the Nu number at impingement is enhanced, the maximum Nu number is obtained at Re= 16000 compared with distilled water. In detail, the Nu number for MWCNT-Al_2O_3 (90:10) –DI water HNF with 0.05% volume concentration stands at 180, 18.7% augmentation in comparison to DI-water. In addition, HNFs with volume concentrations of 0.1%, 0.025 %, and 0.15% experienced higher Nu_{ip} versus DI-water at Re=16000, respectively. This trend was roughly the same from the beginning of the test in different Re numbers. It is well concluded that in Re=16000, the effect of Rayleigh-Taylor instability is evident, which means the waveforms' shapes on the boundaries of the jet flow decreases considerably, which causes the lower boundary condition thickness on the hot surface, improving the HTC. Besides, in the fluid flow using multi-phase fluid or HNF, there are different sublayers in the flow regime (created on the hot surface, specifically in turbulent regime). It can improve the Brownian motion, which is resulted in augmentation in the convection heat transfer and higher Nu number. A minor improvement for all vol% particle concentration fluid was obtained at the lower Re numbers. At Re number =8000, the impinging surface Nu number was improved by 16% when using the 0.15 vol% fluid, and the slightest improvement of 7.14% was seen in the 0.025 vol% fluid. Compared to DI water, the 0.15 vol% and 0.1 vol% fluids gain at 14.17% and 14.2%, respectively.

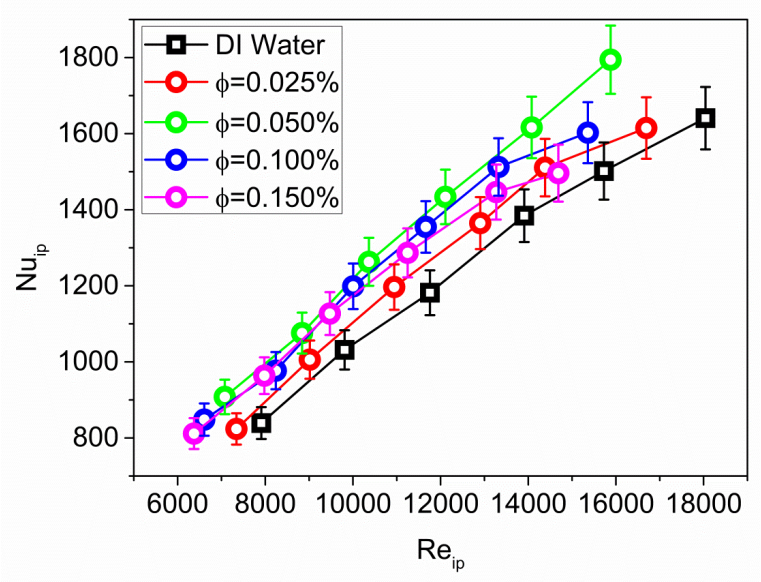

Figure 18 Experimental Impingement Nusselt number values for varying volume fractions of MWCNT/Al_2O_3(90:10)–DI water HNFs at varying impinging Reynolds numbers

Figure 19 (a) shows the Nu number and Weber number investigated at the impinging surface for varying particle concentration HNF. From Figure 19 (a), it is clear that the 0.05 vol% fluid is the best performance fluid, and the 0.15 vol% fluid is the worst and has a negative impact on the Nu number as seen by the curve is lower than of DI water. The maximum Nu_{ip} observed for the MWCNT-Al_2O_3 (90:10) –DI water HNF with the volume concentration of 0.05% standing at Nu_{ip}= 1795 at We= 6500. The improvements of 9% and 16.7% are evaluated for HNF with volume concentration 0.05% compared to Distilled water and 0.15vol% MWCNT-Al_2O_3 (90:10) –DI water HNF, respectively. It should be noted that by comparing the Equations of Re and We numbers, it could be proposed that these two dimensionless numbers are related together. In detail, Weber's number consists of the Re number and the adequate surface tension. The slightest improvement for all vol% particle concentration fluid was obtained at the lower Weber number. At We= 1200, for the best performing vol% fluid of 0.05 vol% concentration, the Nu number was improved by 7.4% and 12.33% compared to DI water and 0.15 vol% fluid.

Figure 19 (b) demonstrates the Nu_{ip} vs Pe_{ip} numbers in the different volume concentrations of HNFs and distilled water with a different mass flow rate at the nozzle. The Péclet number was analysed at its heat transfer form and at the impinged surface using the thermal diffusivity coefficient, which is accounted for in the Prandtl number used to make up the Péclet number. The 0.05 vol% HNF has the most significant improvement in the Nu number. The maximum enhancement of 9.75% is observed at the highest Péclet number of 20200. It can be due to the improved thermal and momentum diffusivity at a high Péclet number. The improvement was less at the lower Péclet numbers, as seen in Figure 19 (b); the curves have a steeper slope as the Péclet number increases. At Péclet number =90 000, the improvement in Nu number compared to DI water is 8% for the highest performing fluid 0.05vol% particle concentration. From Figure 19 (b), it can be concluded that the increase in particle vol% concentration increases the Nu number at the impingement surface. However, this is not true for 0.025 and 0.15 vol% concentration fluid. It can be due to the low thermal diffusivity in the 0.025vol% fluid caused by low thermal conductivity and a very high momentum diffusivity in the 0.15 vol% fluid due to its greater mass.

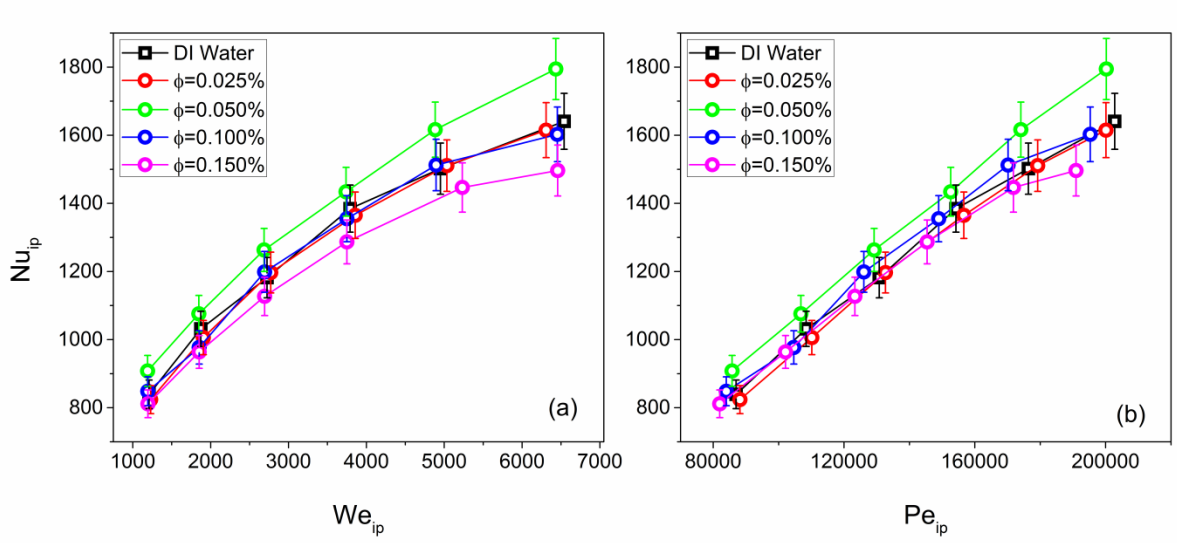

Figure 19 Experimental Impingement Nusselt number values for varying volume fractions of MWCNT/Al_2O_3(90:10)–DI water HNFs at varying impinging (a) Weber number and (b) Peclet number

Figure 20 shows the transient behaviour of the MWCNT-Al_2 O_3 (90:10)-DI water HNFs which allied to the steady-state cooling results. When volume fraction was increased, a desirable effect on the cooling efficiency was seen in comparison with the DI water at a constant volume flow rate. However, it is noted that the cooling effect is almost identical at 0.1vol% and 0.05vol%. In the transient state, the cooling is enhanced by the (0.025, 0.05, 0.1, and 0.15vol%) HNFs were approximately -1.5, 6, 5, and 9%, respectively, when compared to DI water. So, using 0.15% particle concentration, HNF had the biggest cooling effect, providing the reasons below for the cooling efficiency increases with an increase in vol% concentration particle (Ting-zhen MING, 2015). As particle concentration increases, particle deposition is raised in the target surface to create a thin layer that improves the surface wettability and, in turn, increase the heat transfer. The HNF's heat capacity and the surface area are also improved with more particle concentration, raising nanoparticles concentration, increases the random movement of the nanoparticles, which cause an increase in turbulence intensity. Through Brownian motion effects, the convective heat transfer effect becomes larger than other heat transfer modes. However, this trend was not true for the 0.1vol% HNF, as seen in Figure 20. A probable explanation is that the enhancement of thermal conductivity gained (that increased the fluid viscosity) is more effective than high particle concentration. Also, despite an increase in particle concentration (which causes particle

deposition), the heat transfer in the target surface and fluid was enhanced (Ishita Sarkar, 2019) warns that a considerable particle concentration can cause a large amount of deposition at the target surface. The addition of particles also causes the heat transfer in the test specimen and coolant to deteriorate. Because MWCNT/Al_2O_3 nanoparticles had less thermal conductivity compared to the copper target surface, and a deposition layer was formed on the surface. This could explain the trend observed for HNF particle concentration higher than 0.1vol%. Thus, the transient state testing was done for the same Re numbers but not volume flow rates.

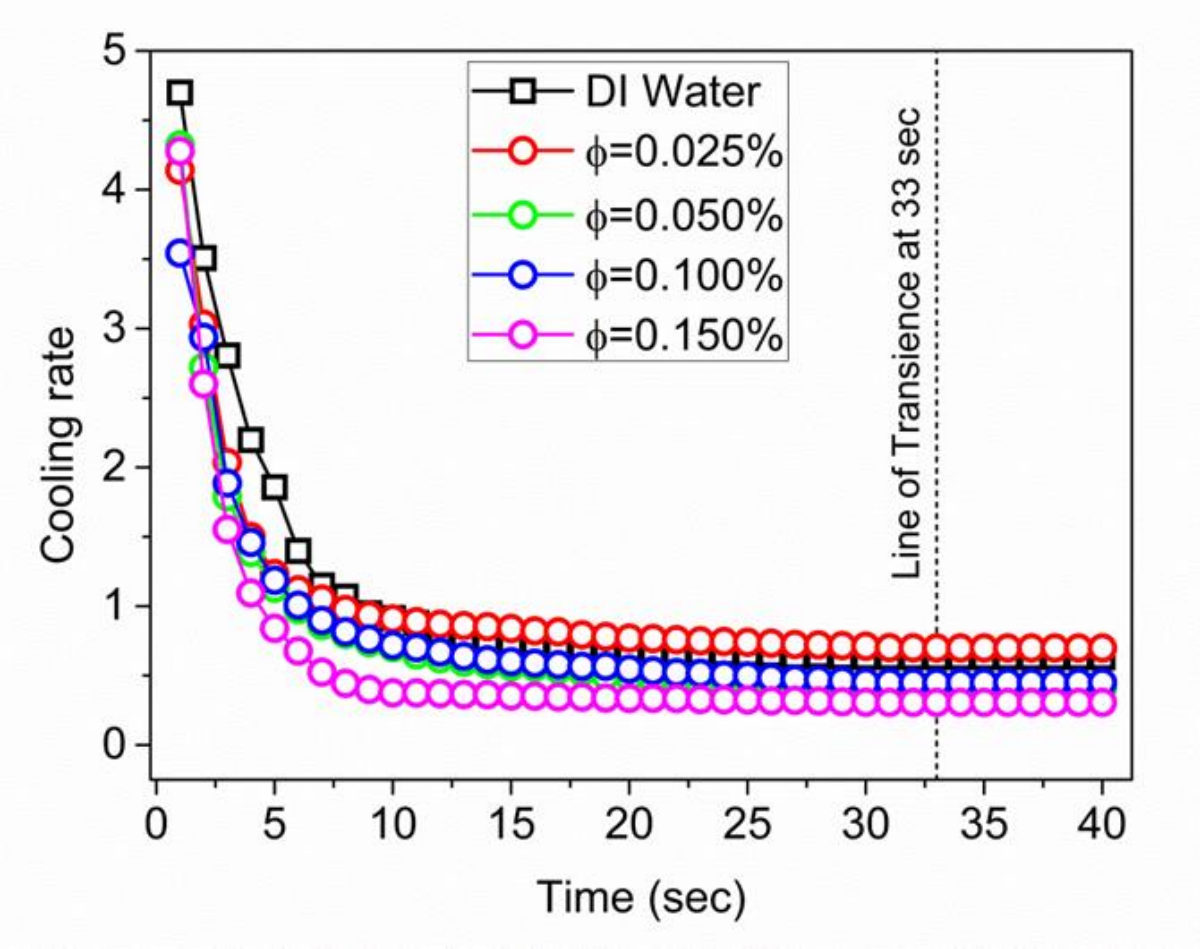

Figure 20 Experimental transient cooling plots for changing particle volume fractions of MWCNT/Al_2O_3(90:10)-DI water HNFs

The flow difficulty of the varying particle vol% concentration HNF was calculated using Equation (4.24). The flow rate loss percentage was calculated relative to the flow rate achieved by DI-water at constant pump power. The results are plotted below in Figure 21 at a temperature 10°C of HNF. It is clear that as particle concentration in HNF increases, the fluid transportation difficulty

increases; this could be due to the denser and more viscous nature of the HNF compared to base fluid DI-water. The slope of the increased flow rate loss was also seen to be steeper as particle vol% concentration increased in the HNF. This method can be utilized to provide a pumping curve for centrifugal pumps used in nanofluid applications due to manufacturers providing curves being done usually for water and not considering the various factors such as viscosity and density change HNFs encompasses.

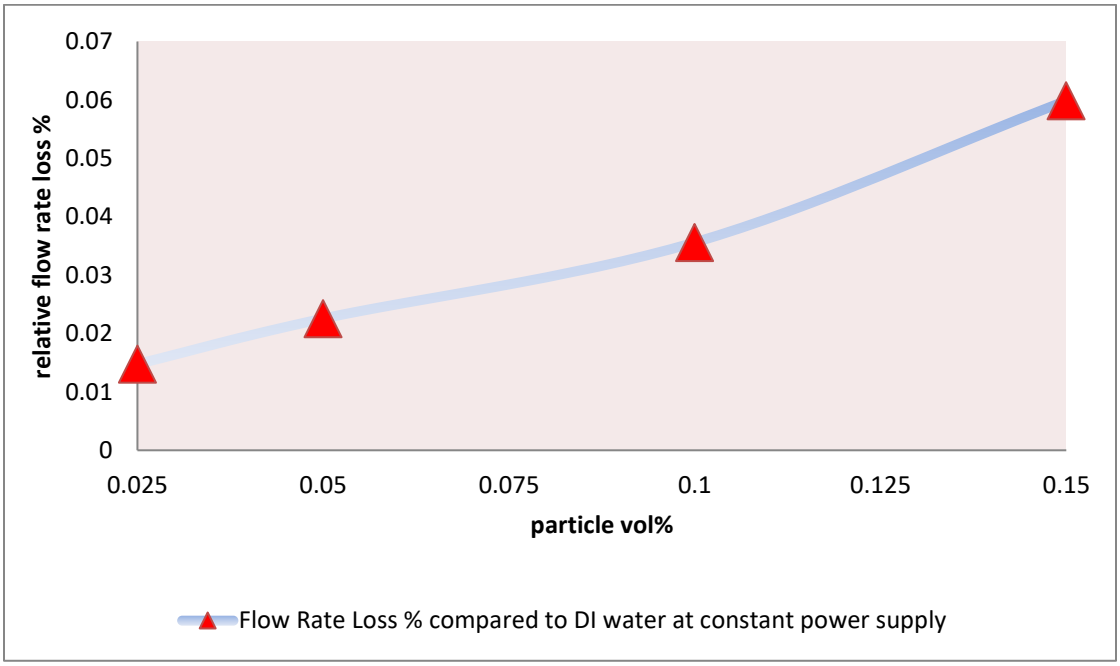

Figure 21 MWCNT/Al_2O_3(90:10) -DI water HNF flow difficulty at varying particle vol% concentrations

5.6 Numerical Cooling performance results

Figure 22 shows the contours of velocity and volume fraction of water from the start of interaction at the jet to the surface at different times. Establishing these contours is to see how the jet interacts with the hot surface and comes out from the domain. Also, these results are proof of working CFD solver correctly. It is because, as is expected, the jet comes out from the nozzle and impacts the hot surface of the setup. Finally, the working fluid brings the surface's heat to the outside of the domain. The obtained results, validation, and mesh independence conclude that the mathematical model works correctly, and its outcomes are trustworthy.

The velocity magnitude contours show that the velocity is maximum at the centreline of the flow and minimum at the flow boundaries. When the fluid makes contact with the surface, it gradually

slows down from the stagnation point to the surface edge, and this should predict that the maximum heat transfer takes place at the stagnation point. The water speeds up parallel to the edges of the hot surface due to the high pressure. The shear stress, which is caused by the velocity gradient on the hot surface, results in high heat transfer with respect to the definition of Reynolds number. A thin and constant thermal boundary layer at the stagnation zone causes maximum heat transfer because of working flow acceleration through the hot surface. Thus, the transition flow regime happens from the stagnation zone to the boundary layer.

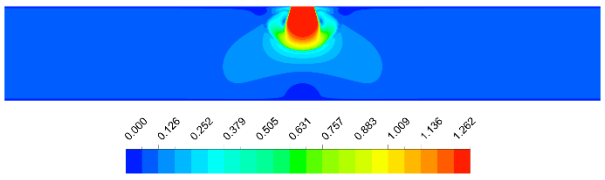

(Velocity)

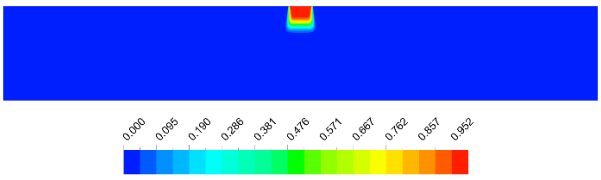

(Liquid Volume Fraction)

t = 0.001 s

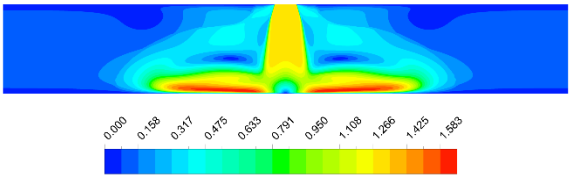

(Velocity)

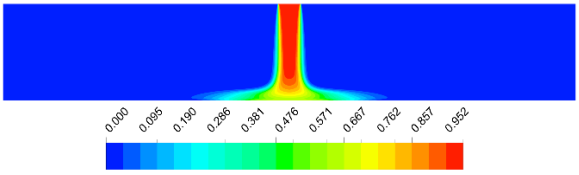

(Liquid Volume Fraction)

t = 0.01 s

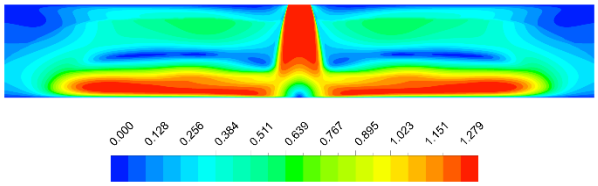

(Velocity)

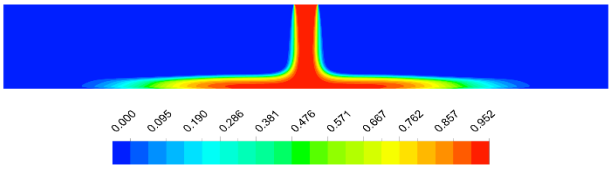

(Liquid Volume Fraction)

t = 0.1 s

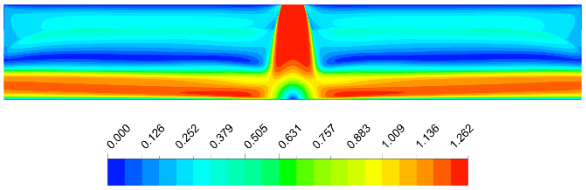

(Velocity)

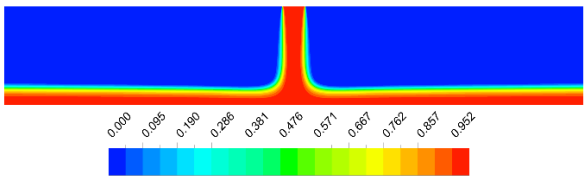

(Liquid Volume Fraction)

t = 1 s

Figure 22 Contours of velocity and volume fraction of water from start to interact to the surface in different times

Figure 23 depicts the temperature contours of the heated solid in different Re numbers and volume fractions of the nanoparticles. According to the obtained results, it is clear that at each Re number, for a higher concentration of the nanoparticles, more heat is extracted from the hot body. Also, when the value of the Re number increases, it has the same impact as the concentration of nanoparticles on the results. Therefore, it is concluded that the most heat extraction has occurred in the highest Re and Volume fraction. There is another statement that we should take into account. If the concentration of the nanoparticles increases significantly, we cannot conclude that there is an enhancement. As the concentration of nanoparticles increases, other parameters play their roles. One of them is the rate of erosion. The other one is high viscosity and density that will affect pressure drop. Therefore, as a suggestion, it can be investigated in further research.

	Re = 8700	Re = 11250	Re = 16250
Pure Water	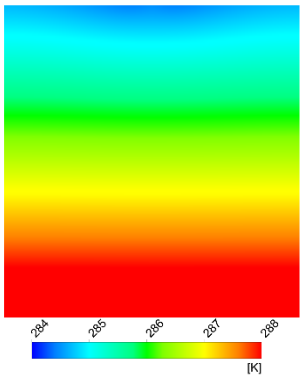	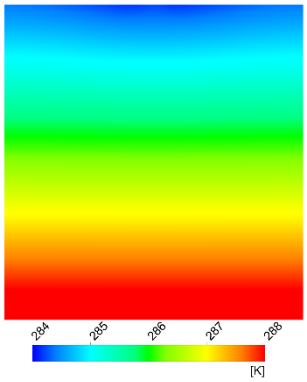	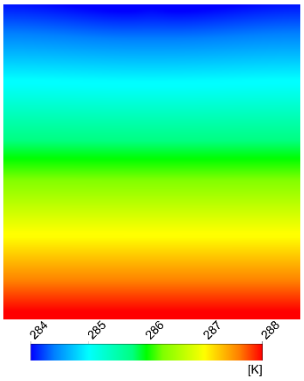
HNF-0.025%	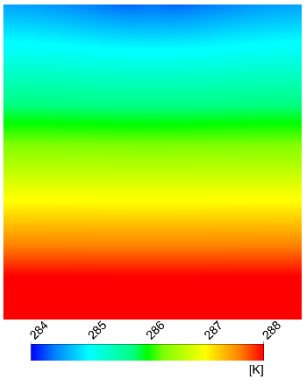	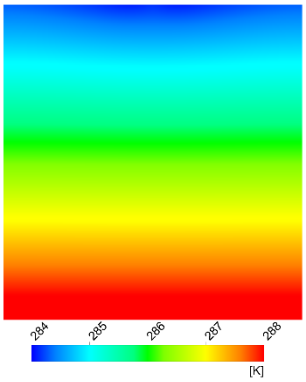	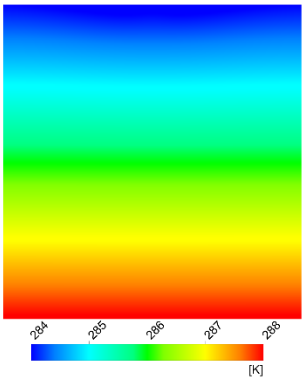

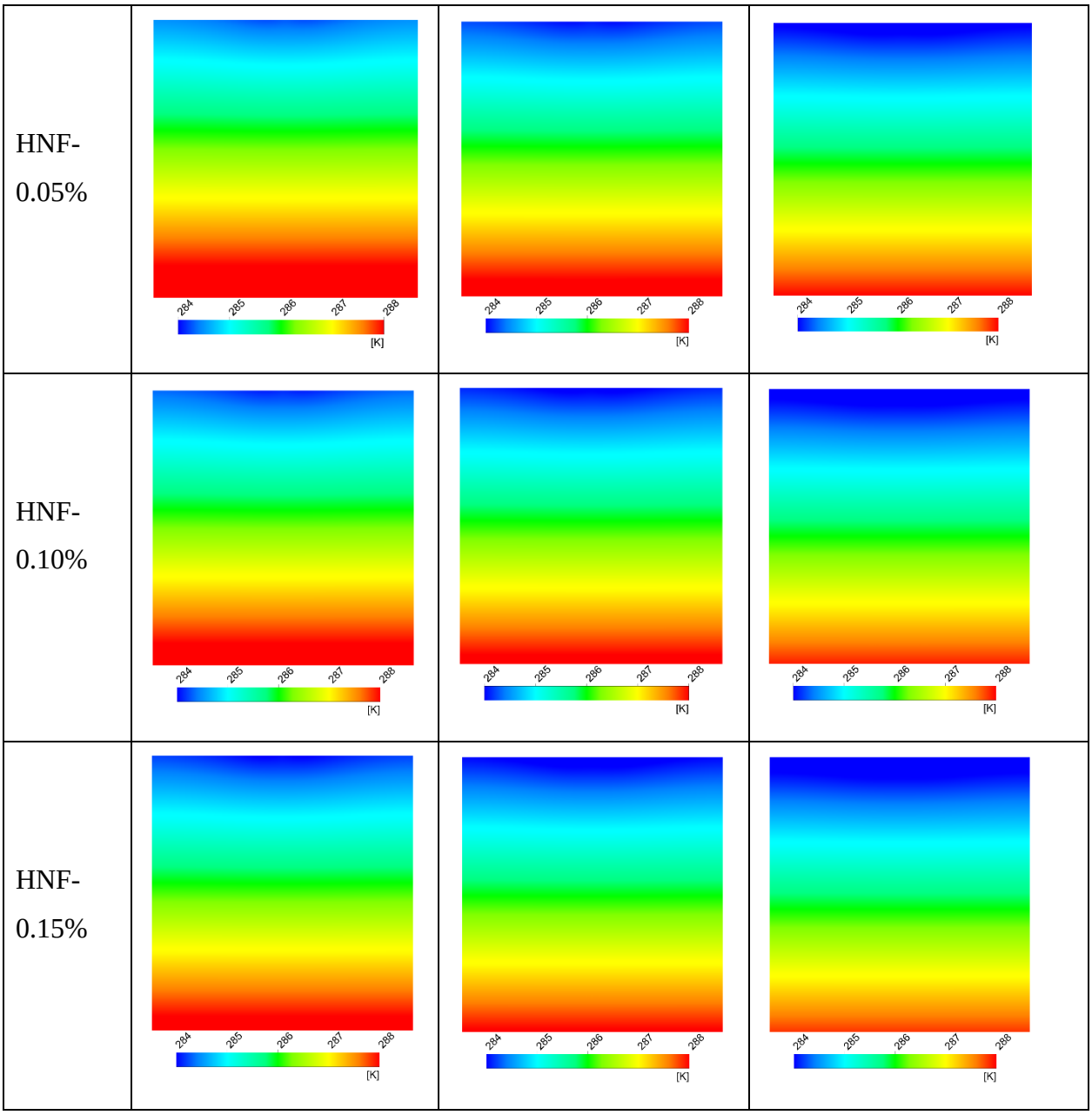

Figure 23 Contours of the temperature of the solid part of the setup in different concentrations of HNF and Reynolds numbers

Re number versus Nu number for pure water is examined to validate the proposed model. Figure 24 (a) validation with (Wilken, 2019) and other results for different HNF concentrations. From validation results, it is evident that the model works perfectly. Also, the figure shows with increasing the concentration of the HNF, the Nu number increased. Figure 24 (b) shows Nu and HTC in different Re numbers. Commonly, these types of information provide us with having accurate judgments about which one of the HNFs prepared is better in heat transfer. According to

these two figures, it is evident that by increasing Re and vol% of nanoparticles, both Nu number and HTC increase. The 0.15 vol% particle concentration fluid sees a maximum improvement of 19.7% in Nu number, and the improvement in the 0.05 vol% particle concentration fluid is 13.7% compared to the experiment value of 17%. These two parameters are on behalf of heat transfer rate. But if we look more closely at the figure, it is clear that the changes can be ignored at the higher concentration of the HNF similar effect was seen in the experiment where the 0.1vol% and 0.15vol% are closely followed by one another. As the experimental results showed, there is no significant improvement for higher concentration. But in all cases, there is a massive improvement in heat transfer when HNF has been utilized.

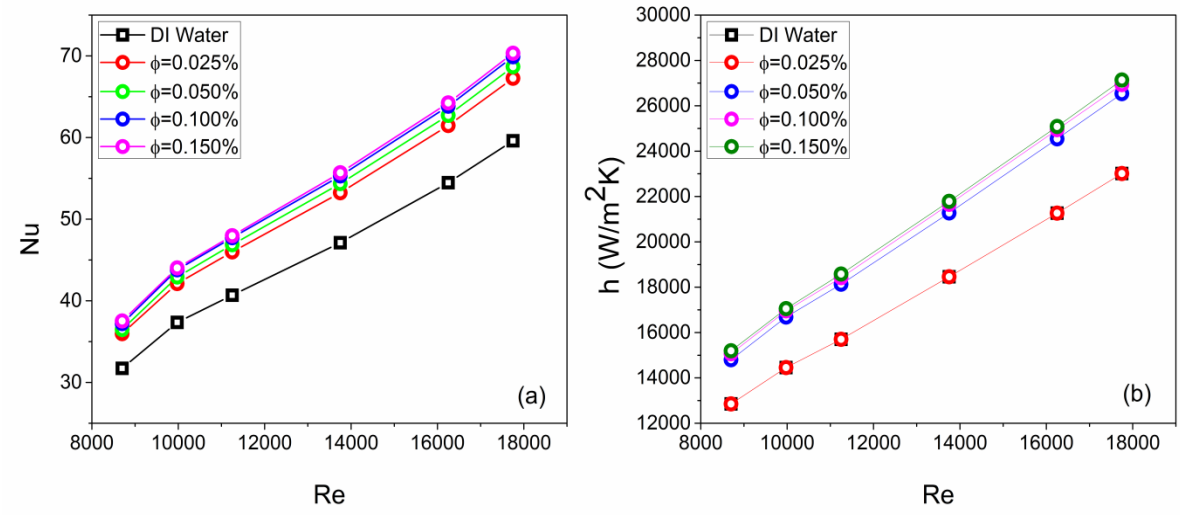

Figure 24 Comparison of (a) Nu and (b) HTF at varying HNF vol% (0.025, 0.05, 0.1 and 0.15%) and varying Reynolds number

Another parameter is calculated for comparing different volume fractions of the HNF is the cooling rate. The cooling rate is a parameter that shows which volume fraction of the nanoparticles has a better impact on cooling the hot surface. It means the shorter the cooling time, the better the volume fraction. Equation 4.21 is used to calculate this parameter. In this Equation, as mentioned before, all temperatures are in centigrade degrees. Figure 25 shows the cooling rate of different volume fractions of HNF when Re = 16250. Re number of 16250 is elected because this Re had the best performance compared to others. As Figure 25 shows, a higher volume fraction of the HNF cooling rate is faster. The best performing fluid is the 0.15vol% particle concentration fluid with

relaxations time 1 second compared to 1.75 seconds in experiment and steady-time (the time the curve is approaching infinity line) is 23 seconds compared to 33 seconds in the experiment. For this case, Table 6 compares the average cooling rate in each volume fraction.

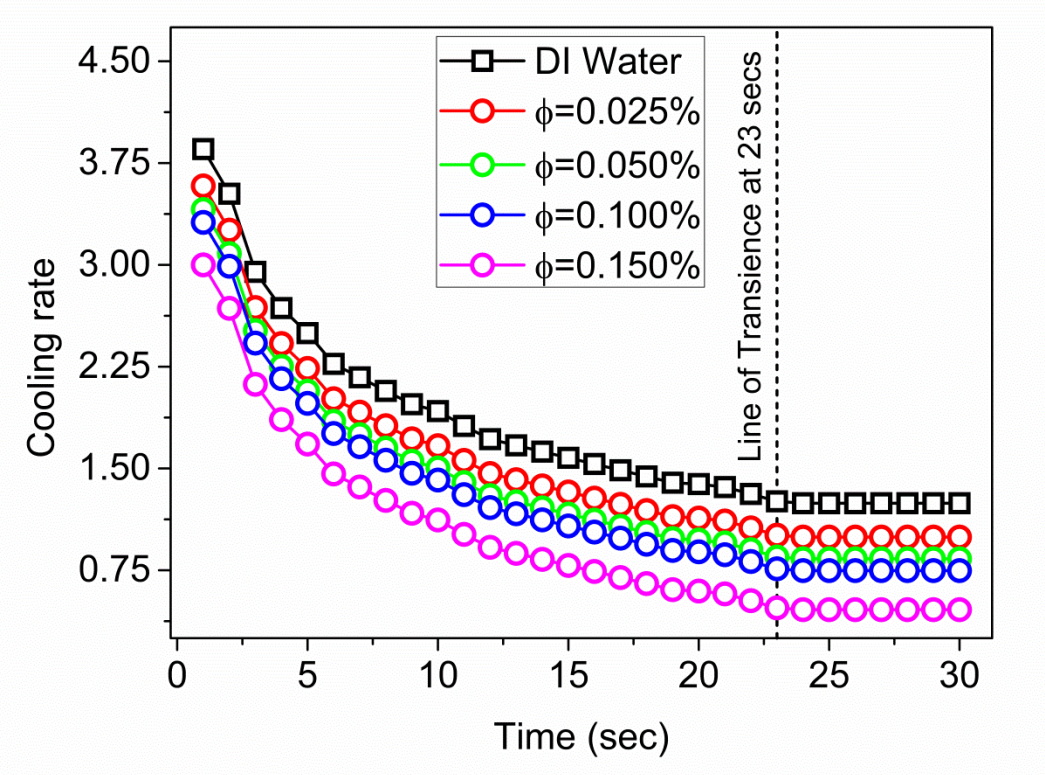

Figure 25 Cooling rate of varying volume fractions of HNF (0.025,0.05, 0.1 and 0.15vol%) at Re = 16250

Table 6 Comparing the average cooling rate in each volume fraction of HNF

Volume Fraction	Ave. Cooling Rate
Water	1.77
0.025%	1.51
0.05%	1.35
0.1%	1.26
0.15%	0.97

6 Correlation development

The simple multiple linear regression calculation is used to find a line of best fit. The line of best fit for data is correlated comprising of two independent values; the vol% concentration and Re number and one dependent Nu number value.

The best fit line is described by Equation (6.1) below, where 'a' and 'b' are coefficients that define the slope of the line and 'c' is the intercept. This calculation determines the values of 'a', 'b', and 'c' for a set of data comprising three variables and estimates the value of Nu for any specified values of φ and Re.

$$Nu=a\varphi+bRe+c \tag{6.1}$$

The correlation was found to be as Equation (6.2) below

$$Nu= 168.83316\varphi + 0.00347Re + 4.63882, \quad \varphi\leq 0.05\% \tag{6.2}$$

The strength of the linear correlation between the two variables is measured by Pearson Correlation Coefficient, as shown in Equation (6.3), where the value R = 1 means a perfect positive correlation and the value R= -1 means a perfect negative correlation.

$$r=\frac{\sum_i (x_i-\bar{x})(y_i-\bar{y})}{\sqrt{\sum_i (x_i-\bar{x})^2}\sqrt{\sum_i (y_i-\bar{y})^2}} \tag{6.3}$$

The correlation was found to have an R-value of 99.561%. Correlation and experimental results comparison plot at 0% 0.025% and 0.05% HNF with 2% deviation margin line, all regions of correlated equation line fall between the 2% margin line, and almost all experimental data also fall between the margin line.

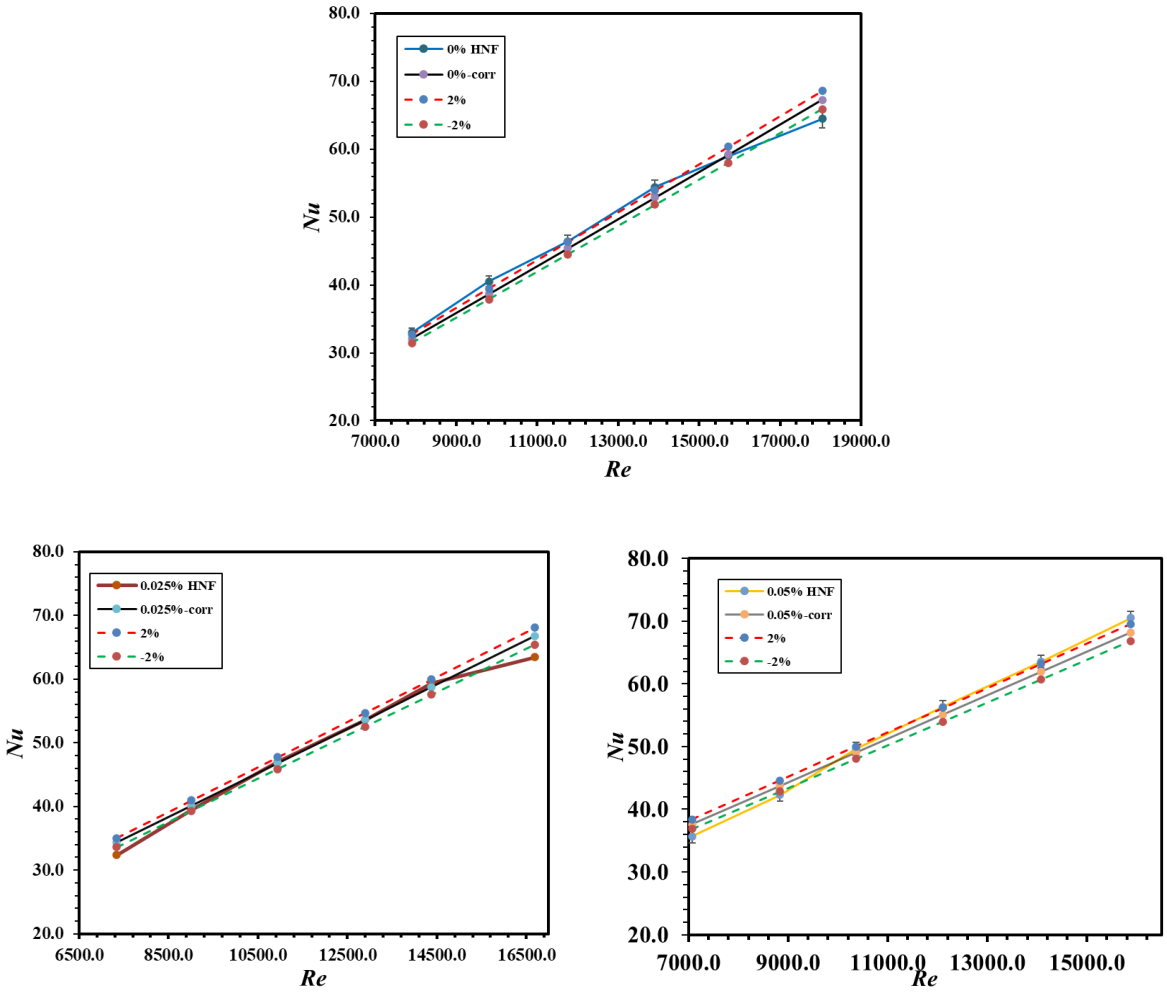

Figure 26 Correlation and experimental results comparison plot at (a) 0% (b) 0.025% and (c) 0.05% HNF

7 Health and safety

The potential risks from exposure to nanoparticles have been highlighted in numerous studies. Therefore, to work safely with nanoparticles, comprehensive research is needed to be done on the health and safety of using these nanomaterials. (EILEEN D. KUEMPEL, 2012) studied matter of the potential safety risks in the use of nanoparticles. They presented nanoparticles are the primary occupational health and safety risk (OHS) associated with NFs. So, an understanding of various particles and their toxicology is needed.

The toxicity of nanoparticles and CNT are not well reported in the literature. CNTs can be bio-persistent and can exist as fiber-like structures. There are currently limited studies reported in the literature on the health effects of CNTs on human beings. However, the use of CNTs is not yet widespread, and there can be a long wait before any disease development is discovered. Animal studies are done to study its effects on humans, showing adverse lung effects (Susana P.B. Sousa, 2020). NIOSH (2010) also reports that animal studies have demonstrated asbestos-type pathology associated with exposure to more extended, straighter CNT structures.

The health hazard is depended on the type of nano-material and the body involved exposure level. For example, (Castillo, 2013) if toxic nanomaterials are inhaled, they can be deposited in the respiratory tract and cause significant damage to tissues and lungs cells, but some other natural nanomaterial cannot have the same degree of damaging effect to the human body. Nanomaterials can act as chemical catalysts and create unanticipated chemical reactions, causing fires and explosions; for example (sugar or wood) need less energy to ignite than other matter particles.

The use of nanomaterials for research is expanding. Employers should gain more information about the potential risk of nanomaterials to control potential exposures. It is suggested that employees should be provided with adequate air filters (HEPA9) and ventilated enclosers with glove boxes and laboratory hoods. It is also recommended that employees hand regularly wash to practice safe hygiene at stop intervals. The spilling of nanomaterial can cause hazards to the environment. It is recommended that proper method followed for cleaning up process. For instance, use wet wiping and vacuum cleaners with HEPA filters to clean up dust clouds instead of dry sweeping or compressed air clean up. Provide personal protective equipment like respirators, gloves, and protective clothing—medical screening.

Different safety structures were manufactured and fitted around the testing rig. Mainly there were two types of shielding; testing section and central shield. The testing section was covered with an initial cylindrical tube to prevent splashing and allow fluid to flow back to the return reservoir. The central shield comprises a fitted Perspex Glass covering the entire rig and preventing particles from splashing and exiting the rig. A large tray is placed under the testing rig to collect leakages or splashes. An emergency water spray system was installed on the setup, which was connected to the water supply located behind the rig. Caution and personal protective equipment (PPE) are critical factors throughout the various cooling tests besides safety in systems structures. The PPE comprises chemical-resistant gloves, safety shoes and eye goggles, a respiratory mask (HEPA), and a laboratory coat.

8 Conclusion

From this research study, we have successfully prepared a hybrid fluid that is capable of heat transfer enhancement compared to its base fluid, stating that nano particle additions in the fluid can have a positive effect on the transfer of energy. Many applications should benefit from this conclusion because we have successfully improved heat transfer without compromising space or pumping power. Many Jet cooling applications such as microchips, turbine and engine cooling are all related to jet cooling applications. There are some conclusions on the effect of using MWCNT-Al_2O_3 as a working fluid in the jet cooling system indicated as,

Hybrid nanofluid:

(1) The negative value of -37 mV of the zeta potential on MWCNT and Al_2O_3 nanoparticles are measured.

(2) The surface tension decreases with particle concentration increasing for all cases except for the lowest concentration HNF.

(3) The thermal conductivity was relatively increasing when adding particles to the base fluid. The 0.15% HNF saw the most significant change in thermal conductivity. The difference in thermal conductivity increased linearly as particle vol% increases in the HNF.

(4) It was also observed for the viscosity measurement of the HNF, the highest particle vol% concentration fluid has the highest viscosity, and the increase is linear with an increase in particle vol%.

Jet Cooling by HNFs in Experiment:

(5) The maximum cooling rate was reported for the nanofluid with a particle volume concentration of 0.15%.

(6) In a steady-state flow regime, an increase in the value of the Re number leads to a higher Nusselt number.

(7) The HTC was seen to increase as vol% concentration was increased; however, after the 0.05vol% concentration of the HTC started to have a decreasing trend. The 0.15vol% and 0.1vol% are almost evenly enhanced.

(8) The maximum augmentation in Nusselt number was evaluated for 0.05vol% with a 17% increase compared to DI water.

(9) When considering Weber's analysis, improvements of 9% and 16.7% in Nu number are evaluated for 0.05vol% HNF compared to distilled water and 0.15vol% HNF. The 0.05vol% HNF is the best performance fluid, and the 0.15vol% fluid is the worst and harms the Nusselt number, as seen by the curves lower than DI water.

(10) Considering the Péclet number analysis, the 0.05vol% HNF has the most significant improvement in the Nusselt number. The maximum enhancement of 9.75% is observed at the highest Péclet number of 202000.

Jet Cooling by HNFs in CFD:

(11) It is evident that by increasing Re and vol% of nanoparticles, both Nu number and HTC increase. Maximum improvement of 19.7% in Nusselt number is seen by the 0.15 vol% particle concentration fluid, and the improvement in the 0.05vol% particle concentration fluid is 13.7% compared to the experiment value of 17%.

(12) The best performing fluid is the 0.15vol% particle concentration fluid with relaxations time 1 second compared to 1.75 seconds in experiment and steady-time (the time the cooling curve is approaching infinity line) is 23 seconds compared to 33 seconds in an experiment.

Recommendations:

It is well concluded that at Re=16000, the effect of Rayleigh-Taylor instability is evident. Rayleigh-Taylor instability happens between two fluids with different densities causes the waveform shape in the flow regime due to the interactions between the particles of two fluids. In the experiment, a high-Speed camera is suggested to capture the boundary layer thickness for varying particle vol% concentrations of the MWCNT-Al_2O_3 nano-fluid in the jet impingement to see the effect of these boundary layer thickness on the HTC and Nusselt number similar to the study of Sir G.I Taylor (Taylor, 1950) when recognising that Rayleigh's interfacial instability also occurs for accelerations other than gravity. Furthermore, a new experiment configuration should be developed for magnetic effect and testing with different nanofluids at different concentrations and ratios of particles instead of only (10:90) ratio. This study would find an optimum balance of MWCNT and Al_2O_3 nanoparticles in the jet Impingement fluid to achieve the most significant heat transfer rate enhancement. It should also be beneficial to develop a configuration that can test for different gases instead of air only.

9 Reference

A. Ghadimi, R. S. (2011). A review of nanofluid stability properties and characterization in stationary conditions. *Internal Journal heat mass transfer 54*.

A. M. Tiara, S. C. (2016). Effect of alumina nanofluid jet on the enhancement of heat transfer from a steel plate. *Springer-Verlag Berlin Heidelberg- heat and mass transfer*.

A. R. Moghadassi, S. M. (2009). *A MODEL OF NANOFLUIDS EFFECTIVE THERMAL CONDUCTIVITY.* Journal of Thermal Analysis and Calorimetry, Vol. 96 (2009).

A.K. Singh, V. R. (2008). Microwave synthesis of silver nanofluids with polyvinylpyrrolidone (PVP) and their transport properties. *Colloid Plym Sci.*

Adnan, M. (2017). Thermal performance and thermal properties of hybrid nanofluid laminar flow in a double pipe heat exchanger. *Experimental Thermal and Fluid Science*, 37-45.

Afshin Ahmadi Nadooshan, H. E. (2018). Measuring the viscosity of Fe3O4-MWCNTs/EG hybrid nanofluid for evaluation of thermal efficiency: Newtonian and non-Newtonian behavior. *Journal of Molecular Liquids*, 169-177.

Amin Asadi, I. M. (2020). An experimental study on characterization, stability and dynamic viscosity of CuO-TiO2/water hybrid nanofluid. *Journal of Molecular Liquids*.

Amin, J. (2018). Two-phase modeling of magnetic nanofluids jets over a Stretching/shrinking wall. *Thermal Science and Engineering Progress*, 375–384.

Amir Asadikiaa, S. A. (2020). Characterization of thermal and electrical properties of hybrid nanofluids prepared with multi-walled carbon nanotubes and Fe2O3 nanoparticles. *International Communications in Heat and Mass Transfer*.

Amir Kakavandi, M. A. (2018). Experimental investigation of thermal conductivity of nanofluids containing of hybrid nanoparticles suspended in binary base fluids and propose a new correlation. *International Journal of Heat and Mass Transfer*.

Andrew W. Cook, D. Y. (2009). Rayleigh-Taylor instability and mixing. *Scholarpedia*, 4(2):6092.

Aparna Z, M. M. (2019). Thermal conductivity of aqueous Al2O3/Ag hybrid nanofluid at different temperatures and volume concentrations: An experimental investigation and development of new correlation function. *Powder Technology*, 714-722.

B. Boudraa, R. B. (2021). Numerical investigation of jet impingement cooling an isothermal surface using extended jet holes with various binary hybrid nanofluids. *International Communications in Heat and Mass Transfer*.

Balla, H. (2013). Numerical study of the enhancement of heat transfer for hybrid CuO-Cu Nanofluids flowing in a circular pipe. *Journal of oleo science*.

Beringer, J. (2012). *Review of particle physics.* Physical Review D - Particles, Fields, Gravitation and Cosmology.

Bharat A. Bhanvase, V. B. (2018). *Nanomaterials for Green Energy-A volume in Micro and Nano Technologies.* Elsevier.

Bhattacharjee, S. (2016). DLS and zeta potential – What they are and what they are not? *Journal of Control*.

Bin Sun, Y. Z. (2019). Experimental study on heat transfer characteristics of hybrid nanofluid impinging jets. *Applied Thermal Engineering*, 556-566.

Brinkman, H. (1952). *The viscosity of concentrated suspensions and solutions.* The Journal of Chemical Physics.

Carla Grobler, M. S. (2015). Experimental Study on Cavity Flow Natural Convection in Porous Medium Saturated with Al203 60% EG-40% Water... *11th International Conference on Heat Transfer, Fluid Mechanics and Thermodynamics.* https://www.researchgate.net/publication/281550930.

Castillo, A. M. (2013). *Nanomaterials and workplace health & safety.* European Trade Union Institute.

Constanza Toledo, R. C. (2021). Binary Medical Nanofluids by Combination of Polymeric Eudragit Nanoparticles for Vehiculization of Tobramycin and Resveratrol: Antimicrobial, Hemotoxicity and Protein Corona Studies. Journal of Pharmaceutical Sciences, 1739-1748.

Dan Huang, Z. W. (2016). Effects of hybrid nanofluid mixture in plate heat exchangers. *Experimental Thermal and Fluid Science*, 190-196.

Deqing Mei, Y. F. (2021). *Analysis of surface tension for nano-fuels containing disparate typesof suspended nanoparticles.* Powder Technology 388 (2021) 526–536.

Dr. Ashwini Kumar, A. K. (2020). Heat Transfer and Pumping Characteristics of Nanofluid Jet Impingement. *National Conference on Conventional Energy Resources & Technologies India*.

Dunn, P. F. (2014). *Measurement and Data Analysis for Engineering and Science 3rd Edition 9780429169168.* Boca Raton: https://doi.org/10.1201/b16918.

E.V. Timofeeva, J. R. (2009). Particle shape effects on thermophysical properties of alumina nanofluids,. *Journal of applied physics*.

EILEEN D. KUEMPEL, C. L. (2012). Risk Assessment and Risk Management of Nanomaterials in the Workplace: Translating Research to Practice. *The Annals of Occupational Hygiene, Volume 56, Issue 5*, 491-505.

Enrique-Manuel Garcia-Merida, A. A.-C.-C. (2021). Numerical Analysis of the Cooling of a Flat Plate Using Nanofluids at Low and High Reynolds Numbers. *Heat Transfer Engineering Volume 42*, 1648-1662.

Eric C. Okonkwo, I.-O. D. (2019). Comparison of experimental and theoretical methods of obtaining the thermal properties of alumina/iron mono and hybrid nanofluids. *Journal of Molecular Liquids*.

Esmaeil Jalali, O. A. (2019). Heat Transfer of Oil/MWCNT Nanofluid Jet Injection Inside a Rectangular Microchannel. *Symmetry* .

Essam M. Elsaid, M. S.-w. (2021). Mixed convection hybrid-nanofluid in a vertical channel under the effect of thermal radiative flux. *Case Studies in Thermal Engineering*.

Everts, M. (2014). *Heat transfer and pressure drop of developing flow in smooth tubes in the transitional flow regime.* Pretoria: University of Pretoira Web.

Farid Soltani, D. T. (2020). Experimental measurements of thermal conductivity of engine oil-basedhybrid and mono nanofluids with tungsten oxide (WO3) and MWCNTs inclusions. *Powder Technology*.

Faroogh Garoosi, G. B. (2013). Numerical simulation of natural convection of nanofluids in a square. *International Journal of Heat and Mass Transfer 67 (2013) 362–376*.

Fatih Selimefendigila, H. F. (2020). Al2O3-Water Nanofluid Jet Impingement Cooling With Magnetic Field. *Heat Transfer Engineering*.

Fazel Hosseinzadeh, F. S.-K. (2016). *Numerical Investigation of the Nanoparticle Volume Fraction Effect on the Flow, Heat Transfer, and Entropy Generation of the Fe3O4 Ferrofluid under a Non-uniform Magnetic Field.* Strojniški vestnik - Journal of Mechanical Engineering 62(2016.

Fei Xue, M. E. (2019). FLOW AND HEAT TRANSFER IN A RIB-ROUGHENED TRAILING-EDGE COOLING CHANNEL WITH CROSSOVER IMPINGEMENT. *International Journal of Gas Turbine, Propulsion and Power Systems Volume 10*.

Gabriela Huminic, A. H. (2020). Study of the thermal conductivity of hybrid nanofluids: Recent research and experimental study. *Powder Technology*.

Georgiana Madalina Moldoveanu, G. H. (2018). Experimental study on thermal conductivity of stabilized Al2O3 and SiO2 nanofluids and their hybrid. *International Journal of Heat and Mass Transfer*.

H.H, B. (2013). Numerical study of the enhancement of heat transfer for hybrid CuO-Cu Nanofluids flowing in a circular pipe. *Journal of oleo science*.

Hadi Ghodsinezhad, M. S. (2016). Experimental investigation on cavity flow. *International Communications in Heat and Mass Transfer*.

Hemat Ranjbar, M. R.-N. (2015). *Experimental and theoretical investigation on Nano-fluid surface tension.* Journal of Natural Gas Science and Engineering 27 (2015) 1806e1813.

HIKMET Ş. AYBAR, M. S. (2015). *A Review of Thermal Conductivity Models for Nanofluids.* Heat Transfer Engineering.

Ho Chang, H. T. (2008). *SYNTHESIS AND MAGNETIC PROPERTIES OF Ni.* Taipei: Natinal Taipei University of Technology.

Hussein, A. M. (2017). Thermal performance and thermal properties of hybrid nanofluid laminar flow in a double pipe heat exchanger. *Experimental Thermal and Fluid Science*, 37-45.

I.M. Krieger, T. D. (1959). A mechanism for non-Newtonian flow in suspensions of rigid spheres. *Transactions of the Society of Rheology*.

Ishita Sarkar, S. C. (2019). Application of TiO2 nanofluid-based coolant for jet impingement quenching of a hot steel plate. *EXPERIMENTAL HEAT TRANSFER VOL. 32, NO. 4*, 322–336.

J. Koo, C. K. (2004). A new thermal conductivity model for nanofluids. *Journal of Nanoparticle Research*.

J.C. Joubert, M. S. (2017). *Enhancement in heat transfer of a ferrofluid in a differentially heated square cavity through the use of permanent magnets.* Pretoria: Journal of Magnetism and Magnetic Materials 443 (2017) 149–158.

Jafarimoghaddam, A. (2018). Two-phase modeling of magnetic nanofluids jets over a Stretching/shrinking wall. *Thermal Science and Engineering Progress 8 (2018)*, 375–384.

K Marzec, A. K.-P. (2014). Heat transfer characteristic of an impingement cooling system with different nozzle geometry. *Journal of Physics: Conference Series 530 012038: XXI Fluid Mechanics Conference*.

Karimi, A., Goharkhah, M., Ashjaee, M., & Shafii, M. B. (2015). *Thermal Conductivity of Fe2O3 and Fe3O4 Magnetic Nanofluids Under the Influence of Magnetic Field.* International Journal of Thermophysics, Volume 36, Issue 10-11, pp. 2720-2739.

Kashinath Barik, S. C. (2020). The enhancement of laminar jet cooling effectiveness at very high surface temperature by using Al2O3 nanofluid as a coolant. *WIlEY Heat transfer Asian Research*.

KeNan Liu, Y. Z. (2021). Improved heat transfer of the engine oil by changing it to hybrid nanofluid: Adding hybrid nano-powders. *Powder Technology*, 56-64.

Khalil Khanafer, K. V. (n.d.). *A critical synthesis of thermophysical characteristics of nanofluids.* 2011: International Journal of Heat and Mass Transfer 54 (2011) 4410–4428.

Kulvir K Dhinsa, C. J. (2004). TURBULENCE MODELLING AND IT'S IMPACT ON CFD PREDICTIONS FOR COOLING OF ELECTRONIC COMPONENTS. *Inter Society Conference on thermal phenomena*.

L Syam Sundar, E. V. (2016). Thermal conductivity and viscosity of hybrid nanofluids prepared with magnetic nanodiamond-cobaltoxide (ND-Co3O4) nanocomposite. *Case Studies in Thermal Engineering*.

L. Colla, L. F. (2012). Water-Based Fe2O3 Nanofluid Characterization: Thermal Conductivity and ViscosityMeasurements and Correlation. *Advances in Mechanical Engineering* .

L. Syam Sundar, M. K. (2013). *Investigation of thermal conductivity and viscosity of Fe3O4.* International Communications in Heat and Mass Transfer 44 (2013) 7–14.

L. Syam Sundar, M. K. (2017). Experimental investigation of the thermal transport properties of graphene oxide/Co3O4 hybrid nanofluids. *International Communications in Heat and Mass Transfer*.

L. Syam Sundara, Z. S. (2020). Combination of Co3O4 deposited rGO hybrid nanofluids and longitudinal strip inserts: Thermal properties, heat transfer, friction factor, and thermal performance evaluations. *Thermal Science and Engineering Progress*.

Li, J. (2008). *Computational analysis of nanofluid flow in microchannels with applications to micro-heat sinks and bio-MEMS.* North Carolina ,PhD.

Lupton T. L, M. D. (2008). *The effect of varying confinement levels on the heat transfer to a miniature impinging air jet.* Eindhoven, Netherlands: Eurotherm.

M. Molana, S. B. (2013). *Investigation of Heat Transfer Processes Involved Liquid Impingement Jets: A review.* Brazil: Brazilian Journal of Chemical Engineering Vol. 30, No. 03.

M.R. Mohaghegh, A. B. (2019). Single- and two-phase water jet impingement heat transfer on a hot moving surface. *Journal of Thermal Analysis and Calorimetry 137:1401–1411*.

M.Reza Azizian, P. D. (2008). Thermo physical Properties of Nanofluid. *Thermo physical Properties of Nanofluid*, (p. all).

Maxwell, J. C. (1873). *Maxwell on Heat and Statistical Mechanics:*. Bethlehem ,london: University association press.

Mikako Takeda, T. O. (2009). *Physical Properties of Iron-Oxide Scales on Si-Containing Steels.* JAPAN: Materials Transactions, Vol. 50, No. 9 (2009) pp. 2242 to 2246.

Mingzheng Zhou, G. X. (2015). Heat transfer performance of submerged impinging jet using silver nanofluids. *Springer-Verlag Berlin Heidelberg- heat and mass transfer*.

Miroslave kmecova, O. S. (2019). Circular Free Jets: CFD Simulations with Various Turbulence Models and Their Comparison with Theoretical Solutions. *IOP Conf. Series: Materials Science and Engineering 471*.

Mohsen Amjadiana, H. S. (2020). Heat transfer characteristics of impinging jet on a hot surface with constant heat flux using Cu2O–water nanofluid: An experimental study. *International Communications in Heat and Mass Transfer*.

Mostafa Mahdavia, M. M. (2020). Fluid flow and heat transfer analysis of nanofluid jet cooling on a hot surface with various roughness. *International Communications in Heat and Mass Transfer 118*.

Muhammad Ali Rob Sharif, K. K. (2009). Evaluation of Turbulence Models in the Prediction of Heat Transfer Due to Slot Jet Impingement on Plane and Concave Surfaces. *Numerical Heat Transfer Fundamentals 55(4)*, 273-294.

Muhammad Saqib, I. K. (2020). RECENT ADVANCEMENT IN THERMOPHYSICAL PROPERTIES OF NANOFLUIDS AND HYBRID NANOFLUIDS: AN OVERVIEW. *International Journal of Computational Analysis*.

Munish Guptaa, V. S. (2020). Heat transfer analysis using zinc Ferrite/water (Hybrid) nanofluids in a circular tube: An experimental investigation and development of new correlations for thermophysical and heat transfer properties. *Sustainable Energy Technologies and Assessments*.

N. Ali, J. T. (2018). A review on nanofluids: fabrication, stability, and thermophysical properties. *Jornal of nanomatter*.

Naimish S. Pandya, A. N. (2021). Influence of the geometrical parameters and particle concentration levels of hybrid nanofluid on the thermal performance of axial grooved heat pipe. *Thermal Science and Engineering Progress*.

Neeshoun Asokan, P. G. (2020). Experimental investigation on the thermal performance of compact heat exchanger and the rheological properties of low concentration mono and hybrid nanofluids containing Al2O3 and CuO nanoparticles. *Thermal Science and Engineering Progress*.

O. Zeitoun, M. A.-A. (2013). The Effect of Particle Concentration on Cooling of a Circular Horizontal Surface Using Nanofluid Jets. *Nanoscale and Microscale Thermophysical Engineering*.

O'Hanley, H. (2012). Measurement and model validation of nanofluid specific heat capacity with differential scanning calorimetry. *Advances in Mechanical Engineering*.

Oronzio Manca, P. M. (2011). Numerical study of a confined slot impinging jet Numerical study of a confined slot impinging jet. *Nanoscale Research Letters*.

P.V.S.N. Murthy, C. R. (9 July 2013). *Magnetic effect on thermally stratified nanofluid saturated non-Darcy porous.* International Communications in Heat and Mass Transfer 47 (2013) 41–48.

Pak B.C, Y. C. (1998). Hydrodynamic and heat transfer study of dispersed fluids with submicron metallic oxide particles. *Experimental Heat Transfer an International Journal,*.

Pradip Radhakrishnan Subramaniam, S. C. (2012). *United states of America Patent No. US20120023969 A1,US 12/845,017*.

Praveen Kumar Kanti, K. S. (2021). Experimental investigation on thermo-hydraulic performance of water-based fly ash–Cu hybrid nanofluid flow in a pipe at various inlet fluid temperatures. *International Communications in Heat and Mass Transfer*.

RR. P. Chhabra, V. S. (2017). *Coulson and Richardson's Chemical Engineering: Volume 1A: Fluid Flow: Fundamentals and Applications (Coulson & Richardson's Chemical Engineering) 7th Edition.* Butterworth-Heinemann.

R. Vold, M. V. (1983). Colloid and interface chemistry. *Reading, MA: Addison-Wesley Pub. Co,*.

R.L Hamilton, O. C. (1962). Thermal conductivity of heterogeneous two-component systems. *Industrial & Engineering chemistry fundamentals,*.

Rapp, B. E. (2017). *Microfluidics: Modeling, Mechanics and Mathematics: A volume in Micro and Nano Technologies.* Elsevier.

Ravikiran Balaga, K. B. (2019). Effect of temperature, total weight concentration and ratio of Fe2O3 and f-MWCNTs on thermal conductivity of water based hybrid nanofluids. *Materials Today: Proceedings*.

Rayleigh, L. (1883). Investigation of the character of the equilibrium of an incompressible heavy fluid of variable density. *Proceedings of the London Mathematical Society*, 14:170-177.

Recep Ekiciler, M. S. (2021). A comparative heat transfer study between monotype and hybrid nanofluid in a duct with various shapes of ribs. *Thermal Science and Engineering Progress*.

Reza Bakhtiari, B. K. (2021). Preparation of stable TiO2-Graphene/Water hybrid nanofluids and development of a new correlation for thermal conductivity. *Powder Technology*.

Roozbeh Taherialekouhi, S. R. (2019). An experimental study on stability and thermal conductivity of water-graphene oxide/aluminum oxide nanoparticles as a cooling hybrid nanofluid. *International Journal of Heat and Mass Transfer*.

S. Aminossadati, B. G. (2009). Natural convection cooling of a localised heat source at the bottom of a nanofluid-filled enclosure. *European Journal of Mechanics-B/Fluids*.

S. Chakraborty, I. S. (n.d.). Synthesis of Cu-Al LDH nanofluid and its application in spray cooling heat transfer of a hot steel plate. *Powder Technol*.

S. Zeinali Heris, H. S. (23 January, 2012). *The effect of magnetic field and nanofluid on thermal performance of two-phase closed thermosyphon (TPCT).* International Journal of the Physical Sciences Vol. 7(4), pp. 534 - 543,.

S.M. Mousavi, F. E. (2019). A detailed investigation on the thermo-physical and rheological behaviorof MgO/TiO2aqueous dual hybrid nanofluid. *Journal of Molecular Liquids 282 (2019) 323–339*.

S.O Giwa, M. S. (2020). Experimental study of thermo-convection performance of hybrid nanofluids of Al 2 O 3 -MWCNT/water in a differentially heated square cavity. *International Journal of Heat and Mass Transfer 148*.

Saad Tanvir, L. Q. (2012). Surface tension of Nanofluid-type fuels containing suspended nanomaterials. Nanoscale Res Lett, 18;7(1):226.S.Sh.Hosseini, S. V. (2011). *A Review of*

Relations for Physical Properties of Nanofluids. Iran: Australian Journal of Basic and Applied Sciences.

SAHEED A ADIO, M. S. (2015). Factors affecting the pH and electrical conductivity of MgO–ethylene glycol nanofluids. *Bulletin of Materials Science 38*, 1345-1357.

Samarshi Chakraborty, P. K. (2020). Stability of nanofluid: A review. *Appliend Thermal Engineering* .

Shivani S. Chawhan, D. P. (2021). Investigation on thermophysical properties, convective heat transfer and performance evaluation of ultrasonically synthesized Ag-doped TiO2 hybrid nanoparticles based highly stable nanofluid in a minichannel. *Thermal Science and Engineering Progress*.

Suleiman Akilu, A. T. (2018). Properties of glycerol and ethylene glycol mixture based SiO 2 - CuO/C hybrid nanofluid for enhanced solar energy transport. *Solar Energy Materials and Solar Cells (IF7.267)*.

Suleiman Akilu, A. T. (2019). Characterization and modelling of density, thermal conductivity,and viscosity of TiN–W/EG nanofluids. *Journal of Thermal Analysis and Calorimetry*.

Susana P.B. Sousa, T. P. (2020). Health and Safety Concerns Related to CNT and Graphene Products, and Related Composites. *Journal of Composites Science* .

Swinehart, D. (1962). The Beer-Lambert law. *Journal Chemica Education 39*.

T.-H. Tsai, L.-S. K.-H.-T. (2009). *Thermal Conductivity of Nano°uid with Magnetic Nanoparticles.* PIERS ONLINE, VOL. 5, NO. 3.

Tahar Tayebi, A. J. (2016). Free convection enhancement in an annulus between horizontal confocal elliptical cylinders using hybrid nanofluids. *An International Journal of Computation and Methodology; Numerical Heat Transfer, Part A: Applications*.

Taylor, G. (1950). The instability of liquid surfaces when accelerated in a direction perpendicular to their planes. *Proceedings of the Royal Society of London*, A201:192-196.

Timothy Anderson, J. C. (2014). *Natural Convection Heat Loss from an Open Room* . Auckland: researchgateway.ac.nz.

Ting-zhen MING, Y. D.-l.-x. (2015). Transient thermal behavior of a microchannel heat sink with multiple impinging jets. *ournal of Zhejiang University-SCIENCE A (Applied Physics & Engineering)*, 894 -906.

V. Murali Krishna, M. S. (2021). Numerical investigation of heat transfer and pressure drop for cooling of microchannel heat sink using MWCNT-CuO-Water hybrid nanofluid with different mixture ratio. *Materials Today: Proceedings*, 969-974.

V.Vicki Wanatasanapana, M. A. (2020). Effect of TiO2-Al2O3 nanoparticle mixing ratio on the thermal conductivity, rheological properties, and dynamic viscosity of water-based hybrid nanofluid. *Journal-of-materials-research-and-technology*.

W. Yu, S. C. (2003). The role of interficial layers in the enhanced thermal conductivity of nanofluids: a renovated maxwell model. *Journal of nanoparticle research*.

Wajiha Tasnim Urmia, M. R. (2020). An experimental investigation on the thermophysical properties of 40% ethylene glycol based TiO2-Al2O3 hybrid nanofluids. *International Communications in Heat and Mass Transfer*.

Wang Peng, L. J. (2014). A Numerical Investigation of Impinging Jet Cooling with Nanofluids. *Nanoscale and Microscale Thermophysical Engineering* .

Webb, B. W. (1995). Single-Phase Liquid Jet Impingement Heat Transfer. *J. P. Hartnett (Ed.), Advances in Heat Transfer,*, 105-217.

Wilken, N. J. (2019). *Experimental investigation of free-surface jet-impingement cooling by means of TiO2-water nanofluids.* Pretria: University of Pretoria- Web published.

Xuan, Y. a. (2000). *Conceptions for Heat Transfer Correlation of Nanofluids.* International Journal of Heat and Mass Transfer.

Y. Li, J. Z. (2009). A Review on developement of nanofluid preparation and characterization. *Powder Tecnol*.

Yanfang Zhu, M. Z. (2021). MWCNT-WO3/water-ethylene glycol antifreeze hybrid nanofluid MWCNT-WO3/water-ethylene glycol antifreeze hybrid nanofluid. *Journal of Molecular Liquids*.

Yaohua ZHAO, T. M.-F. (2002). Conjugated Heat Transfer on a Horizontal Surface Impinged by Circular Free-Surface Liquid Jet. *JSME international journal. Ser. B, Fluids and thermal engineering*, 307-314.

Yunus A.Cengel, A. J. (2015). *Heat and mass transfer,fundamentals & application.* New York: McGraw-Hill Education.

Zekavat, S. A. (2013). *Electrical Engineering Concepts and Applications.* Upper Saddle River, New Jersey: Pearson Higher Education.

10 Appendix

Appendix A: Thermocouple Calibration.

Thermocouples are essential experiment equipment and therefore need to be calibrated well. Both K–type and t-type thermocouples used here are based on the two different electrical conductors that join at various temperatures. All thermocouples do not produce the same accuracy. There is always a deviation due to many factors, such as the data channel and logger used for capturing. The manufacturers' data must be checked, and the thermocouples must be calibrated for a successful experiment. A simple calibration was carried out to test for flow meter accuracy. The flow meter was calibrated with the pump power, and a volumetric reading was done to compare the flow meter reading. A thermal bath (Polyscience PD20R-A12E, USA, -+0.005°) is utilized at a stable temperature to test all eleven critical thermocouples used in the experiment. The temperature of the thermocouple is compared to that of a thermal bath which uses internal PT-100 probes (0.1°C accuracies). Temperature between 10°C and 60°C was used with increments of 5°C. The average of the 50 readings of the thermocouple was designed against the average temperature by a thermal bath PT-100 probes. Utilizing a similar technique to (Wilken 2019), the excel built-in Regression function was employed to test the data set for accuracy level.

The linear regression function is defined as Equation (A.1):

$$T_{cal} = \frac{T_{uncal} - c}{\hat{m}} \tag{A.1}$$

Where the $\hat{m}$ And c is the slope and intercept of the thermocouple and thermal bath temperature line when a plot against one another. The values of slopes and intercepts for each thermocouple are shown below in Table 7. The intercept is all negative, meaning that the thermocouple temperature was read slightly less than the thermal bath temperature.

Table 7 Slopes and Intercepts of the thermocouple calibration regression function.

Thermo-Couple	Slope$\hat{m}$	Intercept c
1	1.00012	-0.50938
2	0.999266	-0.4912
3	1.002514	-0.5756
4	1.000786	-0.50346
5	1.000087	-0.50666
6	1.00046	-0.51809
7	1.000184	-0.5047
8	0.999933	-0.5132
9	0.998669	-0.46192
10	0.999825	-0.50682
11	0.998975	-0.45663

Two different thermos-couples were chosen to plot the uncalibrated and calibrated temperature as shown in Figure 27 to Figure 30 below. Four calibrated and uncalibrated temperatures of approximately 10,25,40,55 was selected and devised.

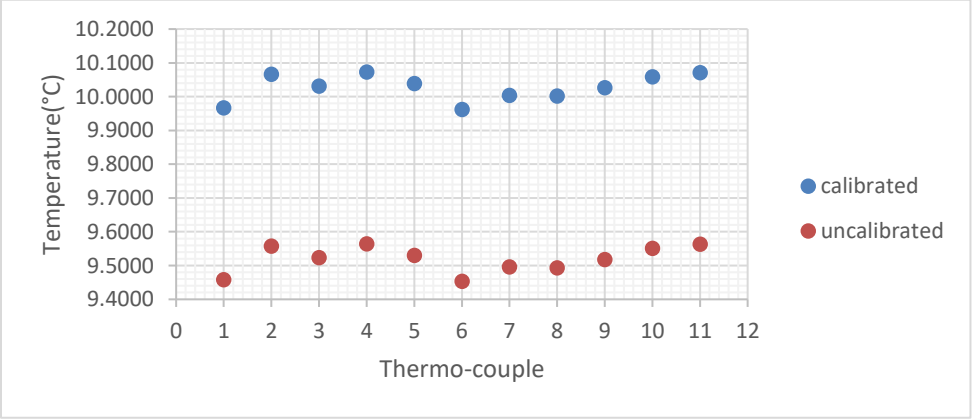

Figure 27 Calibrated and un-calibrated thermocouples temperature readings at approximately 10°C

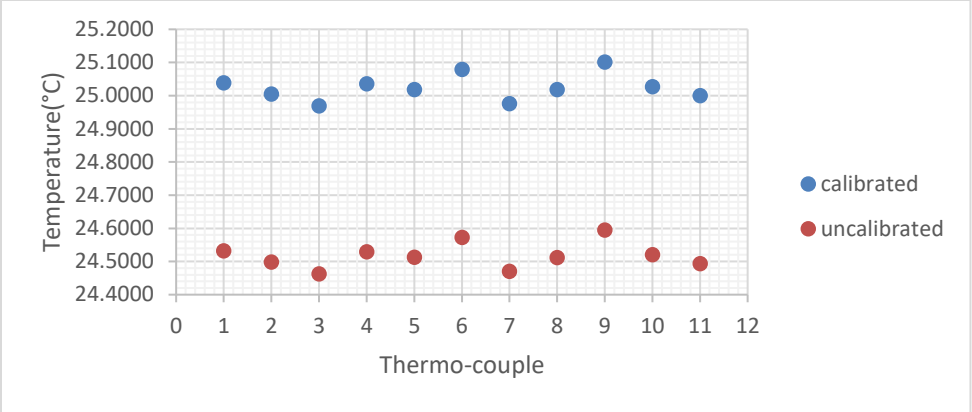

Figure 28 Calibrated and un-calibrated thermocouples temperature readings at approximately 25°C

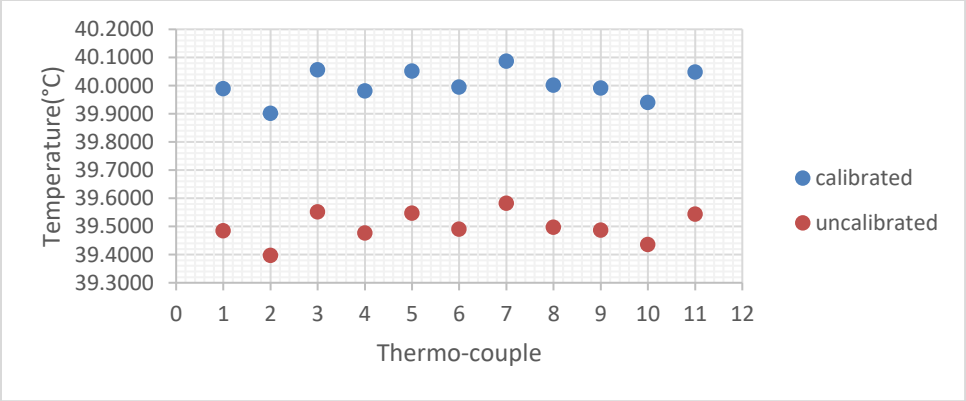

Figure 29 Calibrated and un-calibrated thermocouples temperature readings at approximately 40°C

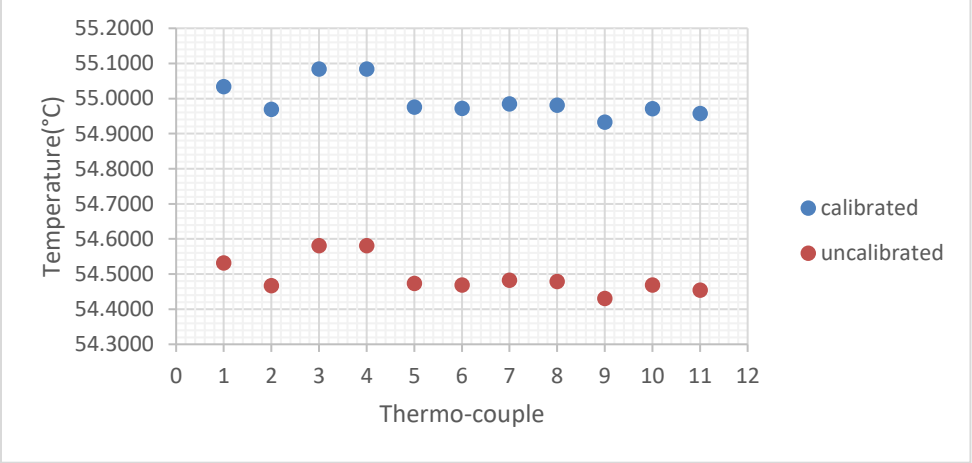

Figure 30 Calibrated and un-calibrated thermocouples temperature readings at approximately 55°C

The above Figures (27-30) indicate that the calibration process was successful, with an average deviation of 0.3°C in the thermocouple temperature. The uncertainty of the thermocouple was calculated as 0.2°C, which correlated to the manufacturer's specifications.

The process of calibration for the eleven thermal couples in the experiment was considered, where six K-type and five T-type thermocouples were calibrated. Calibration creates the most thermocouple uncertainty of 0.119 ℃. The thermocouples were not soldered onto the set-up, but they were fixed by other means. The thermocouples were coated in an appropriate silicone thermal paste supplied by (Unick Chemical Corp.) to eliminate any air gaps in the heated copper cylinder.

Appendix B: Sample Calculation

All calculation sheet sample calculations are done at max Reynolds number and the 0.1% particle volume concentration HNF.

Flow reading using volumetric measuring method:

$$\dot{V}=\frac{V}{t}$$

$$=\frac{1.1}{0.5}=2.2\frac{l}{min}$$

Flow reading using the Burkert Ultrasonic flow meter, the correlation for the meter is shown in Table 8 below:

Table 8 Burket Ultrasonic Flowmeter correlation

flow meter correlation	
Current(mADC)	Flow(litre/min)
4.000	0.1
4.673832	$\dot{V}=$
20.000	50

Average reading from experimental data: DC current=4.090 mADC there for the flow rate is calculated as;

$$\dot{V}=\frac{(50\text{-}0.1)(4.673832\text{-}4.00)}{20\text{-}4}+0.1=2.20151\frac{litre}{min}=3.667\times10^{-5}m^3/s$$

The diameter of the Jet is 1.65mm; therefore, the area of the jet is $A_j = 2.138 \times 10^{-6}\ m^2$ and therefore, the velocity of the jet is 17.1515m/s using the flow rate calculated above from the flow meter.

The experimental bulk fluid temperature is 11.0605°C calculated using a jet inlet temperature of 10.01°C and exit temperature of fluid of 12.111°C, and all water properties were calculated at Bulk fluid temperature.

$$\rho_w=995.9483738\ kg/m^3$$

$$\mu_w = 0.001546052 \frac{kg}{ms}$$

$$k_w = 0.58412612 \text{ W/mk}$$

$$C_{p,w} = 4189.576775 \text{ J / kgK}$$

The density of HNF is calculated using Equations (5.3) found in section 5 of the report.

$$\rho_{hnp} = (0.1*\rho)_{Al_2O_3} + (0.9*\rho)_{MWCNT} = 2287 \text{ kg/m3}$$

$$\rho_{hnf} = (1-\varphi)\rho_{bf} + \rho_{hnp}\varphi$$

$$= (1-0.001)995.9483 + (2287*0.001) = 997.2394 \text{ kg/m}^3$$

The specific heat of HNFis calculated using Equation (5.4) found in section 5 of the report.

$$C_{p,hnp} = \left(0.1*C_p\right)_{Al_2O_3} + \left(0.9*C_p\right)_{MWCNT} = 715.5 \text{ J/kgK}$$

$$C_p = \frac{(1-\varphi)\left(\rho C_p\right)_{bf} + \varphi C_{p,hnp}\rho_{hnp}}{\rho_{hnf}}$$

$$= \frac{(1-0.001)(995.9483)(4189.576) + (0.001*715.5*2287)}{997.2394}$$

$$= 4181.6189 \text{ J/kgK}$$

The viscosity of HNF is calculated using the experimental correlation found in section 5 of the report, Equation (5.1)

$$\mu_{hnf} = \mu_{bf}(1.099055 - 0.00166T_{hnf} + 1{,}0855\phi)$$

$$= 0.001546052(1.099055 - 0.00166(11.0605) + 1.0855(0.1) = 0.001839\ kg/ms$$

The thermal conductivity of HNF is calculated using the experimental correlation found in section 5 of the report, Equation (5.2)

$$k_{hnf} = k_{bf}(0.940688 + 0.00428T_{hnf} + 0.4696\phi)$$

$$= 0.58412612\left(0.940688 + 0.00428(11.0605) + 0.469(0.1)\right)$$

$$= 0.6046 \text{ W/mK}$$

The Reynolds number can be found using Equation(4.17) of section 4 of the report

$$Re_{hnf} = \frac{\rho_{hnf} v_j D_j}{\mu_{hnf}} = \frac{997.2394(17.1515)(1.65\times10^3)}{0.001839}$$

$$=15356.8028\ \text{Re}$$

For Nu number the $\dot{q}$,T_s, are found by using the method explained in Equations (5-18,5-19) of section 5 and T_j is found using the average value found using the exit thermocouple (1-5). The inner diameter of the jet nozzle is 1.65mm. The results for surface temperature calculations are shown below in Table 9.

Table 9 Nusselt number calculation table

T(°C)	T(K)	dT	dx	q(J/s)	dx	Tsi(°C)	tsf(°C)
20.06	293.21	1.001	0.004	96304.55	0.003	18.61	18.12
21.06	294.21	3.417	0.006	219241.28	0.007	17.66	
24.48	297.63	3.275	0.008	157601.35	0.013	18.17	
27.76	300.91	5.912	0.010	227607.29	0.021	17.55	
33.67	306.82				0.031	18.6	

$$\dot{q}=-k_s\frac{\Delta T}{\Delta x}$$

$$\dot{q}_{bar}=\frac{\sum_{i=1}^{n}(\Delta x\cdot\dot{q})_{i,i+1}}{\sum_{i=1}^{n}\Delta x_{i,i+1}}=187055.345\ \text{J/s}$$

$$T_{s,i}=T_{TC,i}-\frac{\dot{q}_{bar}\,\Delta x_{s,i}}{k_c}$$

$$T_{surf}=\frac{T_{s,i\,1}+T_{s,i\,2}+T_{s,i\,3}+T_{s,i\,4}+T_{s,i\,5}}{5}=18.118\ ℃$$

$$Nu=\frac{hD_j}{k}=\frac{\dot{q}}{T_s-T_j}\left(\frac{D_j}{k}\right)=\frac{161034.468}{17.277-10.012}\left(\frac{1.65\times10^{3}}{0.5747}\right)=62.96Nu$$

For transient analysis, The Surface temperature for each time-step was calculated using the same Equations (4.15) and (4.16) and method as steady-state analysis. The non-dimensional cooing rate is calculated using Equation (4.21) of section 5.

$$\theta=\frac{Ts-Tj}{Tj}$$

For the volume flow rate enhancement was done at a constant power of the pump, the flow rate was lost due to using the different nanoparticle vol% MWCNT/AL_2O_3(90:10)-water HNF compared to base fluid DI water is calculated using Equation (5-24) from section 5.

$$\dot{V}_{loss}\% = \frac{\dot{V}_w}{\dot{V}_{hnf}}$$

Appendix C: Uncertainty

Numerous measuring instruments, tables, and Equations (including its parameters) are used for the calculation of results. In this section, all uncertainty relating to the Instruments, Equations, and thermal properties used for MWCNT/ Al_2 O_3(90:10)-DI water HNFs investigation is evaluated.

The uncertainty was divided into two sections on for the measuring instruments uncertainly and other for thermal property uncertainty of MWCNT/Al_2O_3(90:10)-DI water HNF. For a single observation, the following Equation (4.25) and Equation (4.26) by (Everts, 2014) and (Dunn, 2014) was used to calculate the uncertainty.

According to (Dunn 2014), regression analysis is utilized to define the relation of two or more variables. They try to test the effects of more than one independent variable on a dependent variable despite multiple forms of regression analysis. The Linear Regression analysis is carried out when one- variable is known. The known variable is the independent variable, and the gained variables are the dependent variable. Due to that, uncertainty arose. After completing the calibration process, A linear regression analysis method was utilized to determine the uncertainty of various thermocouples.

C.1. Instrumentation

A confidence level of 95% was achieved by using 600 points of measurement multiplied by the appropriate time –variables for all instrument measured values. The ultra-sonic-flow meter used (Type 8081, supplied Burkett) was rated to have an accuracy of 0.01% at max and 2% at measured value. The measured value was checked with physical volumetric measurement of all vol% concentrations of MWCNT/Al_2O_3(90:10)-DI water HNFs and the average was found to deviate approximately 2%, which confirms the accuracy provided by the supplier. The thermocouples were calibrated, and the process is explained above in appendix A. The general method was to check the accuracy of each thermocouple in a thermal bath (Polyscience PD20R-30-A12E, USA),

where an internal probe PT-100 with very high accuracy is used to compare the results, and a linear regression method was applied to find the calibrated temperature of thermocouples. The average uncertainty percentage of the eleven thermocouples were found to be 0.119 ℃. The current and voltage measurement was taken using an Amp meter (type 2053) and voltmeter (type 2052), respectively. The test accuracy of these instruments was provided as 0.05A and 5V by the supplier (Yokogama). A Vinier Calliper (Tricle Brand, China) was used to measure the testing section dimensions, including the surface diameter and thermocouples distance used for calculation. According to the manufacturer, the Vernier scale has an accuracy of 0.02mm (Tricle Brand, China).

C.2. Fluid Properties

The base fluid DI-water and HNF MWCNT/AL_2O_3(90:10)-DI water at different vol% concentrations was analysed for the investigation. The uncertainty of all thermo-physical properties used in the calculation was examined.

Water Properties Uncertainty

The water properties used in this investigation for calculation were derived from ((Yunus A.Cengel, 2015)) with accuracy calculated is shown below in Table 10.

Table 10 Water Thermo-physical uncertainty

Thermophysical property	Uncertainty
Density [kg/m^3]	0.01%
Specific heat [j/kg·K]	0.07%
Thermal conductivity [w/m·K]	2.35%
Dynamic viscosity [kg/m·s]	1.45%

HNF Thermo-physical properties Uncertainty

The thermo-physical properties of the various volume concentrations of MWCNT/AL_2O_3(90:10)-DI water HNF were estimated utilizing many other measurements and Equations. So, the following sections discuss the properties and their corresponding uncertainty independently based on the correlation used.

Viscosity

Viscosity is measured experimentally using a Sine Wave-viscometer (SV-10, A&D, Japan) with manufacture accuracy of 1% over a range of 0.3 to 10 000 mPa.s.

Thermal Conductivity

The experimental empirical correlation was used to calculate the thermal conductivity of the MWCNT/AL_2O_3(90:10)-DI water HNF, and different vol% concentration. The correlation is given an Equation (C.1).

$$k_{HNF}=k_{water}(0.940688+0.00428T_b+0.4696\varphi)$$

$$\delta k_{HNF}=\sqrt{\left(\frac{\partial k_{HNF}}{\partial k_{bf}}\delta k_{bf}\right)^2}$$

$$\delta k_{HNF}=(0.940688+000428T_b0.4696\varphi)\times\delta k_{water} \quad (C.1)$$

Specific Heat/ Density

After considering that the manufacturing value of nano-particles MWCNT and Al_2O_3 specific heat and density have no uncertainty, the Equation of uncertainty is derived Equation (C.2) and (C.3) respectively:

$$C_{p,HNF}=\frac{\varphi\left(C_p\rho\right)_{np}+(1-\varphi)\,\varphi\left(C_p\rho\right)_{hnf}}{\rho_{hnf}}$$

$$\delta C_{p_{hnf}}=\sqrt{\left(\frac{(1-\varphi)\rho_{bf}}{\partial\rho_{hnf}}\delta\rho_{bf}\right)^2+\left(\frac{(1-\varphi)C_{p_{bf}}}{\rho_{hnf}}\delta\rho_{bf}\right)^2+\left(-\frac{\varphi C_{p_{np}}\rho_{np}+(1-\varphi)C_{p_{bf}}\rho_{bf}}{\rho_{hnf}^2}\delta\rho_{hnf}\right)^2} \quad (C.2)$$

$$\rho_{HNF}=2.1\varphi+3.97\varphi+(1-\varphi)\rho_w=\rho_{np}\varphi+(1-\varphi)\rho_w$$

$$\delta\rho_{HNF}=\sqrt{\left(\frac{\partial\rho_{HNF}}{\partial\rho_{bf}}\delta\rho_{bf}\right)^2+\left(\frac{\partial\rho_{HNF}}{\partial\rho_{np}}\delta\rho_{np}\right)^2}$$

(C.3)

$$\delta\rho_{HNF}=\sqrt{\left((1-\varphi)\cdot\partial\rho_{bf}\right)^2+\left(\varphi\cdot\rho_{np}\right)^2}$$

The density of the nano-particle is given; therefore can be assumed to have no uncertainty, and the Equation is simplified to:

$$\delta\rho_{HNF}=\sqrt{\left((1-\varphi)\cdot\partial\rho_{bf}\right)^2}$$

Calculated Parameters Uncertainty

Heat flux

The heat flux between any two thermo-couples within the copper cylinder (test specimen) was estimated using Fourier's heat conduction law as follows:

$$\dot{q}=-k_s\frac{\Delta T}{\Delta x}$$

$$\delta\dot{q}=\sqrt{\left(\frac{k_c\Delta T}{\Delta x^2}\delta\Delta\right)^2+\left(-\frac{k_c}{\Delta x}\delta\Delta T\right)^2}$$

The total heat flux was taken using the weighted average Equation (4.15), with Δx being the distance between the five thermocouples (Δx_1 =0.004mm, Δx_2 = 0.006mm, Δx_3 = 0.008mm, Δx_4= 0.01mm).

The resultant overall uncertainty in the heat flux Equation was derived as Equation (C.4);

$$\frac{\delta\dot{q}_{weight}}{\dot{q}_{weight}}=\left[\left(\frac{4\cdot\delta\dot{q}_{12}}{4\dot{q}_{12}+6\dot{q}_{23}+8\dot{q}_{34}+10\dot{q}_{45}}\right)^2+\left(\frac{6\cdot\delta\dot{q}_{23}}{4\dot{q}_{12}+6\dot{q}_{23}+8\dot{q}_{34}+10\dot{q}_{45}}\right)^2+\left(\frac{8\cdot\delta\dot{q}_{34}}{4\dot{q}_{12}+6\dot{q}_{23}+8\dot{q}_{34}+10\dot{q}_{45}}\right)^2+\left(\frac{10\cdot\delta\dot{q}_{45}}{4\dot{q}_{12}+6\dot{q}_{23}+8\dot{q}_{34}+10\dot{q}_{45}}\right)^2\right]^{0.5} \quad (C.4)$$

Nusselt Number

$$Nu=\frac{hD_j}{k}$$

The uncertainty can be expressed as Equation (C.5).

$$\delta Nu=\sqrt{\left(\frac{\partial Nu}{\partial h}\cdot\delta h\right)^2+\left(\frac{\partial Nu}{\partial D_j}\cdot\delta D_j\right)^2+\left(-\frac{\partial Nu}{\partial k}\cdot\delta k\right)^2} \quad (C.5)$$

The nozzle supplied by (Lechler) was assumed to have no uncertainty, and the uncertainty Equation (C.6) becomes,

$$\frac{\delta Nu}{Nu}=\sqrt{\left(\frac{\delta h}{h}\right)^2+\left(-\frac{\delta k}{k}\right)^2} \quad (C.6)$$

All the results from the MATLAB results for uncertainty for thermo-physical properties, equipment and mathematical Equations are shown in Table 11 below.

Table 11 Uncertainty of measuring equipment's and thermal properties of MWCNT/Al_2O_3(90:10)-DI water HNFs

Parameter	Minimum Uncertainty	Maximum Uncertainty
Heat flux	0.25%	0.31%
Heat transfer coefficient	3.07%	3.76%
Nusselt number	3.89%	4.32%
Flow rate	1.8%	1.9%
Temperature	0.17%	1.2%
Amp meter	2.0%	2.0%
Voltmeter	1.7%	1.7%
Viscosity	1.39%	1.45%
Thermal conductivity	2.31%	2.42%
Surface Tension	0.96%	1.12%